EXCESS PRESSURE AND RESERVOIR COMPARTMENTALIZATION IN THE SABLE SUBBASIN, OFFSHORE NOVA SCOTIA

by

Carla Heleen Skinner

Submitted in partial fulfilment of the requirements
for the degree of Master of Science

at

Dalhousie University
Halifax, Nova Scotia
May 2016

Table of Contents

List of Tables

List of Figures

Abstract

In the Sable Subbasin, pressure distribution in sediments is important from economic, environmental, and drilling safety perspectives; but it has not been consistently explained in the literature. Fluid pressures have been observed in Jurassic and Early Cretaceous reservoirs in over 200 wells and generally increase with depth in unexpected increments from hydrostatic pressure to immense excess pressure (approaching lithostatic gradient) - a system known as “stepped excess pressure”.

The pressure systems of the Scotian Margin were extensively studied from 1989 to 2003 by several researchers without reaching a consensus on mechanisms and timing of excess pressure generation and dissipation (Mudford and Best 1989; Wielens 2003; Williamson and Smyth 1992). Hydrocarbon generation during the Cretaceous was cited as a pressure source, supported by basin modelling results. Recent thermal modelling (South Venture O-59 well) suggests ongoing hydrocarbon generation (Wong et al. 2016).

In the Sable region, excess pressured sections are lithified with thin intra-formational seals, and high net-to-gross ratios of porous sandstone to tight sandstones, shales, and low permeability limestones. It is difficult to rationalize current excess pressure without late hydrocarbon generation (or another late pressure source) within the region given micro-nano Darcy flow across thin imperfect seals that should allow for pressure equilibration over hundreds of thousands to several million years.

In this study, the pressure distribution in the Sable Subbasin was investigated with a sub-regional 3D static reservoir model of the reservoirs associated for five gas fields: South Venture, Venture, Arcadia, Citnalta, and Uniacke. The model was built by interpreting 1520 km^2 of 3D seismic data, that was integrated and calibrated with data from 27 wells. The model was populated with excess pressure data and lithologies interpreted from wireline logs and well tests, and inspected to test the hypothesis that excess pressure distribution is controlled by reservoir connectivity, which is ultimately controlled by permeability.

Pressure and fluids were interpreted to be currently entering the system by ongoing generation of hydrocarbons. At each of the fields, a similar arrangement of reservoir connectivity and pressure distribution were observed, although the ages of the rock units involved change from field to field due to progradational advance of the shelf and progressive formation of “expansion trends”. Expansion trends are isolated, high accommodation space depocentres formed in the hanging walls of down-to-basin listric faults, which formed as a results of depositional loading and salt movement at depth. These listric faults also set up low-relief, hanging wall, fault-bend folds - the principal hydrocarbon traps of the Subbasin. In the “deep” section, where reservoirs are stratigraphically and structurally isolated, the fluids and pressures are interpreted to be actively dissipating by mechanical leak. In the “intermediate” section, pressure equilibration within pressure cells occurs where the displacement of minor crestal faulting exceeds the thickness of minor intra-formational seals allowing for “stair stepping” up juxtaposed permeable units. In the “shallow” section, which is above the listric fault system, the reservoirs are contiguous and hydrostatically pressured.

List of Abbreviations Used

API	American Petroleum Institute (oil gravity)
CD	Commercial Discovery
CDL	Commercial Discovery License
CNSOPB	Canada-Nova Scotia Offshore Petroleum Board
DST	Drill Stem Test
Fm	Formation
FH	Final Hydrostatic (Pressure)
FIT	Formation Integrity Test
FLOT	Formation Leak Off Test
FSI	Final Shut In (Pressure)
GWC	Gas-Water Contact
HP	Hydrostatic Pressure
ISIP	Initial Shut In (Pressure)
km	kilometer
LOP	Leak Off Pressure
Ma	Million years
Mbr	Member
MD	Measure Depth
MDT	Modular Formation Dynamics Tester
ms	millisecond
OWC	Oil-Water Contact
OWT	One Way Time
P	Pressure
PIT	Pressure Integrity Test
RCA	Reservoir Connectivity Analysis
RFT	Repeat Formation Test
SD	Significant Discovery
SDL	Significant Discovery License
SI	Shut In (Pressure)
SIP	Shut In Pressure
TVD	True Vertical Depth
TVDSS	True Vertical Depth Sub-Sea
TWT	Two Way Time
$\mathbf{V_{sh}}$	Volume of Shale
WFT	Wireline Formation Test
WK	Well Kick (Pressure)
Φ	Porosity
P	Density
δ or **Δ**	Difference between 2 values

Glossary

Abnormal Pressure - Subsurface condition in which the pore pressure of a geologic formation exceeds or is less than the expected (or hydrostatic) pressure

American Petroleum Institute - A classification system developed by the American Petroleum Institute to describe the gravity/viscosity of gas-free crude oils expressed as °API. Gravities can vary from low (>31.1°API), medium 31.1-22.3°API), heavy (22.3-10.0°API) to extra-heavy (<10°API) crude oils and extend to tars and solid forms.

Capillary Pressure - Pressure differential between 2 immiscible fluid phases occupying the same pores caused by interfacial tension between the 2 phases that must be overcome to initiate flow

Commercial Discovery - A discovery of petroleum that has been demonstrated to contain petroleum reserves that justify the investment of capital and effort to bring the discovery to production

Excess Pressure - Subsurface pressure that is abnormally high, exceeding hydrostatic pressure at a given depth

Drill Stem Test (DST) - A method for isolating and testing the pressure, permeability, and productive capacity of a geological formation during the drilling of a well; provides important measurements of pressure behaviour and information on fluid type with sample collection

Fracture Pressure - Pressure required for the formation of fractures in a rock at a given depth

Hydrostatic Pressure - Normal (predicted) pressure for a given depth, or the pressure exerted by a column of water from the formation's depth to sea level

Formation Leak Off Test (FLOT) - A method for determining the strength of the rock through the injection of fluids into the rock at a given depth (also known as a Pressure Integrity Test - PIT)

Lithostatic Pressure - Pressure of the weight of overburden on a formation at a given depth

Pressure Gradient - Change in pressure per unit of depth

Repeat Formation Tester (RFT) - A wireline method for testing pressure of a geological formation during drilling quickly; provides important measurements of pressure behavior and information on fluid type with sample collection

Reservoir Pressure (Pore Pressure) - Pressure of fluids within the pores of a reservoir

Significant Discovery - A discovery indicated by the first well on the geological feature that demonstrates by flow testing the existence of hydrocarbons in that feature and, having regard to geological and engineering factors, suggests the existence of an accumulation of hydrocarbons that has potential for sustained production

Acknowledgements

I would like to take a moment to thank the people who have helped over the course of my graduate research.

I cannot thank my supervisor and committee members, Professor Grant Wach, Mr. Bill Richards, Mr. Neil Watson, and Mr. David E. Brown, enough for the opportunity to pursue research on the Sable Subbasin. Their expertise, guidance, and constructive feedback proved immeasurable, I could not have come close to completing this thesis without them. I would especially like to acknowledge Mr. Bill Richards for the hours spent sharing his knowledge on basin modelling, connectivity analysis, and fascination with all things subsurface.

This work was made possible by the donation of software from Schlumberger Canada Limited, and seismic data from ExxonMobil Canada and the Operators of the Sable Project (SOEP). Databases maintained by the Canada-Nova Scotia Offshore Petroleum Board and Natural Resources Canada were also critical to the success of the study.

I would like to thank the administrative and technical staff at the Department of Earth Sciences for all their help throughout the years, including Darlene van de Rijt, Norma Keeping, and John Thibodeau.

I would like to thank my parents, and grandmother who taught me the value of determination, hard work, and kindness. Last but not least, I would like to thank my husband for his encouragement, patience, and love.

Chapter 1: Introduction

Offshore Nova Scotia extends from the low water line to the edge of the continental margin, and covers approximately 402,000 km^2 (Smith et al. 2014). A total of 207 wells of all types have been drilled since 1967, and based on these there have been 23 discoveries that are associated with 35 Significant Discovery Licences (SDLs) and 8 of which are acknowledged as Commercial Discoveries (CDs) (Smith et al. 2014). It is worth noting that seven of the eight CDs are located within 50 km of Sable Island, confirming that Sable Subbasin is critical to the offshore proven commercial petroleum systems.

Reservoir pressure distribution in the Sable Subbasin is important from economic, environmental, and drilling safety perspectives. This study investigates the subsurface pressure distribution and reservoir connectivity in the Sable Subbasin.

1.1: Statement of Motivation

Unpredicted pressure changes (i.e. sudden onset of excess pressure) have occurred in wells drilling in the Scotian Basin, which are potentially dangerous situations if not properly identified, understood, and managed. Excess pressure in the Sable Sub-basin has been mapped at a low resolution, but the causes for excess pressure have not been resolved (Wielens 2003). Earlier work demonstrated excess pressure in the basin is inconsistent and only loosely associated with specific depths or formations (Mudford and Best 1989; Wielens 2003; Williamson and Smyth 1992). Studies of excess pressure in the region initially focused on describing the pressure mechanisms of the Scotian Basin including location, magnitude, and depth. However, faults in the Sable Subbasin were assumed to be either dynamic (allowing gas/fluid to migrate through) or static (not allowing gas/fluid to migrate); this supposition that all faults behave the same way is unreasonable and improbable (Richards et al. 2008). It is probable that more than one excess pressure formation mechanism is operating in the Sable Subbasin as excess pressure is observed in multiple formations. This study has access to newer vintage digital seismic and well log data, and the use of new software, which allows for a novel approach for studying pressure in the region.

Increased understanding of the geological context and contributing factors to excess pressure in pressure cells or compartments can reduce drilling and environmental risks and financial costs during exploration and development of offshore resources.

1.2: Study Area

The Scotian Basin is located east offshore Nova Scotia, and comprises several smaller subbasins including the Sable Subbasin (Figure 3.1). The study focuses on the northeast Sable Subbasin, in particular the Uniacke to South Venture hydrocarbon fields. This study crosses the expansion trend associated with the rifting and opening of the North Atlantic Ocean; thus the stratigraphy and deposition have been affected by tectonic movement (faults).

1.3: Objectives

The objectives of this study are to:

(1) Identify potential pressure sources within the Sable Subbasin
(2) Determine how pressure could migrate and dissipate
(3) Clarify the role of faults and fault juxtaposition of permeable units with respect to (1) and (2).

These objectives are met by:

(1) Defining a seismic stratigraphic framework within the study area for the Late Jurassic to Cenozoic strata on the Scotian Shelf and Slope, calibrated to available wells.
(2) Delineating faults present within the stratigraphic framework.
(3) Constructing and interpreting a 3D geocellular model of the study area with lithologies, fluid types, and pressures.

1.4: Hypothesis

The distribution and dissipation of pressure in the Sable Subbasin is controlled by reservoir connectivity, which is ultimately dependent on permeability and a result of interplay between the regional structure, stratigraphy, diagenesis, and seal integrity.

1.5: Thesis Organization

This thesis is organized 7 chapters and supporting appendices in order to present the work and results.

Chapter 2 discusses the relevant background theory on subsurface pressure, measurements, and excess pressure. Chapter 3 presents material on the Scotian Basin including regional structure, stratigraphy, petroleum systems, and previous excess pressure studies. Chapter 4 describes the datasets used for the study and how the data were collected. Chapter 5 reviews the pressure, geocellular and interpretation workflows developed as a part of this thesis. Chapters 6 presents the results and interpretations. Finally, Chapter 7 explains the conclusions and implications from this study, including final recommendations.

Chapter 2: Pressure

2.1: Hydrostatic Pressure

Hydrostatic pressure is a function of fluid density and the height of the fluid column. It can be expressed by the equation:

$$P = \rho * g * h$$

Equation 2.1: Hydrostatic pressure (P) equation, where P is the hydrostatic pressure; ρ is the fluid density; g is the gravity acceleration; and h is the height of the fluid column.

Pressure is also frequently expressed in terms of a pressure gradient, which is a function of the fluid density and depth. It can be expressed by the equation:

$$P = \frac{\rho_2 - \rho_1}{D_2 - D_1}$$

Equation 2.2: Pressure gradient equation; and ρ_2 and ρ_1 are the different pressures measured at depths D_2 and D_1 respectively.

The reference point for subsurface pressure is atmospheric pressure (at sea level), which is 101.28 kPa. Below the surface, fluid pore pressure increases at a rate dependent on the fluid density in the interconnecting pores. As the pressure gradient is dependent on the salinity of the formation water, in the absence of known water composition an average water gradient of 10.15 kPa/m is often used. If pressure measurements are made offshore, the reference datum is sea level.

2.2: Lithostatic Pressure

Lithostatic pressure is the combined weight per unit area of the overlying sediments and fluids at a specified depth. It is also commonly referred to as overburden, overburden pressure, overburden stress, or S_v (vertical stress) (Equation 2.3).

$$S_v = \rho_b * D$$

Equation 2.3: Lithostatic pressure equation, where S_v is the lithostatic pressure; ρ_b is the average bulk density; and D is the vertical depth from datum.

The bulk density is a function of the rock matrix, fluid densities, and porosity. It can be expressed by the equation:

$$\rho_b = \rho_m(1-\varphi)+\rho_f(\varphi)$$

Equation 2.4: Bulk density equation, where ρ_m is the density of the rock matrix; ρ_f is the density of the pore fluid; and ϕ is the porosity.

The significance of lithostatic pressure to pressure evaluation is two-fold:

(a) When the fluid pore pressure reaches lithostatic pressure, all the weight of the overburden is being supported by the fluid, therefore there is effectively no matrix support. If the rock is unconsolidated, grain-to-grain cohesion will be eliminated; the rock will then behave as a non-Newtonian liquid. If the rock is consolidated, the increasing fluid pore pressure typically induces hydraulic fracturing before lithostatic pressure is reached (depending on the tensile strength of the rock).

(b) Most methods for estimating pore pressure in shales use the lithostatic pressure as an input, therefore the more precisely it can be calculated, the more confidence there is in the pressure prediction.

2.3: Fracture Pressure

Any rock has a finite strength that is dependent on its lithology/composition, stress condition, and existing weaknesses (i.e. faults or fractures). The amount of pore pressure the rock can tolerate before failure is the fracture pressure. Above this, the minimum stress exceeds the tensile strength of the rock. Typically, the fracture gradient is less than the lithostatic gradient. Determining the fracture gradient requires data on the stress conditions existing in the formation. The stresses are a function of the tectonic and sedimentation histories of the region during the formation of the basin. Three principle stresses that act on the rock orthogonal to each other at depth (Figure 2.1).

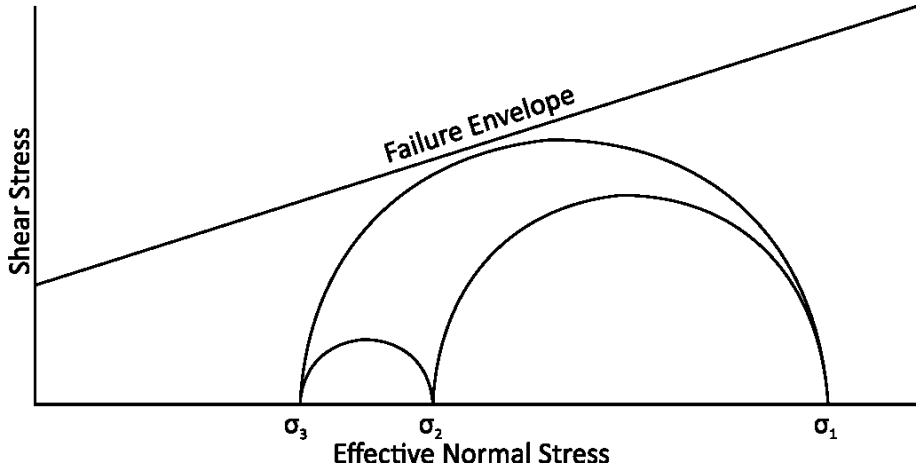

Figure 2.1: The state of stress is defined by σ_1, σ_2, and σ_3; which are the maximum, intermediate, and minimum compressive principal stress components respectively. When the Mohr circle touches the Failure Envelope, faults are activated.

2.4: Pressure Measurement

2.4.1: Formation Pressure

Reservoir pressures are measured directly by wireline pressure measurement tools. Indirect pressure data can be deduced from the mud weight required to prevent fluid influx into the borehole and 'kicks' when this is exceeded; these are often the only pressures available in impermeable shales (unless there are isolated porous intervals).

Formation pressure can only be measured directly when there is sufficient permeability for fluids to reach equilibrium with a downhole pressure gauge in a reasonable time frame. Accordingly, direct pressure measurements can be completed in reservoirs, but can only be estimated in low permeability lithologies (i.e. shales, tight sandstones, silts, or limestones). A common method for direct pressure measurement is the Wireline Formation Test (WFT) that includes the Repeat Formation Tester (RFT) and the Modular Formation Dynamics Tester (MDT). Another method for direct pressure measurement is the Drill Stem Test (DST). It is important to note that during the 1980's there was a change from using strain gauges to quartz gauges in pressure measurement tools.

Commonly encountered problems during testing are (a) tight sections, (b) seal failure, and (c) supercharging. When operators are drilling, they can be reluctant to leave a given tool in place for long periods of time for build-up tests because the tool may become stuck. Therefore, when testing in low permeability zones when longer than 15 minutes is required for build-up, the tests are often abandoned and noted in the log. In the case of seal failure, if the probe(s) cannot be isolated from the mud and the pressure reading remains close to or at the mud pressure, then the operator will record a seal failure.

Finally, supercharging occurs in low permeability zones as a result of the (higher pressured) borehole fluid invading the (lower pressured) formation. This can "charge" the formation in the testing zone, which is then measured and sampled by the tool. The pressure measurements will appear uncharacteristically high, and when plotted with other measurements against depth, will be evident as anomalies.

2.4.1.1: Repeat Formation Tester (RFT)

The RFT tool is an openhole wireline logging instrument used to measure formation pressure and collect samples of formation fluids. The tool has an unlimited number of pressure measurements but can only collect a few samples of formation fluid per run. Simply, hydraulic rams hold the tool against the borehole wall and a piston pushes a small probe against the formation. Packers above and below seal the probes from the well bore fluids, and allow formation fluids to flow into the pretest chambers. A pressure gauge records the inflow into the pretest chambers and the pressure build-up. The rate the pressure increases is primarily a function of the formation permeability. A high permeability zone can build-up pressure in as little as a minute, while a low permeability zone may take up to 15 minutes. Following this, a formation pressure test is completed, providing a measurement of the "hydrostatic" pressure; hydrostatic in this case refers to the drillers definition, which is actually reflective of the mud weight and is used for calibration. If the system is stable, the pre-test and post-test pressures should not differ by more than a few kPa. The build-up (or shut in) formation pressures logged against time may require correction to get the true formation pressure. A Horner Plot can be

constructed to allow extrapolation to time-infinity, allowing the formation pressure to be determined.

2.4.1.2: Modular Formation Dynamics Tester (MDT)

The MDT tool is also an openhole wireline logging instrument, and has multiple probes that allows for measurement of vertical and horizontal rock permeability. This tool is also able to collect more samples than the RFT tool as it has more sample chambers. The MDT tool test is run the same as the RFT tool.

2.4.1.3: Drill Stem Test (DST)

If hydrocarbons have been encountered and there is sufficient net pay over a reservoir interval, a production test can be run whereby formation fluids are allowed to flow to surface over an extended period of time (hours to days). The DST is completed in the open or cased borehole, where the interval of interest is isolated with packers (similar to RFT and MDT) and the casing is perforated. In a normal DST, an initial flow period is completed where formation fluids are allowed to flow up the drill pipe to "flush" out any mud infiltrates in the reservoir. Pressure is monitored before, during, and after. The pressure is then allowed to build-up and the final Initial Shut In Pressure (ISIP) is recorded – this is the best assessment of the true formation pressure. If the pressure is slow to build, then sometimes an extrapolated pressure is calculated instead. This indicates that true formation pressure has not been reached (similar to the RFT).

After the initial shut in period, the well is opened to flow for an extended time (typically 8 hours), allowing fluids to flow to surface and samples to be collected. The downhole pressure and wellhead pressure are observed during the flow, with the expectation of stable fluid flow conditions. The well is then shut in again, and pressure is allowed to build-up. The Final Shut In Pressure (FSIP) is the recorded; it may be lower than the ISIP because a volume of the reservoir in the near the wellbore has been produced.

DST data is often less accurate for pressure measurements due to the position of the gauge - it is not located at exactly the same depth as the sample collection, therefore corrections are required to the pressures measured. DST data is still preferable for permeability calculations (due to the extended flow period) and to establish flow rate. In

addition, any skin effect and reservoir damage (as a result of drilling) can be assessed, which is more difficult with RFT data. Also, more accurate formation temperature can be measured during a DST.

2.4.1.4: Well Kick

A well kick occurs when the formation pressure exceeds the borehole mud pressure (when static or flowing) and is observed as borehole fluid gains at the surface in the mud tank. The density of the drilling mud is known, therefore downhole pressure is known, and a minimum formation pressure can be estimated if the depth of the invading formation fluids is known. Underbalanced drilling (mud weight below formation pressure) can also cause a well kick; therefore, it is important to resolve why a well kick has occurred.

2.4.1: Fracture Pressure Measurement

2.4.1.1: Formation Leak Off Test

Formation Leak Off Tests (LOT) are conducted immediately after the hole is cased to (a) check the integrity of the cement at the casing shoe, (b) between the wellbore and casing above the shoe, and (c) to evaluate the borehole strength for future mud weight. After casing and cementing, the well is re-entered and the casing shoe (cement) is drilled through followed by several meters of rock. Normally in a FLOT, the effective mud pressure is increased in the borehole via pumping until fractures are introduced. FLOTs are generally used as indicators of the fracture strength of the fresh formation and represent the upper limit for mud pressure in the open hole section. In reality, the upper limit is not approached as there may be weaker parts of the formation where the limit is actually lower; faulted or fractured sections of formations would likely open at a lower pressure than the FLOT trend would indicate.

The FLOT is performed by drilling a short section (a rat hole) approximately 3 m below the cement casing shoe and shutting in the well. The mud continues to pump into the borehole, increasing the effective mud weight until mud volume is lost, which is recorded as a pressure response. If the cement is intact, then the mud loss is a result of the formation rock failure in the open hole section. Often, the leak off point is not reached

but a definite maximum pressure is reached (without mud losses) that is considered high enough to safely proceed with drilling. This is then known as a Formation Integrity Test (FIT) since leak off was not reached.

As part of a drilling plan, an estimate of the fracture gradient is required so the well will have an appropriately designed casing program. Planned mud weights in the well must also be close but slightly above the formation pressures expected (overbalanced), and casing points must be planned to prevent borehole fracture (based on the fracture pressure gradient prediction). When drilling in normally pressured sections, the casing design is predominantly based on the length of the open hole that can be drilled without difficulty. The casing points are generally placed in fine-grained lithologies, especially above zones of interest. When drilling in excess pressured sections, casing is controlled by the proximity of the pore pressure gradient and the fracture gradient - the closer the gradients are, the more casing strings are required. Casing is required when the mud needed to control the formation pressure approaches the fracture pressure in the open hole section.

2.5: Principles of Subsurface Pressure Analysis

2.5.1: Pressure versus Depth Plots

Pressure data (x axis) is plotted against depth (y axis) to determine formation pressure with respect to hydrostatic, fracture, and lithostatic pressures, and this plot provides the opportunity to assess fluid density, fluid contacts, and fluid type. Data points that plot on or near the hydrostatic pressure gradient are interpreted as “normally pressured” water, contiguous with a water column to the hydrostatic datum (typically sea level in an open marine offshore environment). Pressures that plot higher than a hydrostatic pressure line are abnormally high and are considered “excess pressured”. Pressure points that plot lower than a hydrostatic pressure line are abnormally low and are “underpressured”.

$$\Delta P = P - P_h$$

Equation 2.5: Formation pressure equation, where the The amount of pressure (ΔP) is the difference between the formation pressure (P) and the hydrostatic pressure (P_h) at a given depth.

Note, pressure-depth lines on pressure-depth plots are colloquially referred to as "gradients", which is an incomplete description. Pressure-depth lines have a gradient that reflects fluid density and an offset from a datum line such as sea level hydrostatic, that reflects under or over pressure. The hydrostatic pressure line is not necessarily a straight line, and does not necessarily have a consistent gradient in the strict sense. The density of water varies with both salinity and temperature. Similarly, gas and oil lines (or "gradients") are not necessarily straight and vary with composition (gravity segregation) and temperature.

2.5.2: Fluid Pressure Gradients

2.5.2.1: Water

Water gradients are calculated equations of state, typically using Pressure Volume Temperature (PVT) software, as there are quite a few variables that affect the gradient. For example, fresh water with a density of 1.00 g/cm^2 will have a gradient of 9.80 kPa/m. If it is a saturated brine with a density of 1.20 g/cm^2 it will have a gradient of 11.75 kPa/m.

The water gradient can be simply estimated using the difference in pressure at two different depths in the same interconnected formation, using the equation:

$$P_w = \frac{P_2 - P_1}{D_2 - D_1} = \frac{\delta P_w}{\delta D}$$

Equation 2.6: Water pressure gradient equation, where P2 and P2 are the pressure measurements at depth D2 and D1 respectively.

The gradient will be the same, regardless of absolute pressure, however the mud weight required to balance the formation pressure does depend on the absolute pressure and depth.

2.5.2.2: Oil (20-60° API) and Gas

Crude oils are generally classified by their density / viscosity and described by their gravity (°API). Conventional oil has a density less than water (with exception of very heavy

oils of < 10° API) which have densities equal to or greater than water), therefore their gradients will not be a steep as water. For example, an oil that is 20° API will have a gradient of 9.14 kPa/m, while an oil that is 60° API will have a gradient of 7.62 kPa/m. Gas has the lowest density of the fluids; therefore, it correspondingly has the lowest gradient. In the case of dry gas, gradients range from 2.25 - 3.20 kPa/m. Hydrocarbon gradients are calculated using the same formula as the water gradient (P_o is the oil gradient; P_g is the gas gradient). The more data points collected in any permeable section, the more accurate the gradient, a minimum of 2 points are required to determine a gradient. It is also important to remember that in deviated wells, the true vertical depth subsea (TVDSS) must be used for calculating gradients (as opposed to the measured depth (MD)).

2.6: Excess Pressure and Permeability

Simply put, excess pressure results from the inability of pore fluids to escape at a rate that allows equilibration with a column of static water connected to the atmospheric surface. There are three main groups of processes that generate excess pressure: (1) stress-related, (20 fluid volume increase, and (3) load transfer. Assuming a source of excess pressure is present, then permeability and connectivity become the primary control on the occurrence and distribution of excess pressure.

Permeability is a function of the rock properties (grain size, shape, and tortuosity) and the fluid properties (density and viscosity), and is imbedded in Darcy's Law (Equation 2.7). It is measured in Darcies (D) or milliDarcies (mD), or m^2 in SI units. The magnitude of excess pressure and the rate at which it builds up or dissipates at is an interplay between the process generating the pressure and the permeability of the encasing rocks.

$$Q = \frac{k*A*\Delta P}{\mu*L}$$

Equation 2.7: Darcy's Law equation for a single fluid phase, where Q is the volume rate of flow; k is the permeability; A is the area the flow is across; ΔP is the pressure drop across length L; L is the length scale; and μ is the fluid viscosity. More complex forms of the equation exist that describe fluid flow for multiple phases.

Where multiple phases are present in fine grained low permeability rocks, permeability to the non-wetting phase can become zero – it is immobile. For example, gas

trapped by a water-wet shale is trapped until the buoyancy force of the gas column exceeds the minimum capillary entry pressure of the connected pore space through the shale seal. Consequently, in addition to being controlled by the permeability, excess pressure dissipation can also be controlled by the capillary effects where hydrocarbons are encountered.

A seal was defined by as a rock that prevents the natural buoyancy upward migration of hydrocarbons, and he recognized the importance of capillary (or membrane) leakage and seals (Watts 1987). As described above, below a certain threshold pressure, seals can be barriers to hydrocarbon flow – the hydrocarbons are unable to flow because the displacement/entry pressure (controlled by capillary properties) of the seal rock cannot be reached. In 1990, Hunt adjusted the definition to refer to any rock that prevents all pore fluid migration (water, oil, and gas) over geologic time (Hunt 1990). Deming (1994) disputed the ability of rocks to maintain zero effective permeability over geologic time, and he reasoned it is more appropriate to view pressure accumulation and dissipation as continuous processes that change the pressures of abnormally pressured rocks over time (Figure 2.2).

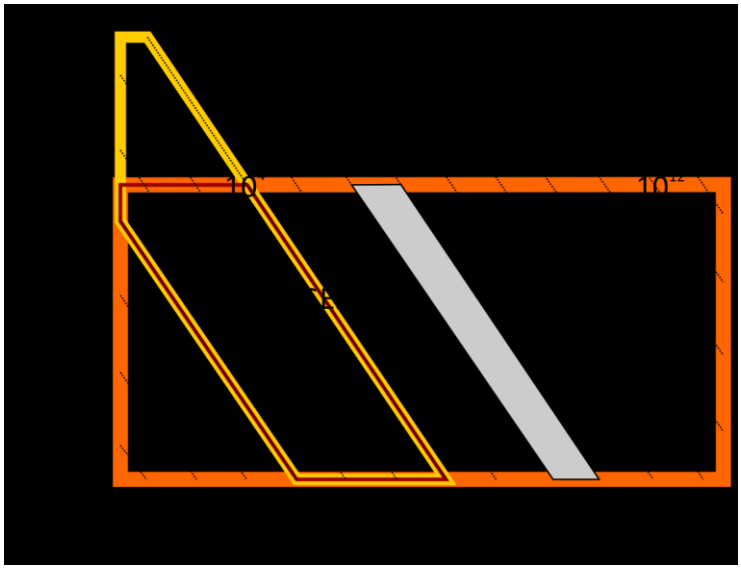

Figure 2.2: Maximum times over which a shale of a given thickness (y axis) and permeability (x axis) can confine excess pressures (Deming 1994). Grey shaded area indicates approximate minimum permeability required to sustain a 100-1000 m thick seal over 1 my. Yellow outline indicates average Sable Subbasin shale permeability of 10^{-20} to 10^{-22} m^2, while orange outline indicates shale thickness from 10 to 1000 m. Red outline indicates overlap of thickness and permeability, suggesting the maximum time shales of these conditions could impede flow is 10^4 years.

Excess pressure dissipation can also be achieved through fracturing. In tectonically active regions, reactivation of faults is another potential release for pressure. It should be noted that if the pore pressures increase to the fracture pressure of the rock during excess pressure generation, then the rock will hydraulically fracture and pressure may be rapidly released until the fractures reseal.

Excess pressure is a disequilibrium state and will change with time (depending on the development of the system), unless a state of zero effective permeability is reached (Deming 1994). Excess pressure magnitude and distribution will change during the generation phase and the dissipation phase. Today we are only able to look at the present stress state of the excess pressure system - pore pressure may have been higher or lower in the past.

Fluid properties of hydrocarbons have particular importance to excess pressure because of their buoyancy (based on density contrast) and the capillary pressure effect controlling relative permeability and entry pressure (therefore the effective sealing

capacity of the rocks). Buoyancy and fluid density are inversely related. Gas is the most buoyant fluid, and becomes denser (decreasing its buoyancy) at higher pressures. Pressure increases and decreases over time can affect the hydrocarbon composition in the basin, especially if pressure falls above or below the bubble point (the depth and temperature conditions at which the first bubble of gas comes out of solution in oil) .

2.6.1: Mechanisms of Excess Pressure Generation

2.6.1.1: Stress-Related Mechanisms

2.6.1.1.1: Disequilibrium Compaction (Vertical Loading Stress)

The vertical stress (or overburden stress) in a sedimentary basin is caused by the weight of the overlying rocks at a given depth, and can by expressed by the equation:

$$S_v = Z * \rho_b * g$$

Equation 2.8: Overburden stress equation, where S_v is vertical stress; Z is the thickness; ρ_b is the density of the overlying rocks; and g is the gravity acceleration.

$$\rho_b = \rho_{ma}(1-\phi) + \rho_{fl}(\phi)$$

Equation 2.9: The density log can be used to determine the average bulk density using the rock matrix density (ρ_{ma}), fluid density (ρ_{fl}) and porosity (φ).

The overburden stress is also supported by the fluid, the pore pressure (P), and the balance is spread between grain contacts, the effective stress (σ'). The relationship between vertical effective stress and the overburden stress is defined with Terzaghi's equation:

$$\sigma'_v = S_v - P$$

Equation 2.10: Terzaghi's equation, where σ'_v is the vertical effective stress; S_v is the overburden stress; and P is the fluid pore pressure.

In a normally pressured system, the vertical effective stress at a given depth is simply the difference between the overburden stress and hydrostatic pressure.

Increases in mean effective stress due to sediment loading during burial and simultaneous changes in horizontal stress can cause compaction, reducing pore volume and forcing out formation fluid(s) (Goulty 1998). The porosity loss rate will vary with lithology, and each lithology has a lower limit where no additional compaction is possible,

therefore any more porosity loss will be due to chemical compaction. Sandstones have a comparatively low compaction rate, from approximately 40-45% porosity at deposition, to as low as 5-7% due to grain rearrangement (packing) and minor dissolution at contacts. This contrasts sharply with clays, which have a faster compaction rate, and go from 65-80% porosity at deposition to as little as 5-10%, also due to grain rearrangement. This is due to the differing shapes and sizes of sand grains (generally more equidimensional) and clay grains (generally more platey) (Katsube and Williamson 1994).

In slow burial conditions, the equilibrium between the overburden stress and pore fluid volume reduction due to compaction can be more easily sustained. However, in rapid burial conditions, there is a quicker discharge release of fluids due to the rapidly increasing overburden stress. In areas where the fluids are unable to be released fast enough, the pore fluid pressure increases, a situation identified as disequilibrium compaction. Conditions which favour disequilibrium compaction are rapid burial and low-permeability lithologies, therefore it is commonly found in thick clay and shale sequences during continuous rapid burial. The excess pressure forms in adjoining high-permeability reservoir rocks due to isolation or encapsulation within the low permeability unit.

The magnitude of excess pressure formed as a result of disequilibrium compaction is controlled by the (a) vertical stress and coupled horizontal stress, (b) rock compressibility, (c) fluid and pressure dissipation through seals, and (d) pressure redistribution through connected high permeability units. Dewatering is controlled by the permeability of fine-grained rocks, and during initial burial both the porosity and permeability are reduced due to compaction and dewatering.

2.6.1.2: Fluid Volume Increase Mechanisms

2.6.1.2.1: Mineral Transformation - Water Release

2.6.1.2.1.1: Gypsum-Anhydrite Dehydration

The transformation of gypsum to anyhydrite is temperature controlled, and results in the loss of chemically-bound water. This reaction is suspected to be an important excess pressure generation mechanism in evaporite dominant area during shallow burial (Jowett et al. 1993). The transformation occurs between 40-60°C at normal pressure and has the

potential to generate significant excess pressure. However, many excess pressured basins do not contain sufficient evaporite sections and the excess pressure is located deeper.

2.6.1.2.1.2: Smectite Dehydration

Smectite is a multi-layer clay with water bound between the layers; as the particles dehydrate and water is removed, the mineral lattice gradually collapses. Although the clay particles collapse, the bound water being released actually causes an overall volume increase of up to 4% (Osborne and Swarbrick 1997). The dehydration of smectite is not thought to be a primary mechanism for excess pressure, but a secondary one.

2.6.1.2.1.3: Smectite-Illite Transformation

In mud-rich basins, a methodical change from smectite to illite is frequently observed, and is generally linked to the transition to high excess pressure (Bruce 1984); thereaction is controlled by time and temperature, sediment framework, and permeability. The transition from smectite to illite occurs over 70-150°C and seems unrelated to the age of the sediments or the burial depth. The precise chemistry of the reaction is unknown; therefore, the overall volume change is not known. Osborne and Swarbrick (1997) completed a set of reactions that indicated a volume change range from a 4% increase to an 8% decrease (assuming the mudrock comprises 100% smectite). Overall this would suggest the contribution to the magnitude of excess pressure is small.

2.6.1.2.2: Hydrocarbon Generation

The generation of hydrocarbons from kerogen maturation is kinetically controlled, that depends on both time and temperature. The two main reactions in hydrocarbon generation are (1) kerogen maturation to generate hydrocarbons, and (2) thermal cracking of oil to gas. Kerogen maturation generally occurs at 2-4 km depth and at 70-120 °C, while the cracking of oil to gas occurs at 3-5.5 km depth and 90-150 °C (Barker 1990; Tissot et al. 1987).

High pressures are required for primary migration of hydrocarbons from low permeability source rocks to reservoirs. When the kerogen matures to liquid, part of the overburden stress is transferred to the liquid phase and if the liquid is trapped then pore pressure will increase. The magnitude of excess pressure is related to the relationship

between effective stress and porosity. The richer the source rock, the greater the increase in pressure (assuming the same quantity of kerogen is transformed).

2.6.1.2.3: Gas Generation and Oil-to-Gas Cracking

Gas-prone (Type III kerogen) source rock maturation results in a greater increase in fluid volume, with calculated volume expansions of 50-100% relative to the initial kerogen volume (Ungerer et al 1983). At sufficiently high temperatures (120-140 °C) oil converts to lighter hydrocarbons and ultimately to methane, a process known as thermal cracking. At temperatures beyond 180 °C, there is almost complete cracking to gaseous hydrocarbons (Mackenzie and Quigley 1988). At standard pressures and temperatures 1 volume of standard crude oil cracks to 534.3 volumes of gas (and minor graphite residue) (Barker 1990). If this occurs in a perfectly sealed (isolated) system, then there is an immediate and rapid increase in pressure. Hunt et al (1994) observed a strong coincidence between peak gas generation and top excess pressure in the Gulf of Mexico. Cayley (1987) noted that the highest excess pressures in the North Sea are located where the Kimmeridge Clay is the most deeply buried.

2.6.2: Effect of Excess Pressure on the Petroleum System

The effect of excess pressure on the petroleum system has not received equal attention to the study of generation mechanisms. Opinions on the influence of excess pressure vary widely, for example researchers have claimed that the excess pressure in some North Sea reservoirs explain the high porosity (Harris and Fowler 1987), while other researchers have claimed there is no effect (Bjorkum 1996). This section focusses on the potential effects of excess pressure on the petroleum system with respect to reservoir quality, maturation, and migration.

2.6.2.1: Reservoir Quality

Numerous studies have concluded that excess pressure has been an important factor in porosity preservation in reservoir rocks, regardless of the age of the system (Atwater et al. 1986; Harris and Fowler 1987). Reservoir porosity is tied to the capacity for granular rocks to mechanically compact, and to mineral precipitation and dissolution processes. As excess pressure reduces the effective stress (or at the least maintains it with

continued burial), it will result in higher than expected porosity at a given depth. The timing of excess pressure compared to diagenetic porosity alteration is important - if excess pressure precedes a diagenetic process that reduces porosity, then a higher level of porosity should be preserved than if excess pressure was not present.

2.6.2.2: Source Rock Maturation

Evidence from field studies paired with basin modelling suggests that excess pressure affects source rock maturation timing by slowing down maturation reactions at high pressures (Luo et al. 1994). A higher geothermal gradient is often observed in the excess pressured sediments, but that is likely connected to the reduced thermal conductivity of the higher porosity sediments and is not a results of an increased heat flow (Luo et al. 1994). The higher temperatures would be expected to provide higher vitrinite reflectance (VR) results.

2.6.2.3: Migration

Excess pressure as a result of volume increase during hydrocarbon generation or thermal cracking provides a pressure drive mechanism for the petroleum system. Sufficiently high internal pressures (in source rocks) can cause downward or upward migration into carrier beds. The connection between the source rock pressure history and the carrier beds should be assessed; if the beds contain greater pressure than the source rocks, migration will be hindered until the pressure differential is adequate between the bodies.

2.7: Underpressure

Underpressure is defined as occurring when the pore pressure is less than hydrostatic pressure. Natural underpressured systems are not as common as excess pressured, though they are well documented in the foothills of the Western Canadian Sedimentary Basin. Underpressured systems can form in isolated compartments as a results of overburden being removed through uplift and erosion. The pores are then able to expand due to the reduction in confining stress and the elastic nature of rocks, leading to underpressure. Reservoirs can also become underpressured from production, where

the influence of earlier drilled wells is observed on later drilled wells as either a reduction in excess pressure or the formation of underpressure.

2.8: Pressure Compartments and Reservoir Connectivity

Interactions between stratigraphy and structure with the buoyant fluids they contain leads to the formation of compartments. The compartments are connected through leak and/or spill points. There are two types of spill recognized: spill through the "escape of the more buoyant fluid at a break or cusp in the topseal", and breakover with the "loss of the denser fluid driven by excess pressure at a break of saddle in the baseseal" (Vrolijk et al. 2005). A saddle that occurs between two compartments is not a barrier - flow is not prevented; rather the saddle is a connection between the compartments, similarly with cross fault leak.

In hydrocarbon migration and trapping studies, it is generally assumed that traps have sufficient seal strength to prevent leakage. Based on this and the initial generation of oil, gas generation may force oil to spill from traps in a predictable manner. A trap should become charged with water, oil/water, gas/oil, then finally gas. Examination of updip traps should reveal this fluid transition in a logical sequence. Once all the compartments in the system are filled with gas, then any additional hydrocarbons (oil or gas) should continue updip until the rock ultimately crops out releasing them. Gussow (1954) proposed that at the extreme of this theory, entire systems or basins may have become gas dominated, even though oil preceded the gas.

If the seals leak before the trap is filled (closure strength of the seal is surpassed), then the compartment will preferentially leak gas because it has smaller molecules, is more buoyant, and is located above the oil (Sales 1997). The oil will continue to accumulate and any gas that enters the system will leak at the same rate the gas enters. If the oil continues to put pressure on the seal and exceeds the seal strength, then the oil too will start to leak from the compartment. Based on the closure versus seal strength principle, three classes of trap can be defined based on the interaction between closure strength, gas column height, and oil column height (Figure 2.3) (Sales 1997). As compartments fill, the fluid contacts are volumetrically controlled and will change as more hydrocarbons are added to the system (Sales 1997). Once a compartment is full, they become spill point and/or pressure controlled. Fluid contacts that are pressure controlled will stay in their position as fluids continue to flow through the trap.

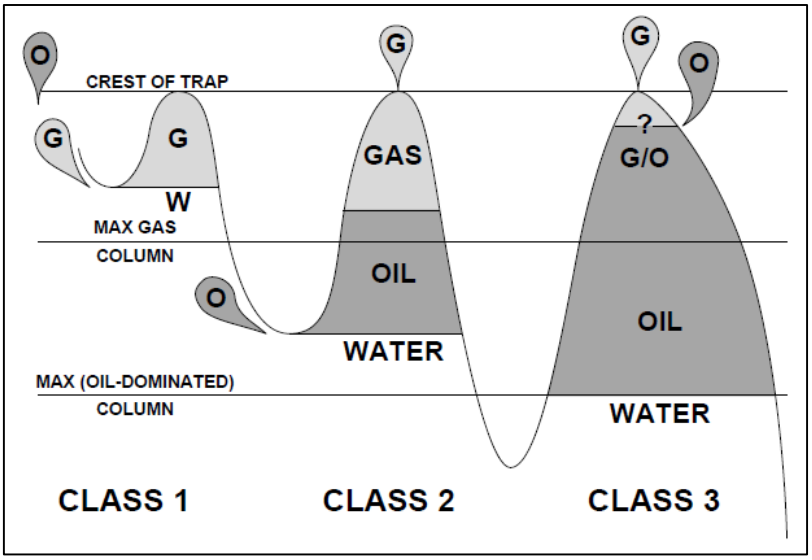

Figure 2.3: Diagram demonstrating each of the three class types, and where each fluid may be spilled or leaked (Sales 1997).

Important assumptions are made by Sales (1997) that are accepted by industry and used in this thesis:

(1) Hydrocarbons migrate as separate phases, based on their densities and controlled by their buoyancies (Tissot et al. 1987)

(2) Seal failure can result from

a. Capillary breakthrough (Berg 1975)
b. Hydraulic fracturing (Watts 1987)

In faulted compartments, the spill point can be a result of juxtaposed permeable units across the fault. If hydrocarbons are migrating through juxtaposed permeable units, this spill point is typically higher than the structural spill point; these compartments are not normally filled to their structural spill point but are filled-to-spill (Figure 2.4). These relationships are best visualized with fault plane profiles and structural maps, which provide a three dimensional view of migration and trapping (Allan 1989). Fault plane profiles (FPPs) demonstrate the relationship between the closure style, the cross-fault geometry, and stratigraphic geometry. The cross-fault spill points define the limits of the compartments and potential migration paths.

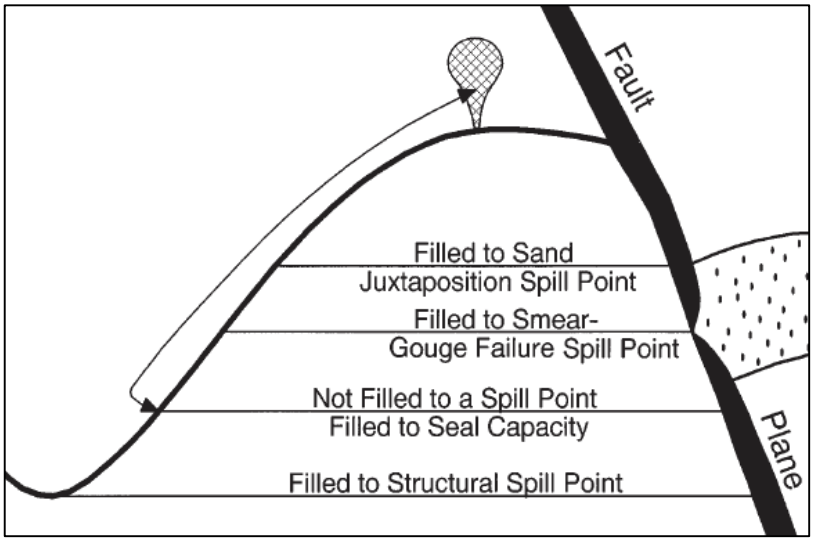

Figure 2.4: Potential spill points in a faulted trap (Sales 1997)

A breakthrough paper on Reservoir Connectivity Analysis (RCA) By Vrolijk et al. (2005) outlined a systematic approach to analyzing complex connectivity in fields; it integrated structural, stratigraphic, fluid pressure & composition data (Vrolijk et al. 2005). The method combines conventional (well understood and accepted) concepts to study connectivity, including:

(a) fault juxtaposition relationships
(b) spill points related to saddles

(c) fluid breakover

(d) seal leak through either mechanical, capillary leak, or baseseal leak (stratigraphic compartments.

This systematic analysis is based on sequential trap fill where hydrocarbon volumes are greater than the trap volume, and can be divided into three phases:

(1) interpret and describe reservoir compartments

(2) define the connection(s) between the compartments

(3) construct an RCA model - a connectivity diagram

The RCA approach is normally completed at the field-scale, however it can also be applied regionally across multiple fields. For this study, the RCA approach has been applied at the regional scale to the Uniacke, Citnalta, Arcadia, Venture, and South Venture fields of the Sable Subbasin (detail on methodology is available in Chapter 5).

The role of faults is important in any discussion of connectivity and migration within the RCA method, especially in the Sable Subbasin where there is a considerable amount of growth faulting related to basin formation. Significant research has been published on the role of faults in fluid connectivity, with many differing opinions as to when, where, and how fault act as either seals or conduits. A very reasonable view taken by Downey (1990, 1994) is that fault planes can sometimes behave as conduits near the surface (due to tensional opening of fractures) and in the deep subsurface (due to fluid pressures exceeding fracture closure pressure) (Figure 2.5). At intermediate depths, fault planes and associated fractures are typically “closed” due to the hanging wall overburden and relatively low pressure of the fluid system. There are exceptions, where the fault is not a plane but rather a zone of permeable material such as sandstone injectite or fault gouge. Upward migration of fluids associated with faults at intermediate depths is achieved through cross-fault movement between juxtaposed permeable strata (juxtaposition windows). In areas with significant changes in fault throw, this enables upward “stair stepping” of fluids.

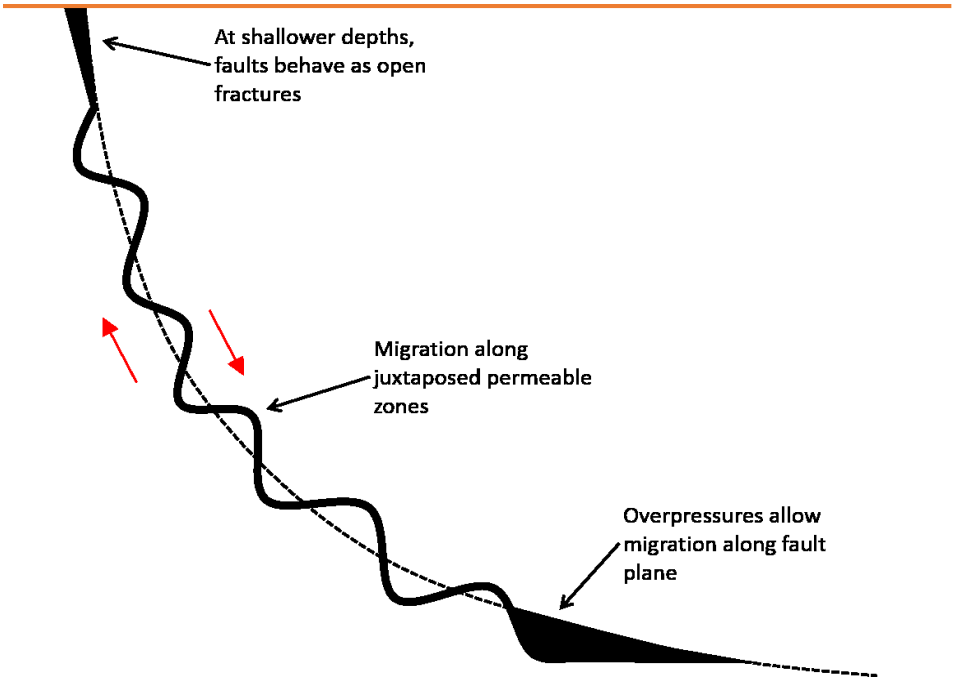

Figure 2.5: Hydrocarbons can migrate along the fault plane at shallow depth where they behave as open fractures, or juxtaposed permeable zones, or due to excess pressure at depth (Downey 1994).

An important consideration is that the presence of clay smear, cataclasis, or diagenesis can create a capillary seal at the juxtaposition windows. Overall, there is consensus that fault gouge can act as a baffle to fluid flow in commercial hydrocarbon production (or even very active petroleum systems), but because gouge is normally discontinuous along the fault surface there is considerable discussion on the effectiveness of this as a seal mechanism over geologic time. The Shale Gouge Ratio (SGR) is used to estimate the shale content of the fault zones (Allan 1989). In general, fault zones in regions with greater shale content (lower net-to-gross ratio) will have higher SGR values, thus can support higher capillary threshold pressures.

Considering juxtapositional relationships in more detail: if permeable lithologies are located on either side of the fault, then hydrocarbons can migrate across; if there are multiple permeable units on either side, then there is the potential to “staircase” or “stair step” up the juxtaposed permeable zones. If there is a permeable unit on one side of the fault and an impermeable unit on the other side, then the ability of the hydrocarbons to migrate across the fault is significantly reduced.

Chapter 3: Scotian Margin

3.1: Regional Structural Setting

The Scotian Margin is a narrow northeast trending continental basin, 125-225 km wide, which extends approximately 1000 km from Georges Bank to the southern Grand Banks. The total area of the basin is approximately 402,000 km^2 (Figure 3.1) (Hansen et al. 2004; Wade and MacLean 1990). The basement comprises structurally complex Cambro-Ordovician metasediments and Devonian granites overlain with Mesozoic-Cenzoic sediments. The geologic history of the basin reflects continental extension and rifting followed by the opening of the North Atlantic Ocean and development of the passive Scotian Margin. Rifting during the Late Triassic to Early Jurassic caused extensional faulting, forming a series of basement ridges and subbasins. The subbasins in the margin include the Mohawk, Emerald, Naskapi, Mohican, Sable, Abenaki, and Orpheus basins (Smith et al. 2014). For overviews of the petroleum systems of the Scotian Margin, please see Wach et al. (2014) and Silva et al. (2015).

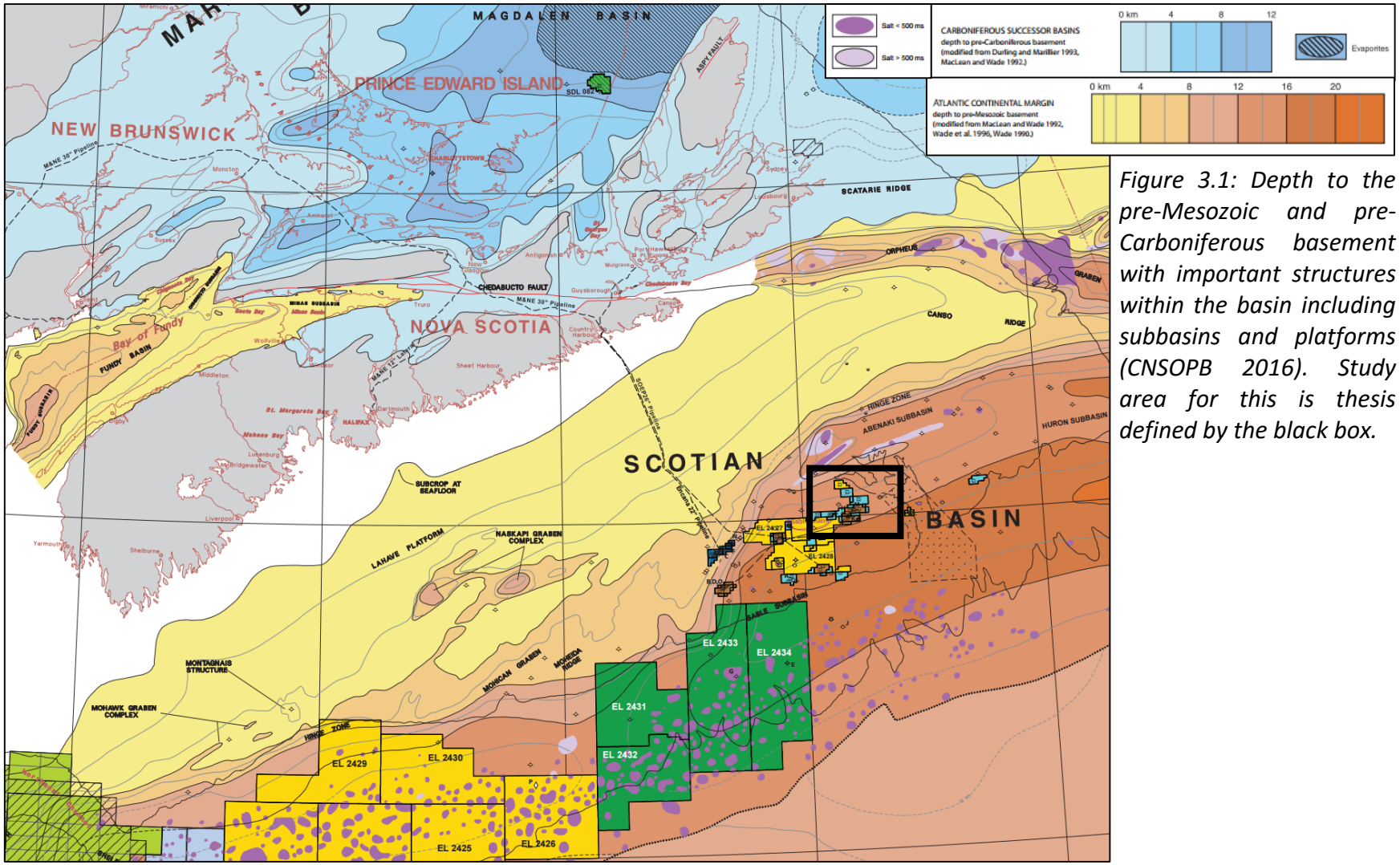

Figure 3.1: Depth to the pre-Mesozoic and pre-Carboniferous basement with important structures within the basin including subbasins and platforms (CNSOPB 2016). Study area for this is thesis defined by the black box.

3.2: Regional Stratigraphy

The stratigraphy of the margin can be broadly divided into five groups: Triassic pre-breakup rift deposits, Early to Middle Jurassic post-breakup clastics and carbonates, Late Jurassic to Early Cretaceous deltaic wedge sediments, Middle to Late Cretaceous transgressive and Cenozoic regressive marine sediments (Figure 3.2).

Crustal attenuation and basement faulting during the Middle Triassic to Early Jurassic rifting formed grabens and half grabens that were filled with the synrift continental clastics of the Eurydice Formation (Smith et al. 2014). These were followed by the deposition of the Argo Formation evaporites and unnamed clastics. Following the Breakup Unconformity was the deposition of the shallow marine dolomites of the Iroquois Formation. These formations emphasize the shift from non-marine to marine depositional environments as a result of the opening of the North Atlantic Ocean (SOEP 1997).

Widening of the Atlantic during the Jurassic creased more open marine conditions along the Scotian Basin margin. This led to a significant marine transgression and allowed for the development of a carbonate bank on the shelf edge, the Abenaki Formation (Scatarie, Misaine, and Baccaro members) (Kidston et al. 2005). Off the shelf edge, there was a rapid increase in the slope resulting in a change from shallow water marine shelf to deepwater depositional environments over very short distances. While the carbonate bank grew on the shelf edge, seaward of this was deposition of deepwater marine shales of the lower Verrill Canyon Formation (SOEP 1997). Landward was the coeval deposition of Mic Mac Formation the shallow shelf calcareous sands, shales, and carbonate muds. Locally within the Sable Subbasin area, structural downwarping provided high accommodation for clastic sediments preventing the development of the Abenaki carbonate bank in that area; instead a small Mic Mac Formation delta was established (Smith et al. 2014).

During the Late Jurassic to Early Cretaceous, clastic sediment deposition increased through a major continental drainage system that created the Sable Delta complex. The delta prograded into the basin with sand-rich delta, delta front and delta plain sediments of the Missisauga Formation and the prodelta shales of the Verrill Canyon Formation

(Wade and MacLean 1990). The sandstones of the Missisauga and Mic Mac formation delta complexes form the reservoirs of the Sable Subbasin. A marine transgression over the delta sequence covered the unit with the thick marine shale of the Naskapi Member of the Logan Canyon Formation (Wade and MacLean 1990).

The rest of the Early Cretaceous is associated with passive margin development and the deposition of the delta to shallow marine progradational lobes of the Logan Canyon Formation interfingered with the basinal-equivalent marine shales of the Shortland shale (SOEP 1997). The Logan Canyon comprises four members, which in descending order, are the Marmora, Sable, Cree, and Naskapi. These members represent alternating regressive (Marmora and Cree) and transgressive (Sable and Naskapi) successions.

During the Late Cretaceous, the region was undergoing the final stages of passive margin development, and a marine transgression deposited the Petrel limestone. Following this was the deeper water deposition of shales of the Dawson Canyon Formation, then chalky limestones of the Wyandot Formation. Finally, this was all capped by deposition of the Paleogene and Neogene Banquereau Formation clastics (SOEP 1997).

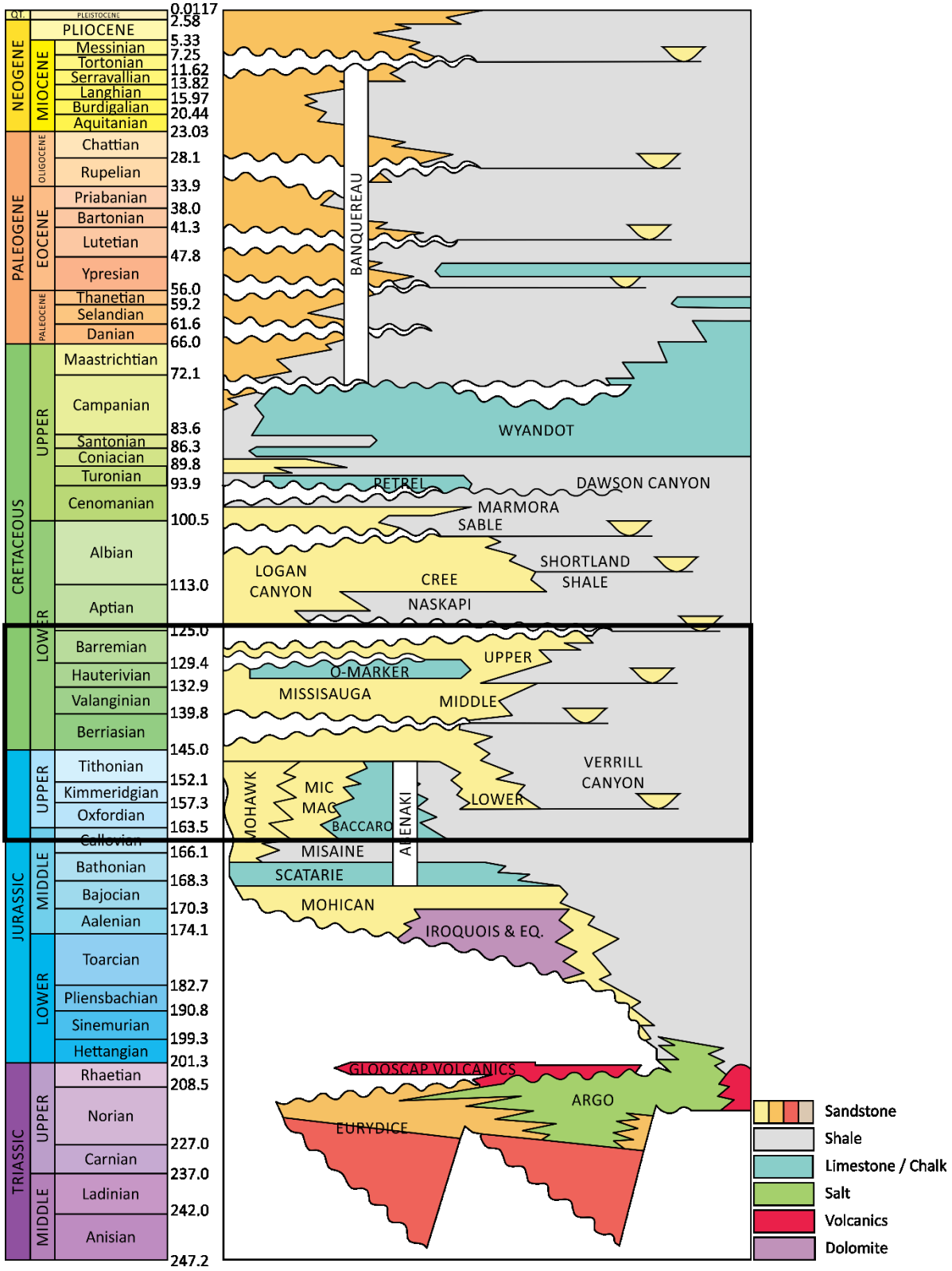

Figure 3.2: Lithostratigraphy for the Scotian Basin (Weston et al. 2012). The (approximate) stratigraphic interval of interest is defined by the black box.

3.3: Hydrocarbon Sources & Trapping

The shales of the Verrill Canyon Formation are the distal marine equivalents of the Mic Mac and Missisauga formations, and are regarded as the most likely hydrocarbon (gas and condensate) source for the Sable Subbasin petroleum system. The shales are type III source rocks, meaning they are generally sourced from plant material and were likely deposited in a terrestrial depositional environment (McCarthy et al. 2011). The shales are described as gas-prone, lipid-poor, and as having low total organic content (TOC).

During and after deposition of the Mic Mac and Missisauga formations, growth faulting due to sediment loading was active, resulting in the formation of rollover anticlines and potential traps for migrating hydrocarbons (Figure 3.3).

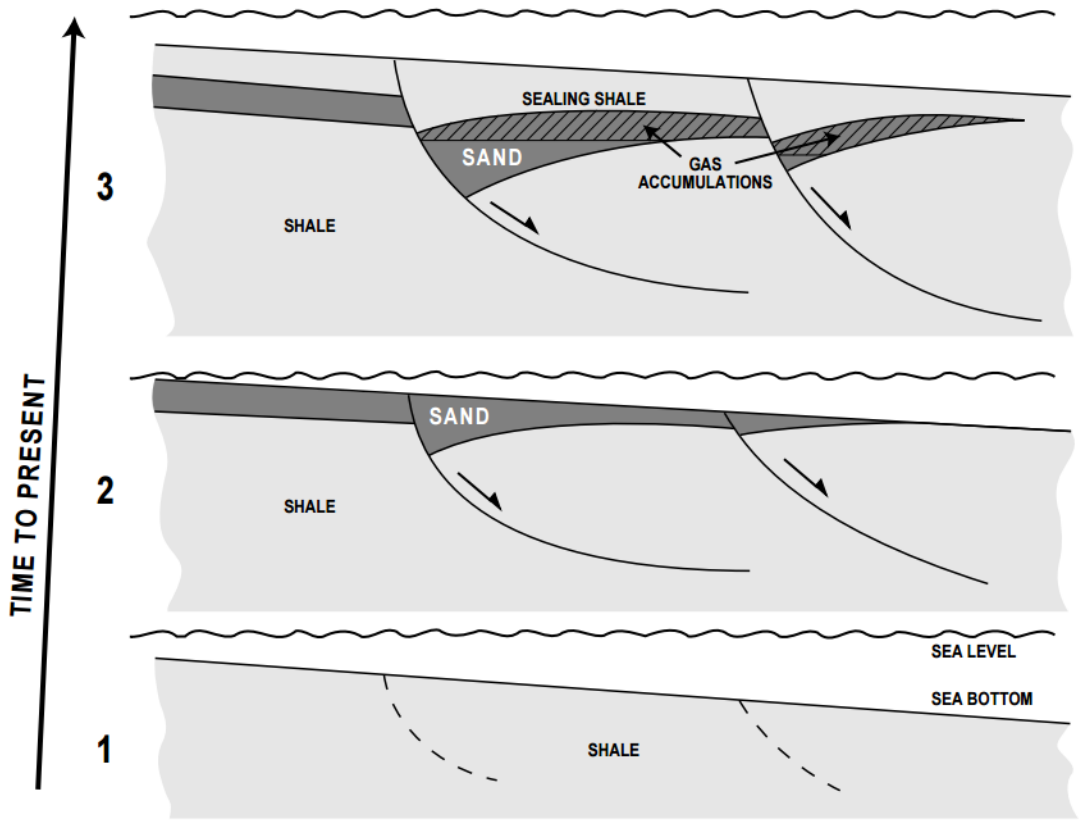

Figure 3.3: Development of growth faults leading to formation of anticlinal trap structures (SOEP 1997)

3.4: Previous Work - Excess Pressure

The gas accumulations in the Sable Subbasin occur in hydropressured and excess pressured reservoirs. Excess pressured reservoirs are defined as those with a subsurface pore-fluid pressure greater than those with hydrostatic pressure (see Chapter 2 for more detail on subsurface pressure). The shallow Missisauga Formation reservoirs of the Venture and South Venture fields are hydropressured, while the deep reservoirs of the same formation are excess pressured. Excess pressure in the subbasin is suspected to be a result of compaction disequilibrium and gas generation, however, multiple theories have been proposed and are summarized in Table 3.1.

One of the first studies focused on excess pressure in the Sable Subbasin studied the Venture gas field (Mudford and Best 1989). The authors observed that pore pressure increases correlated with low permeability shale beds (permeability less than 10^{-20} m^2). Through a 1D (one dimensional) model of single-phase pore pressure development, they concluded that disequilibrium compaction was the primary cause of excess pressure in the gas field.

In 1991, more 1D modelling was completed on the Scotian Shelf and results were then compared to results from the North Sea and Gulf Coast (considered reasonably analogous) (Mudford et al. 1991). Permeability measurements on the shales returned results of approximately 10^{-21} m^2 for effective pressures between 10,000 – 60,000 kPa. The comparison of models from the three regions showed poor agreement, with the Scotian Shelf modelled pressures lower than those of the other two areas. In the North Sea and Gulf Coast, rapid Neogene sedimentation and shaley Cenozoic sediments combine to cause compaction-based excess pressure formation. In contrast to the 1989 study, the difference between them and the Scotian Shelf was interpreted to suggest mechanisms such as lateral fluid migration, mineral diagenesis, and ice loading.

Following the 1D modelling in the previous two studies, 2D (two dimensional) modelling was completed on the Venture field by Forbes, Ungerer, and Mudford (1992). In their study, a basin-scale model was used to attempt the reconstruction of excess pressure formation around the Venture field. The study determined that gas generation

and lateral compression were minor contributors to excess pressure, while disequilibrium compaction was again put forth as the primary mechanism.

Another study in 1992 focused on how gas migration dynamics may have impacted the timing of gas and excess pressure generation (Williamson and Smyth 1992). The researchers compared the Glenelg and Venture fields, which comprise hydropressured and excess pressured reservoirs respectively. They completed 2-phase 1D pore pressure models that showed the two phases of pressuring can be explained by disequilibrium compaction with minor hydrocarbon generation. Importantly this study also noted that major vertical growth faults may have acted as migration conduits for gas from deeper, mature excess pressured reservoirs into shallower, hydropressured reservoirs. Vertical growth faults were not observed at the Venture field; therefore, the gas was restricted to the localized excess pressured accumulations.

Yassir and Bell (1994) completed a geomechanical study of the Mesozoic and Tertiary (Cenozoic) sediments of the Scotian Shelf and identified two weak layers at depth: (1) an excess pressured interval at 4000 m depth, and (2) the Argo salt. The study determined that present-day lateral stress in sediments above the excess pressured zone are "aligned with contours of equal pressure but not with the Tertiary listric faults or shelf edge". They concluded that the rocks of the Scotian Shelf are trying to slide down over the weak excess pressured unit but are unable to do so because of the shape of the basement structure, thereby increasing the overburden load.

Williamson (1995) reexamined the excess pressures of the Sable Subbasin in order to better understand the relationship between the burial, thermal, and maturation history, and how these affected the pressure history. Simple 1D maturity and pore pressure reconstructions were completed and calibrated (where possible) to published maturity, temperatures, and pressures. The reconstructions assumed that compaction disequilibrium and gas generation were the primary excess pressure mechanisms. The study concluded that the basin source rocks underwent rapid (rift-related) subsidence leading to early maturity and gas generation. The rapid subsidence and ongoing sedimentation resulted in compaction disequilibrium and early onset of excess pressure.

The study also noted that the models were particularly sensitive to the assumed seal permeability profiles, and that using present seal permeabilities does not necessarily accurately reflect the permeability evolution of the subbasin.

In 2003, the variable behavior of excess pressure on the Scotian Shelf was studied to determine if there were correlations between excess pressure occurrences and magnitude, top (depth) of onset, burial depth, maturity, and formations (Wielens 2003). Several important conclusions about excess pressure on the Scotian Shelf were reached:

- Excess pressures are not present in all wells
- Are generally at similar magnitudes and depth in wells from the same field
- Do not appear related to particular formation(s)
- Do not appear in the same formation in adjacent wells
- Do not appear related to burial depth
- Do not appear related to formation temperature
- Do not consistently have indications on wireline logs

The study suggested several potential excess pressure mechanisms on the Scotian Shelf, including fluid volume increase, mineral transformation, and hydrocarbon generation; they also discounted compaction disequilibrium as a mechanism. One of the most important conclusions reached was the acknowledgement of the lack of knowledge surrounding the role of faults, recognizing that further research was required.

Most recently, 1D thermal modelling was completed on the South Venture O-59 well to examine thermal maturity of known and suspected source rocks (Wong et al. 2016). The researchers concluded that a late stage increase in basinal heat flow during the Paleogene provided the best fit between simulated results and measured data for temperature and vitrinite reflectance. This thermal input caused a second phase of hydrocarbon generation in the South Venture field, which could serve as a potential pressure source for the Sable Subbasin (Figure 3.4).

Table 3.1: Summary of excess pressure theories for the Sable Subbasin (Forbes et al. 1992; Jansa and Urrea 1990; Mudford and Best 1989; Mudford et al. 1991; Mukhopadhyay 1993; Wielens 2003; Williamson 1995; Williamson and Smyth 1992; Wong et al. 2016; Yassir and Bell 1994).

Year	Researcher	Theory							
		Disequilibrium Compaction	(Late) Hydrocarbon Generation	Migration at Depth	Lateral Fluid Migration	Mineral Diagenesis	Ice Loading	Growth Fault Conduits	Fluid Volume Increase
1989	Mudford & Best	X							
1990	Urrea & Jansa		X	X					
1991	Mudford, Gradstein, Katsube, & Best				X	X	X		
1992	Forbes, Ungerger, & Mudford	X							
1992	Williamson & Smyth	X	X					X	
1993	Mukhopadhyay		X						
1994	Yassir & Bell		X						
1995	Williamson	X	X						
2003	Wielens		X			X			X
2016	Wong, Skinner, Richards, Silva, Morrison, & Wach		(X)						

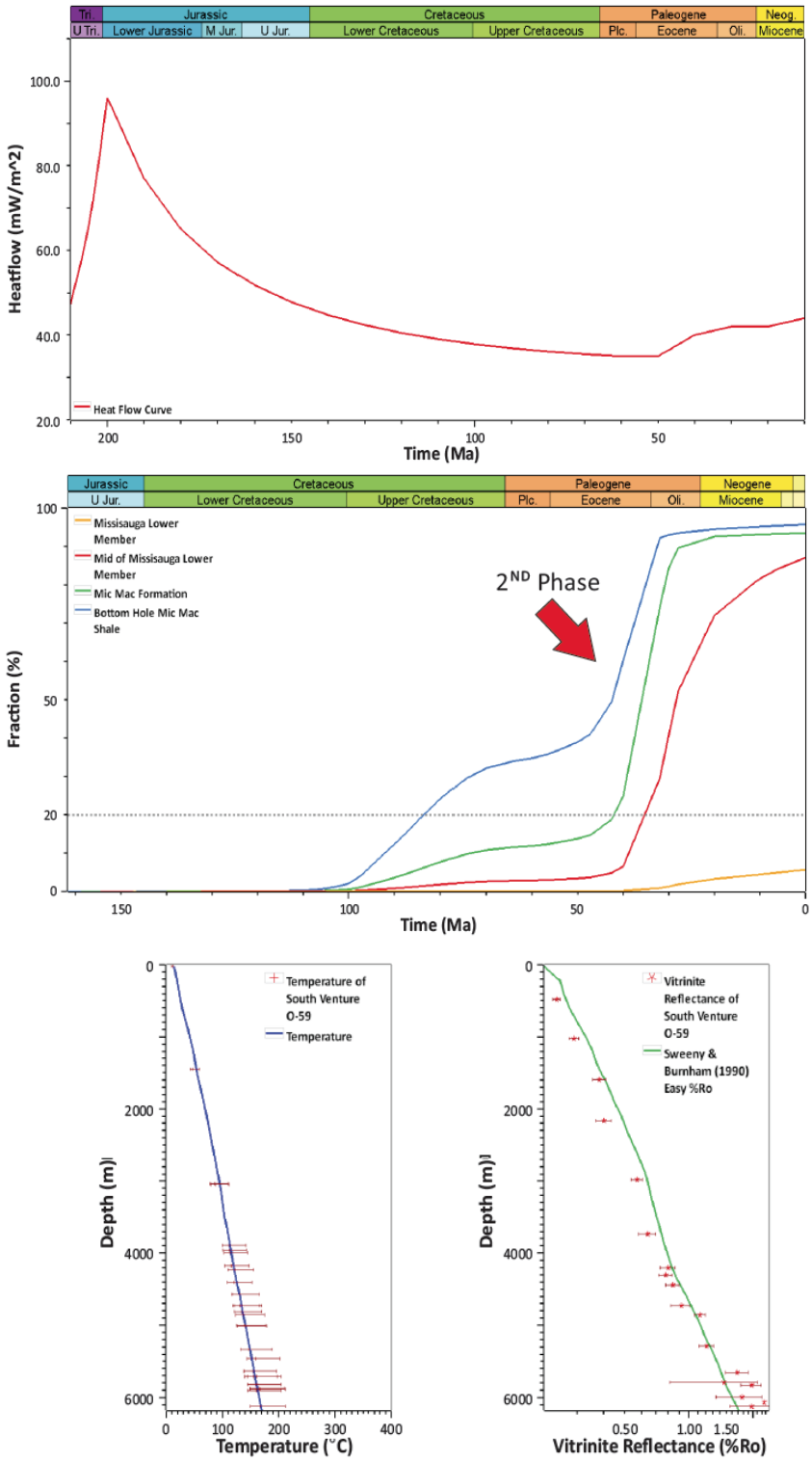

Figure 3.4: Petromod™ simulation results from South Venture O-59 (Wong et al. 2016). (top) Heat flow plot; (middle) source rock transformation ratio (amount of source rock transformed to hydrocarbons) plot with 2nd phase of generation indicated; (bottom-left) temperature-depth plot with simulated and measured data; (bottom-right) vitrinite reflectance-depth plot with simulated and measured data.

3.5: Reservoir Stratigraphy

In the Sable Subbasin, reservoirs are stratigraphically located within the Late Jurassic Mic Mac and Early Cretaceous Missisauga formations. They comprise deltaic to shallow marine sand deposits of the Sable Delta complex. The delta complex was deposited over approximately 50 million years, and over this period the delta advanced and retreated multiple times in a generally north-south direction. The delta complex consists of stacked successions of coarsening-upward cycles, and is thickest in the Thebaud and Venture field areas (SOEP 1997).

Gas has become trapped where there is a working system of reservoir-quality lithology, source rocks, seal lithology (shales and limestones), and structures. The seaward margin of the delta complex has low (15:85 to 30:70) but superior sand-to-shale ratio for trapping gas due to the interfingering of the deltaic sands with pro-delta and marine shales. Moving upward stratigraphically through the delta complex, the sand-to-shale ratio increases. As a result of syndepositional growth faulting, the lithologic, biostratigraphic, and sequence stratigraphic correlation of reservoir intervals between the gas fields of the Sable Subbasin is complicated. This complexity also means a standard nomenclature for the sands between the fields does not exist, and each field has its own classification system (SOEP 1997).

3.6: Reservoir Sedimentology

The reservoir flow units primarily comprise progradational sand-shale cycles that range from 10-50 m thick in cleaning-upward cycles formed as a result of the delta progradation and lobe avulsion. The reservoir sands are generally located at the top of the cycles, and belong to one of three depositional facies: shelf and strand plain, delta plain, and valley-fill (SOEP 1997). The facies are distinguished based on lithology, sedimentary structures, and relationships with adjacent units. The shelf and strand plain and the delta plain facies are both interpreted as being deposited in a mixed-energy deltaic system; it was tidal and wave dominated with local fluvial influences. The valley fill facies are interpreted as being deposited in valley systems that incised into the underlying

delta sediments; valley-fill facies sediments were deposited in tide-dominated estuarine conditions (SOEP 1997).

3.7: Field Descriptions

This section gives a brief summary of the two developed Commercial Discoveries (Venture and South Venture fields) and three undeveloped Significant Discoveries (Arcadia, Citnalta, and Uniacke fields) that form the focus of this thesis (Figure 3.5).

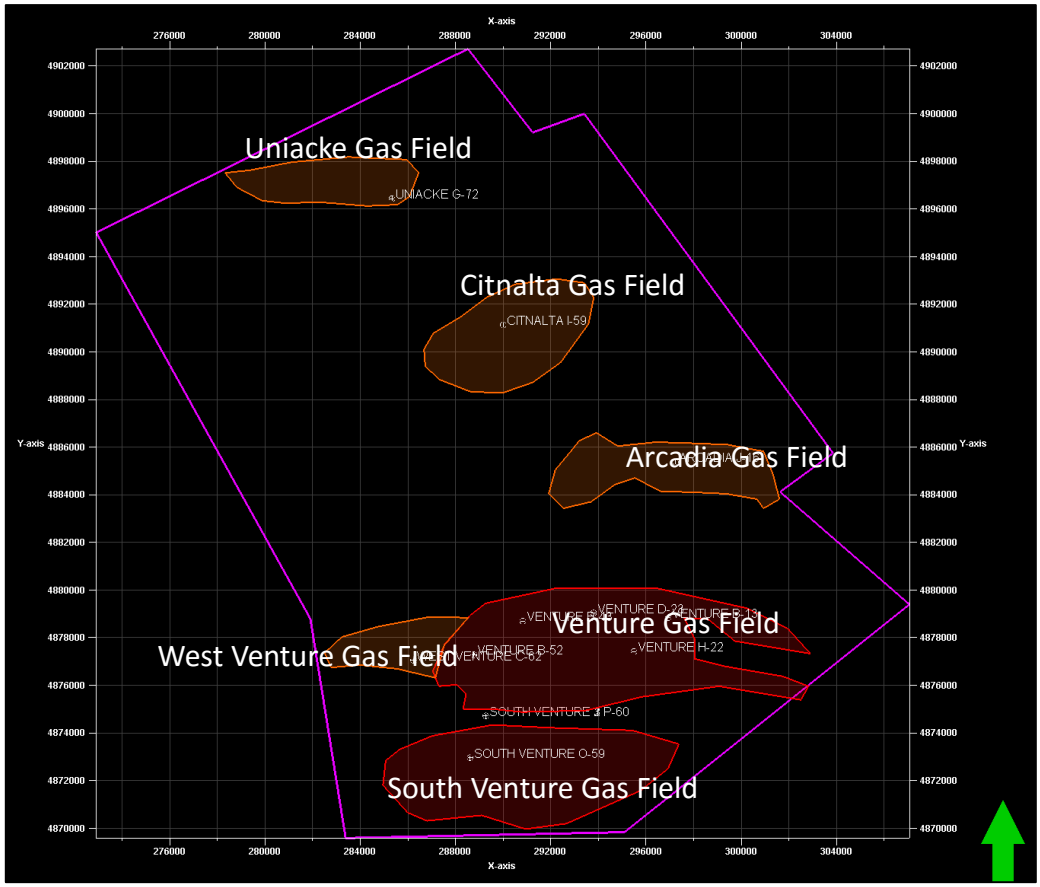

Figure 3.5: Location of the gas fields within the model area (purple outline). Note that the developed fields (Venture and South Venture) are indicated in red, while the undeveloped fields (Uniacke, Citnalta, Arcadia, and West Venture) are indicated in orange.

3.7.1: Venture Field

The Venture structure is a rollover anticline located on the hanging wall of an east-west trending listric growth fault. The anticline structure is approximately 12 km long and 3 km wide, with two crests and associated saddle (SOEP 1997). The discovery well for this

field was Venture D-23, drilled in 1979 on the Venture structure crest with gas discovered in multiple sandstone horizons, both hydropressured and excess pressured. Following the discovery well, four more wells were drilled to delineate the discovery (Venture B-13, B-43, B-52, and H-22). The delineation wells were drilled deeper than the discovery well, and successfully confirmed the presence of deeper (excess pressured) gas. The reservoir horizons of the field are continuous and can be correlated through all of the wells.

The Venture Field reservoir sands are Late Jurassic to Early Cretaceous, and are stratigraphically within the Mic Mac and lower Missisauga formations respectively. The upper reservoir horizons are hydropressured, while the deeper reservoir horizons are excess pressured. The reservoir sandstones are stacked alternating sandstones, shales, and limestones. The limestones encountered in all wells are laterally extensive (flooding surfaces), and are the most useful seismic markers to delineate the fields and individual sand pools.

3.7.2: South Venture Field

The discovery well for this field was South Venture O-59 (1982), which was drilled on a low relief rollover anticline on the hanging wall of a bounding east-west trending growth fault. Gas accumulations were encountered in stacked sandstone horizons that were hydropressured and excess pressured. The South Venture structure is approximately 8 km long and 3 km wide, and is bounded to the north by the Venture Field (SOEP 1997).

The South Venture reservoir sands are also Late Jurassic to Early Cretaceous, and are assigned to the Mic Mac and lower Missisauga formations. The sandstone reservoirs are interbedded with shales, siltstones, and limestones.

3.7.3: Arcadia Field

The Arcadia Field was discovered by the Arcadia J-16 well in 1983 that tested a large rollover anticline structure on the hanging wall of a growth fault. There were six gas-bearing excess pressured reservoir sands identified, and all are within the Mic Mac Formation (Smith et al. 2014; SOEP 1997). The sands are equivalent to the Venture field to the south, although correlations can be challenging across the border faults. The reservoir sands comprise stacked deltaic and shoreface sand sequences that interfinger

with prodelta and marine shales, and intermittent limestones (Smith et al. 2014). The shales and limestones serve as top seals.

3.7.4: Citnalta Field

The Citnalta Field was discovered in 1974 with the Citnalta I-59 well that drilled a large, salt-cored rollover anticline on the hanging wall of a north-bounding fault (Smith et al. 2014; SOEP 1997). Five gas-bearing accumulations were encountered, and are stratigraphically located within the Early Cretaceous to Late Jurassic lower Missisauga and Late Jurassic upper Mic Mac formations respectively (Smith et al. 2014). Unlike the Arcadia Field, the gas reservoirs of the Citnalta Field are hydrostatically pressured. The reservoirs sands comprise deltaic and shoreface sands capped with prodelta and marine shales that act as seals.

3.7.5: Uniacke Field

The Uniacke Field was discovered in 1983 with the Uniacke G-72 well, which was drilled on a rollover anticline on the hanging wall of a growth fault (Smith et al. 2014). The reservoir horizons are stratigraphically within the Late Jurassic Mic Mac Formation. The reservoirs of the Uniacke Field are highly excess pressured and comprise sequences of interfingred deltaic, strandplain, and shoreface sands with prodelta and marine shales (SOEP 1997).

3.7.6: West Venture Field

The West Venture Field was discovered in 1984 with the deviated West Venture C-62 well. The well was drilled on a rollover anticline immediately west of the Venture Field and shares the same north-bounding fault (Smith et al. 2014). The reservoir sands of the West Venture Field are lateral equivalents of the Venture field sands to the east, in the lower Missisauga Formation and are all excess pressured. The reservoir-seal pairs comprise deltaic and strandplain cycles within prodelta and marine shales.

Chapter 4: Datasets & Background

4.1: Datasets

4.1.1: Well Data

A total of 27 wells were used for this study, with an emphasis first on the exploration wells then the production wells (Appendix A). The well logs were provided by Divestco as digital .LAS files with multiple logging runs spliced together. Deviation and checkshot surveys were acquired from Natural Resources Canada online BASIN Database, and incorporated with the .LAS files. The lithology data was donated from CanStrat, and also added to the project. The V_{sh} (Volume of Shale) log used for a calculation-based lithology log was provided by committee member Mr. Bill Richards, and was not calculated as a part of this project.

4.1.2: Pressure Data

Many of the wells had pressure measurements collected during drilling or before production to determine if gas accumulations were commercially viable. The pressure data is available in the well history reports for each well archived by the CNSOPB, but has been digitized and made available on the BASIN Database where it was downloaded from for this project. A detailed table is available in Appendix B.

4.1.3: Seismic Data

The ExxonMobil MegaMerge 3D seismic volume was used to determine the reservoir connectivity, and excess pressure dissipation and distribution in the study area. The MegaMerge 3D seismic volume is a combination of multiple varying vintage and operator 3D surveys processed and merged to form one large survey. The volume was donated to Dalhousie University by ExxonMobil post-processing, therefore the raw data was not available for analysis or to determine the effect of processing.

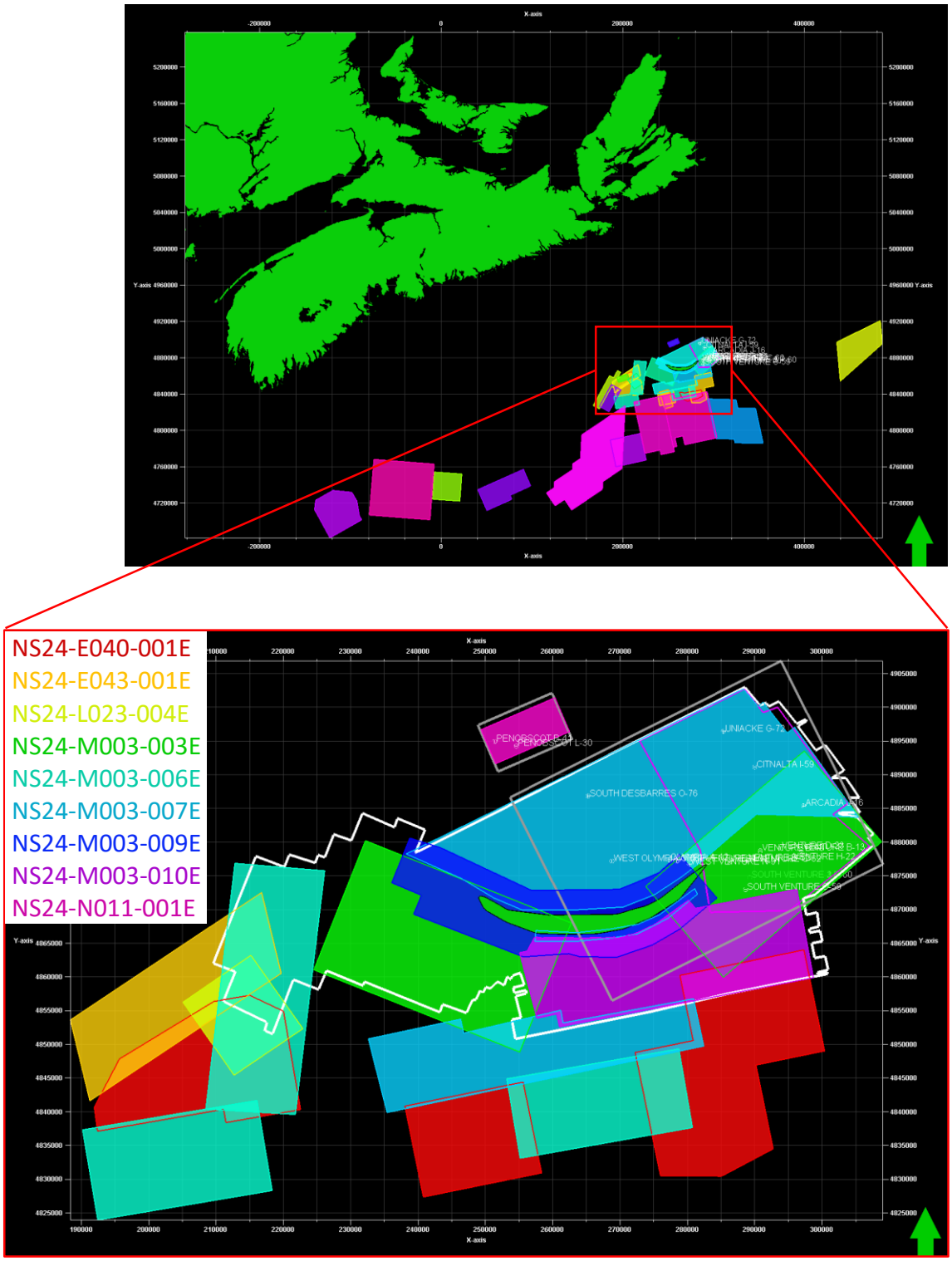

Figure 4.1: (Top) 3D seismic surveys on the Scotian Margin - 23 total. (Bottom) 9 3D seismic surveys occur within the 3D Megamerge area (white outline), of which 5 are within the study area (grey outline), and 3 are within the model area (purple outline). Colour coded text designates the seismic program number as archived by the CNSOPB.

4.2: Seismic Interpretation Background

4.2.1: Reflection Seismology

Reflection seismology is a geophysical exploration technique, and uses the principles of seismology to estimate subsurface properties from reflected seismic waves. Seismic waves are mechanical disturbances that travel through the subsurface at a velocity controlled by the acoustic impedance (I) of the medium. Acoustic impedance is defined by the velocity and density of a rock (Burger et al. 2006) (Equation 4.1).

$$I = v \cdot \rho$$

Equation 4.1: Acoustic impedance (I) is a product of velocity (v) and rock density (ρ) (Burger et al. 2006).

When the seismic wave encounters an interface between materials that have different acoustic impedances, part of the wave energy will refract through and part will reflect off the interface – producing a seismic reflection (Figure 4.2). The strength of the impedance contrast is related to the difference in the materials at the interface, and the larger the contrast - the stronger the seismic reflection (reflection coefficient).

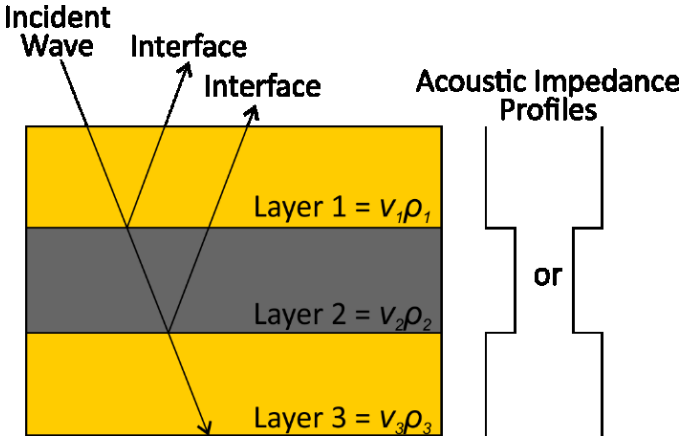

Figure 4.2: Diagram demonstrating the variances in acoustic impedance as seismic waves encounter a stratigraphic boundary (Christians 2015).

The reflection coefficient is determined by the impedance contrast (Equation 4.2).

$$R = \frac{\rho_2 v_2 - \rho_1 v_1}{\rho_2 v_2 + \rho_1 v_1}$$

Equation 4.2: Reflection coefficient (R) equation where $\rho_1 v_1$ and $\rho_2 v_2$ are the acoustic impedance for layers 1 and 2 respectively (Burger et al. 2006).

4.2.2: Seismic Resolution

Resolution is the ability to distinguish between objects, and in seismic is considered in both the vertical and lateral directions. If a unit is not sufficiently thick or laterally extensive then it will be difficult (or impossible) to visualize the unit as a clear reflection. Seismic depth is measured in milliseconds two-way travel time (TWT), which is the length of time the sound wave takes to travel from the source (at surface) to the interface and return to a receiver. As the depth increases, the frequency of the sound decreases due to attenuation and the velocity and wavelength increase. This means that the resolution will decrease with increased depth. Seismic resolution is a function of the dominant wavelength, which is in turn a result of the relationship between velocity and frequency (Equation 4.3).

$$\lambda = \frac{v}{f}$$

Equation 4.3: Dominant wavelength (λ) is a result of dividing the velocity (v) by the frequency (f) (Burger et al. 2006).

4.2.2.1: Vertical Resolution

Vertical resolution refers to how far apart two interfaces must be in order to distinguish separate reflections from them, or how thick a unit must be to allow individual reflections from the top and bottom (Sheriff 1992). In order for two closely spaced reflective interfaces to be discriminated, the minimum thickness is equal to ¼ of the dominant wavelength (tuning thickness) (Equation 4.4).

$$\text{Vertical Resolution} = \frac{\lambda}{4}$$

Equation 4.4: Vertical Resolution is a result of the dominant wavelength (λ) divided by 4 (Sheriff 1992).

Seismic velocity in sedimentary rocks generally ranges from 2000 m/s to 5000 m/s, and increases with depth due to compaction. Standard seismic frequencies used in data acquisition range from 5 – 100 Hz, and higher frequencies with shorter wavelengths provide better resolution (vertical and lateral). In industry, deep acquisition is a priority therefore frequencies generally range from 20 – 50 Hz, with dominant wavelengths from

40 – 250 m. Based on Equation 5.4, this would give a vertical seismic resolution of 10 – 62.5 m

4.2.2.2: Horizontal Resolution

The horizontal resolution is described by the Fresnel zone, which is a frequency and range dependent area of a reflector from which most of the energy of a reflection is returned and arrival times vary by less than half a period from the first acoustic signal arrival (Figure 4.3) (Equation 4.5) (Mondol 2010). In 3D seismic, the Fresnel zone is circular, and any features that extend beyond the zone will be visible.

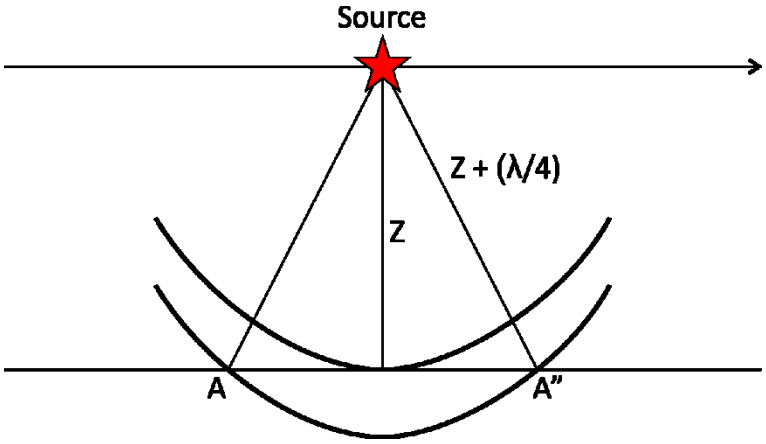

Figure 4.3: Fresnel zone in 3D seismic, with diameter A-A”, depth to interface (Z) and wavelength (λ). The size of the Fresnel zone determines the minimum dimension features that can be resolved (Mondol 2010).

$$\text{Fresnel Zone} = v\left(\frac{T}{f}\right)^{0.5}$$

Equation 4.5: The size of the Fresnel zone is determined by the velocity (v), depth in time (T), and frequency (f) (Mondol 2010).

The size of the Fresnel zone can be reduced through migration of the seismic data to focus the energy spread – reflections that were misaligned due to dip are rearranged and reflection patterns from points and edges are removed. This will reduce the Fresnel zone to approximately ¼ of the dominant wavelength (Equation 4.6).

$$\text{Fresnel Zone} = \frac{v}{4f}$$

Equation 4.6: The size of the Fresnel zone after migration (Mondol 2010).

4.2.3: Seismic Stratigraphy

Seismic stratigraphy is the "study of stratigraphy and depositional facies as interpreted from seismic data" (Mitchum et al. 1977). Reflection terminations (onlap, downlap, toplap, and erosional truncation) define seismic sequence boundaries (Figure 4.4) (Mitchum et al. 1977). A seismic sequence is a relatively conformable succession bounded by unconformities or sequence boundaries (Catuneanu et al. 2009). Sequence stratigraphy is the study a succession of strata deposited during a full cycle of change in accommodation space or sediment supply (Catuneanu et al. 2009). Seismic facies are recognized based on their reflection configuration (geometry), strength, and continuity (Figure 4.5). The identification and interpretation of seismic reflections, and their relationship to interpreted lithologies and facies identified in wells, is critical for recognizing depositional environments.

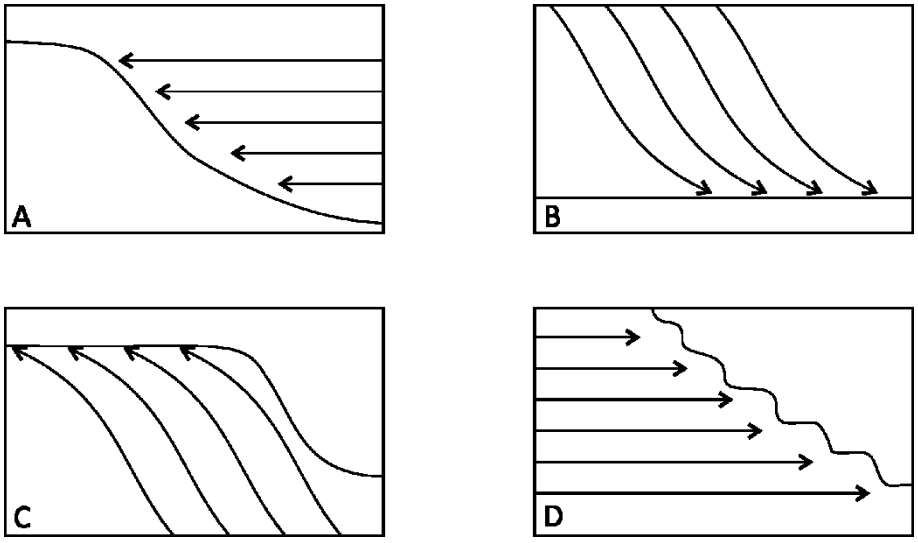

Figure 4.4: Reflection termination patterns (A) onlap, (B) downlap, (C) toplap, (D) erosional truncation (Mitchum et al. 1977).

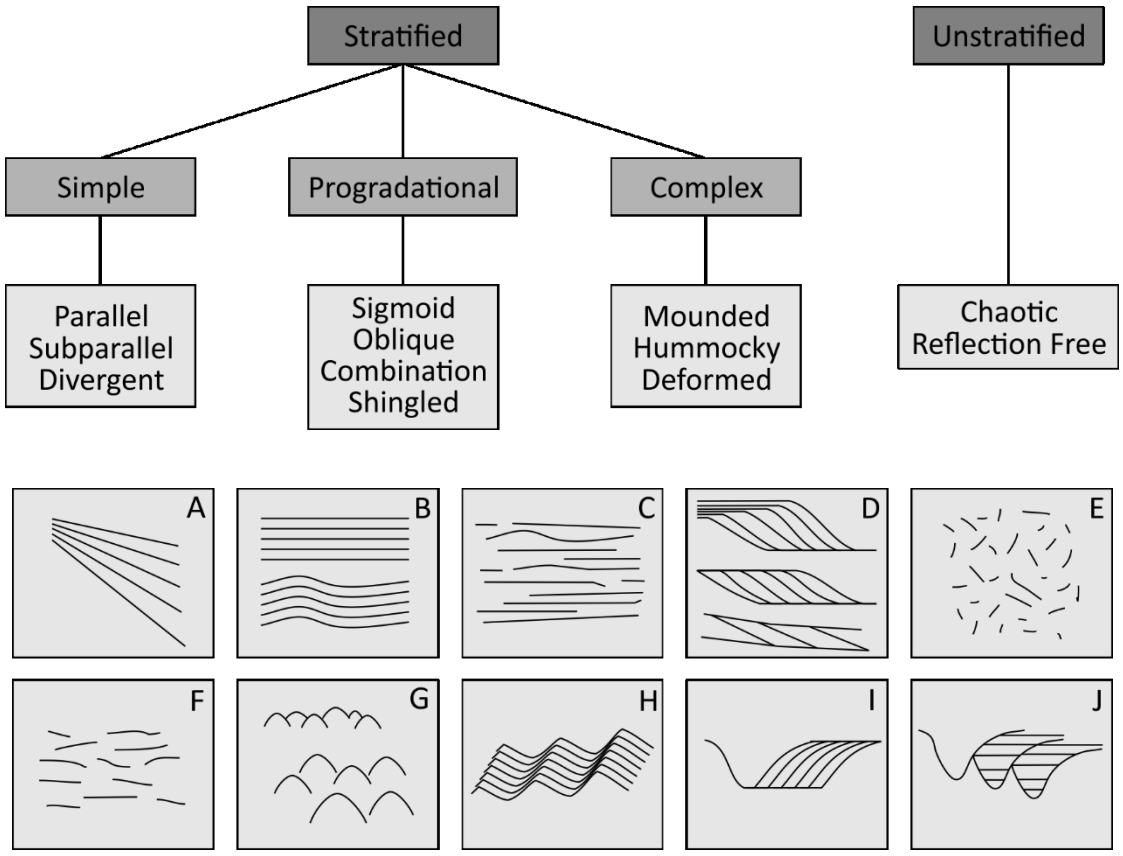

Figure 4.5: Reflection configurations (A) divergent, (B) concordant, (C) sub-parallel, (D) progradational, (E) chaotic, (F) hummocky, (G) hyperbolic, (H) climbing waves, (I) accretionary channel, (J) cut-and-fill channel (Mitchum et al. 1977).

4.2.4: 3D Seismic Surveys

3D seismic surveys began in the mid-1970's as an advancement from 2D seismic surveys. In a 3D marine survey, data are acquired by survey vessels that traverse the designated area of the ocean following a series of parallel lines. The shooting direction is the *inline* track, and the perpendicular direction is the *crossline* direction; when combined these form a grid, allowing the data to form a 3D volume (Mondol 2010). The vessels trail airgun arrays and hydrophone streams. The airgun array comprises airguns that fire simultaneously every 5-10 seconds; the hydrophone steams comprise a group of hydrophones connected in series to eliminate surface noise and provide one seismic trace.

In modern 3D seismic surveys, more than 100,000 traces may be recorded for a single seismic channel. Traces are gathered into common-cell gather - bins (x and y values

are shot point distances, z value is sample) with an assigned trace value (Yilmaz 2008). Bins allow data to be viewed in any orientation the user desires as vertical transects: inline, crossline, or composite line (a line of any direction determined by the user – not constrained to the inline or crossline). 3D surveys are an expansion on 2D surveys, as they allow the user to view data on the z-plane, which is the horizontal plane (closer to and further away from the user location).

4.2.5: Methods for Viewing 3D Seismic Data

3D seismic surveys comprise a volume (or cube) of data, therefore various methods allow the interpreter to "slice" through the volume and extract (or plot) information. The most common methods are vertical seismic sections and horizontal time slices. Vertical seismic sections can be viewed in any direction (inline, crossline, or composite), and provide a cross section-type view. These sections are used to determine morphology and seismic facies of the volume. Features that are too subtle to identify in vertical sections are often better identified in horizontal time slices, which are parallel to TWT (or depth if the volume has been converted).

4.2.6: Seismic Attributes

Seismic attributes are derived from seismic measurements and include: time, amplitude, attenuation, and frequency. The attributes can be extracted along a horizon or within a defined polygon (2D area). Reflection amplitude is a measure of the strength and polarity of a reflection, and depends on the acoustic impedance contrasts between adjacent lithological units. Amplitude is a non-unique attribute; therefore, it is important to remember that different geologic conditions can generate similar amplitudes. In multi-channel seismic data, amplitude is most strongly influenced by contrasts in porosity, bed thickness, and fluid content (Mitchum et al. 1977). Reflection magnitude is similar to amplitude but does not have the associated phase information - this means that it is the absolute value of amplitude.

4.3: Well Log Interpretation Background

4.3.1: Gamma Ray

Gamma ray logging tools measure the (natural) radioactivity of rocks in the borehole, and intensity is given in American Petroleum Institute units (API) (Asquith and Krygowski 2004). Normally shales will have higher gamma emissions than sandstones or limestones due to their higher proportion of clay minerals that have an attraction for elements with radioactive isotopes. For this reason, the gamma ray log can be (and is often) used to distinguish shale from non-shale, and can be used to calculate the volume of shale (V_{sh}).

In this study, gamma ray logs were used for correlation and interpretation purposes. Generally, the shape of the gamma ray curve can be used to identify grain-size trends, with funnel-shaped curves indicating coarsening upwards while bell-shaped curves indicating fining-upwards. In turn, these trends can be used to infer depositional environments (Shanmugan et al. 1995). Care should be taken with this approach as a high fraction of feldspars or micas in sands can increase the gamma emissions (due to their potassium content) than a more siliceous sand.

4.3.2: Density

Density logging tools measure the bulk density of the combined matrix and pore-filling fluids of the borehole rocks. The tools bombard the formation at the wellbore wall with gamma rays from a radioactive source (typically cesium-137) and then measures the attenuation of the gamma rays as they are received at the detectors (Asquith and Krygowski 2004). The amount of attenuation (reduced number of gamma rays returned to the detectors relative to the amount originating at the source) is directly related to the electron density of the formation (the combination of matrix and pore-filling fluids), which is in turn a close approximation for the actual formation density. The greater the electron density of the formation, the greater the attenuation of the gamma rays; therefore, denser formations will have greater attenuation and less dense formation will have smaller attenuation (Asquith and Krygowski 2004). In normal pressured regimes, the density of shale increases with depth (compaction largely associated with pore water loss)

so the density log will measure progressively higher shale densities with depth. However, in excess pressured regimes, increased pore fluid retention can reduce the density of shales (from what they would be in a normal pressured regime) causing the tool to measure lower density values – this is called a reversal. In this study, continuous density profiles were one of two main inputs used to generate synthetic seismograms.

4.3.3: Resistivity

Resistivity logging tools measure the electrical resistivity of formations in the borehole, and measurements are expressed in ohm/m^2/m. Electrical resistivity is the inverse of conductivity and measures the ability of a rock to impede electrical current flow. The total resistivity of a rock (matrix and pore fluid) is determined dominantly by the resistivity of the pore fluids and the formation factor (Asquith and Krygowski 2004). This is because contributions to a combined total resistivity reading are largely those of the less-resistive (more conductive) pore fluids – when all available components are added together on a parallel basis.

The formation factor is a value representing the concentration of the pores and their connectivity. Rocks that are porous but with low permeability will have a higher formation factor because the electrical current flow will be impeded, contributing to higher total rock resistivity. The salinity of the fluid in the pore space has the largest impact on the total resistivity – highly saline waters will have a lower resistivity as electrical currents are easily transmitted. Hydrocarbons are natural insulators (low in ion content) and will have higher resistivity as electrical currents are not readily transmitted. In this study, resistivity logs were used for correlations and to identify fluid contacts.

4.3.4: Sonic

Sonic (also called acoustic) logging tools measure the acoustic interval transit time (in microseconds per foot or microseconds per meter) or *slowness* of rock in the borehole. The sonic log measure the length of time required for a sound pulse to travel from a source at one end of a sonde, through the borehole and formation, and reach the receiver at the other end of the sonde (Asquith and Krygowski 2004). Interval transit time is the inverse of the velocity, therefore the greater the interval transit time, the slower the formation

velocity. Interval transit time is the sum time a sound wave spends in the matrix and fluid of a rock, hence it is related to the porosity of the rock. As porosity is increased, the velocity decreases and interval transit time increases; this is because the sound wave is spending a greater amount of time in fluids, which transmit acoustic signals at (usually) slower velocities than through the rock matrix. In this study, continuous sonic logs were used for correlations and as the more important of the two possible contributing log curves in the generation of synthetic seismograms.

4.3.5: Lithology

Continuous lithology logs (versus depth) used in this study were generated by Canadian Stratigraphic Services (2000) Ltd. ("CanStrat") by analyzing cuttings from wells using petrographic methods. Cuttings are particles of rock that are produced in the borehole as the drill cuts downward; the cuttings are circulated up and out of the borehole with the circulating drill mud, where they are passed through the shale shaker and samples are usually aggregated approximately every 5m of drilled section.

In the process used by CanStrat, cuttings were washed and dried, and then examined at a high level of detail (as compared to a wellsite description). Data on the following attributes were collected: major rock type and percentage, grain size, rounding and sorting of clastic grains, accessory rock types and percentages, porosity type and percentage, oil staining, fluorescence, mineral occurrence, and fossil type and percentage. This data has been digitized into .LAS files at a later time by CanStrat, and these were subsequently imported into Petrel for wells in this study. The major rock type attribute was used for correlations and interpretation.

4.3.6: Checkshot Surveys

Checkshot surveys are a type of borehole-based seismic data that are designed to measure the seismic travel time from the surface to a known depth – this provides a time-depth pair. This data allows depths along the borehole to be converted to TWT and displayed against time-based data (i.e. seismic). Well-seismic ties were established for this study using the checkshot data.

4.3.7: Synthetic Seismograms

Synthetic seismograms are used to correlate seismic data with borehole data. The velocity data of the sonic log and the density data of the density log are used to generate a synthetic seismic trace that closely approximates a trace from a seismic line that passes close to or through the location of the well in which the logs were acquired. The Petrel software computes an acoustic impedance curve from the sonic log velocities and density log data; the acoustic impedance curve is then used to compute reflection coefficients at interfaces between contrasting velocities. The reflection coefficient is convolved with a selected wavelet to produce the synthetic seismogram.

Chapter 5: Methods

The overall workflow for this study can be divided into three linked workflows:

(1) pressure workflow

(2) geocellular model workflow

(3) interpretation workflow.

The objective of these workflows are to populate a geocellular model (2) with lithologies and excess reservoir pressures (1) so the controls on excess pressure distribution can be interpreted (3). The initial hypothesis is that excess pressure in porous and permeable reservoirs, regardless of its generation mechanism(s), is controlled by the connectivity (or lack of connectivity) of those reservoirs. A 3D geocellular model that captures structural and stratigraphic architecture, lithology and pressure data can be interpreted to determine where excess pressure may be entering the system, how it moves through the system, and where it exits the system. If the model were populated with "raw" pressure data, each reservoir would show pressure increases as a function of depth rendered as gradational changes in the colour of the model (and colours that are not unique to each reservoir). The advantage of populating the model with a single number and single colour (if there is no measurement error and density is constant) is there should be no variation in each aquifer excess pressure; in practice averaging of measured values is required.

5.1: Pressure Workflow

The pressure data were downloaded for each well from Natural Resources Canada's online BASIN database and merged to form a master Excel spreadsheet for the drill stem test (DST), repeat formation test (RFT), leak off test (LOT), and well kick (WK) data (Figure 5.1) (Appendix B). Mud weight measurements were not included; although they do provide a rough upper limit on pressure, they are not a direct measurement of formation pressure. The pressure data were reviewed and poor quality data points were removed from the dataset before further analysis; poor quality data points included values that were related to unstable flow, supercharging or dry tests (no numerical criteria applied).

The pressure data were exported from Excel, and imported as a 'well point data set' into the Petrel™ project where they were plotted on a well log cross section comprising all wells. Pressure data were inspected on this cross section and by pressure-depth plots and excess pressure-depth plots in Excel to identify flow units and their bounding well tops and bases. The well tops and bases were subsequently correlated on all wells and are consistent with flow units in the BASIN database and the Sable Offshore Energy Corporation Development Plan Application (1997). Flow units are reservoir zones, sometimes comprising multiple sandstones that contain fluids on the same water or hydrocarbon pressure gradient (ie. common excess aquifer pressure) and can also be described as 'pressure compartments' or 'pressure cells'. Well tops and flow units were imported to the geocellular model as reservoir 'zones'.

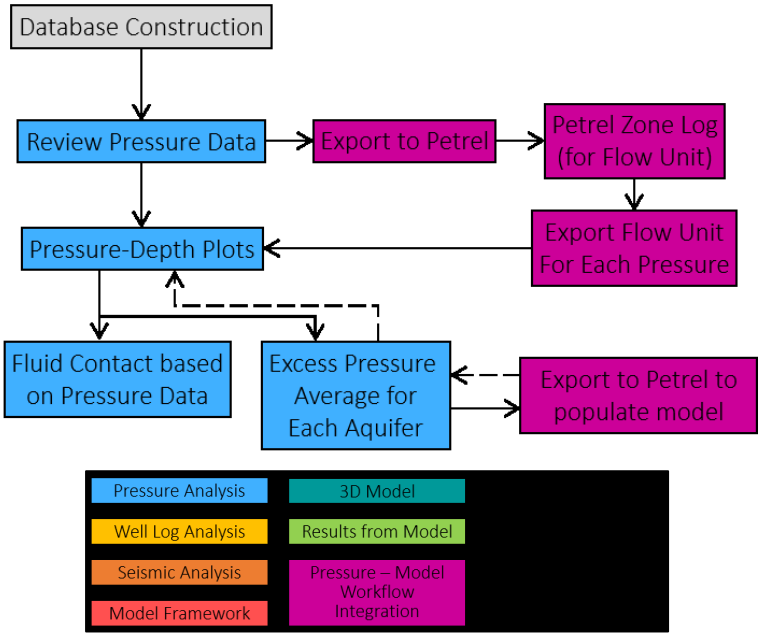

Figure 5.1: Pressure workflow summarizing processes used to integrate pressure data from wells with geocellular model. Legend for workflow in box. More detail on modelling process available in Section 5.2: and Figure 5.2.

At this point in the workflow, the aquifer excess pressure (XSP) data in Excel and the Petrel™ 'well point data set' have not been linked to stratigraphic intervals or flow units. This was subsequently achieved by generating a zone log from the well tops folder, which was then used to automatically assign a flow unit or stratigraphic attributed in the

well point data set. The excess pressure data was then exported to Excel, averaged, and imported to the geocellular model.

Excess pressure-depth plots were inspected in Excel to determine the average pressure for each flow unit in each segment (segments identified in geocellular model workflow below). Although production well data was available from ten wells (the Venture O-32 wells (7 total) and South Venture P-60 wells (3 total)), they were not included when determining pressure averages unless they were the only data available for a particular flow unit. This is because of either pressure depletion due to production or lack of reliable well surveys in wells. The excess pressure averages were exported to Petrel™ to create an excess pressure index for geometrical modelling. Average excess pressure data was used as geometrical modelling requires a single input (excess pressure value) per flow unit per segment.

5.2: Geocellular Model and Interpretation Workflow

The integrated geocellular model and interpretation workflow is in Figure 5.2:

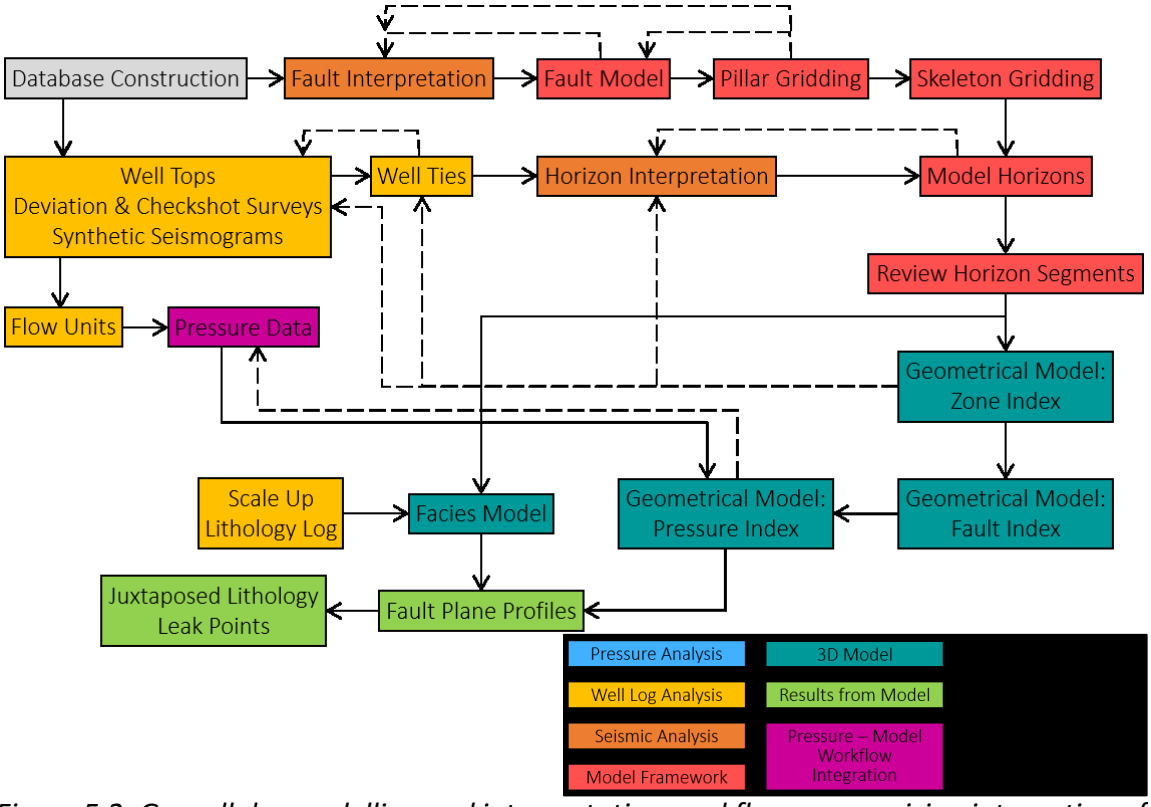

Figure 5.2: Geocellular modelling and interpretation workflow summarizing integration of well log, seismic, and pressure data to examine fault juxtapositions in the study area.

5.2.1: Well Tops and Well Ties

Initial well tops were downloaded as lithostratigraphic picks from the Natural Resources Canada's online BASIN database, and are based on work by the operators and/or the Geological Survey of Canada. Well tops from the BASIN database included main formations and members, and production sands (where available). The well tops were imported into the Petrel™ project, then updated and correlated to wells across the study area.

Deviation and checkshot data were also downloaded from the BASIN database for each well. Deviation files provided correct well paths, which was important for the well tie process and horizon interpretation on the seismic data. The wells in the study area are predominantly vertical as they are exploration wells; exceptions are the production wells; these are deviated to reach intended targets, maximize production capabilities, and minimize total development cost by drilling from central pre-established locations to reduce subsequent individual well tie-in costs. Checkshot data from the BASIN database was initially used to complete the time-to-depth conversion of the wells, however the data proved unreliable for several wells so the original checkshot data in the well reports was reviewed and digitized instead.

Synthetic seismograms were generated from the sonic log and density log. An acoustic impedance log was generated and used to compute the reflection coefficient, which was convolved with a Ricker wavelet (30 Hz) to generate the synthetic seismogram (for example well section for South Venture O-59 available in Figure 5.3).

The checkshot data were used to display the (depth-based) wells on the (time-based) seismic sections. The well tops and synthetic seismograms were displayed on the inline and crossline sections. The synthetic seismogram was compared to the underlying seismic data to assess the goodness of fit - if the well tops plotted in the correct location (seismic reflector interpreted as the matching horizon) then the well was left as is. If the well tops plotted incorrectly (seismic reflector not interpreted as the matching horizon) then the checkshot data were reviewed and adjusted to create a better fit.

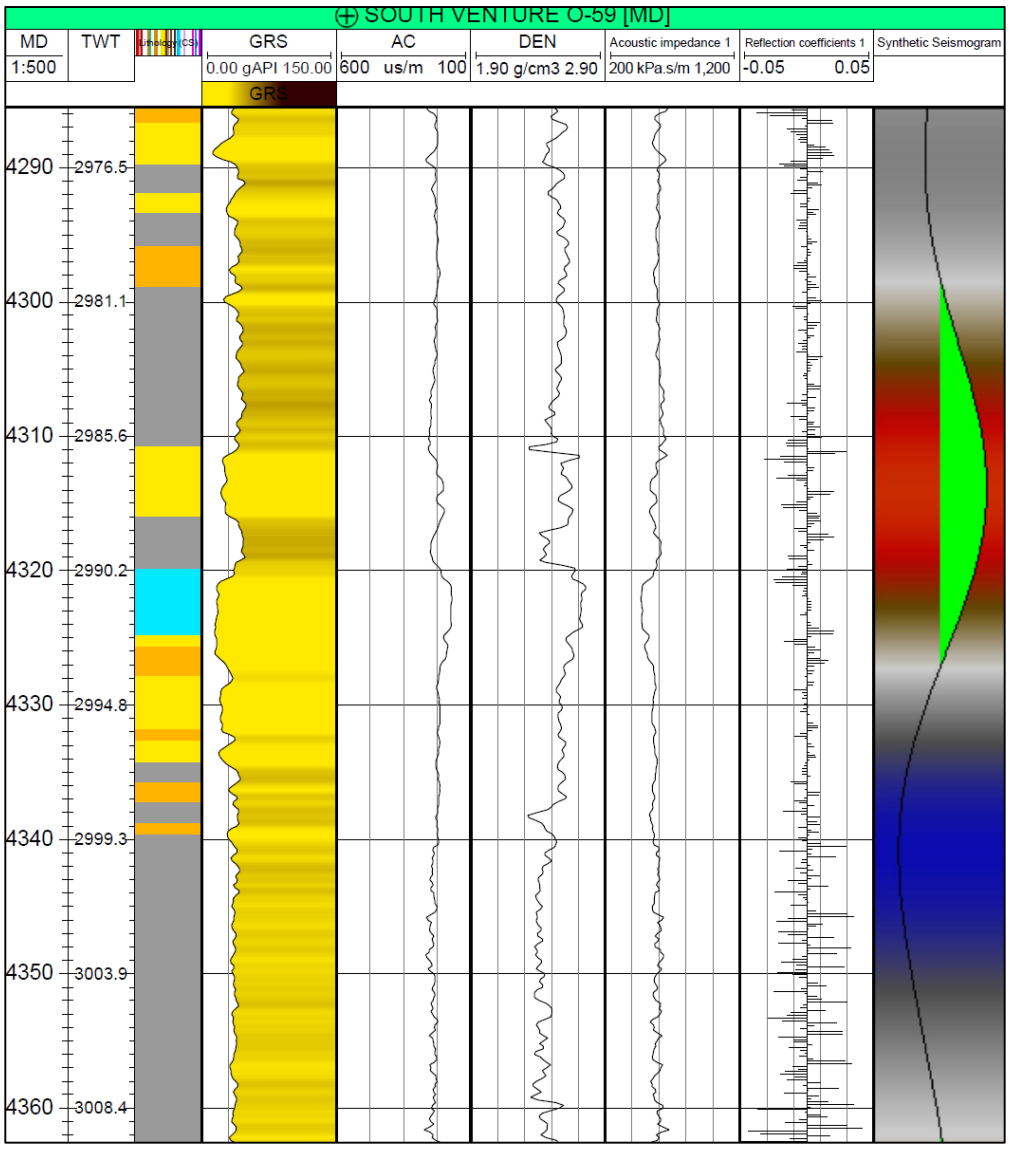

Figure 5.3: Synthetic seismogram workflow for South Venture O-59 with measured depth (track 1), two-way travel time (track 2), lithology based on CanStrat petrographic analysis (track 3), gamma ray log (track 4), sonic / acoustic log (track 5), density log (track 6), acoustic impedance (track 7), reflection coefficient (track 8), and synthetic seismogram with bitmap and wiggle trace (track 8).

5.2.2: Flow Units

Production sand tops were provided from the BASIN Database for several of the wells. These were then reviewed and adjusted where necessary to improve their fit with the well log data.

The flow units were then correlated to wells that did not contain the units. To better constrain the flow units; the tops of the underlying shale units that separate the sands were correlated. This allowed the pressure data for the different flow units to be identified in the higher permeable units during geometrical modelling.

5.2.3: Horizon Interpretation

Horizon interpretation was completed on vertical seismic sections using a combination of manual picking, autotracking (automatically tracks a horizon along a seismic profile in 2D), and autopicking (automatically tracks a horizon along a given area in 3D). The horizons were identified via checkshot corrected synthetic seismograms. Horizon interpretation was completed after fault interpretation to enable precise, accurate horizon terminations at fault planes. Twenty seismic markers were correlated from the Middle Jurassic to Upper Cretaceous succession in the study area (youngest to oldest):

Table 5.1: Seismic markers correlated in study area with estimated geological age based on the Scotian Basin lithostratigraphic chart and stratigraphic relationships.

Horizon Interpreted	Horizon Name	Geological Age
Wyandot Formation	WYA	Late Cretaceous
Petrel Member	PET	Late Cretaceous
Naskapi Member	NSK	Early Cretaceous
O Marker	OMK	Early Cretaceous
South Venture Sand 0	SV0	Early Cretaceous
South Venture Sand 6	SV6	Early Cretaceous
Venture Sand 2 Canyon Base	SST2b	Late Jurassic
Venture Sand 2	SST2	Late Jurassic
3 Limestone	3 LST	Late Jurassic
6 Limestone	6 LST	Late Jurassic
9 Limestone	9 LST	Late Jurassic
Y Limestone	Y LST	Late Jurassic
Z Limestone	Z LST	Late Jurassic
Citnalta Top Carbonate Envelope	CIT TCE	Late Jurassic
Citnalta Bottom Carbonate Envelope	CIT BCE	Late Jurassic
Penobscot Top Carbonate Envelope	PEN TCE	Late Jurassic
Penobscot Bottom Carbonate Envelope	PEN BCE	Late Jurassic

The limestone horizons are laterally continuous, and are interpreted as marine flooding surfaces. They were correlated first across the study area, based on the work of Wade and MacLean (1990) (Figure 5.4). These were then used to establish reservoir correlations between the fields. The limestones were interpreted as having downslope tongues coming off the main reef, which have edges that seem to have influenced where listric faulting occurred - potentially due to lithological heterogeneity.

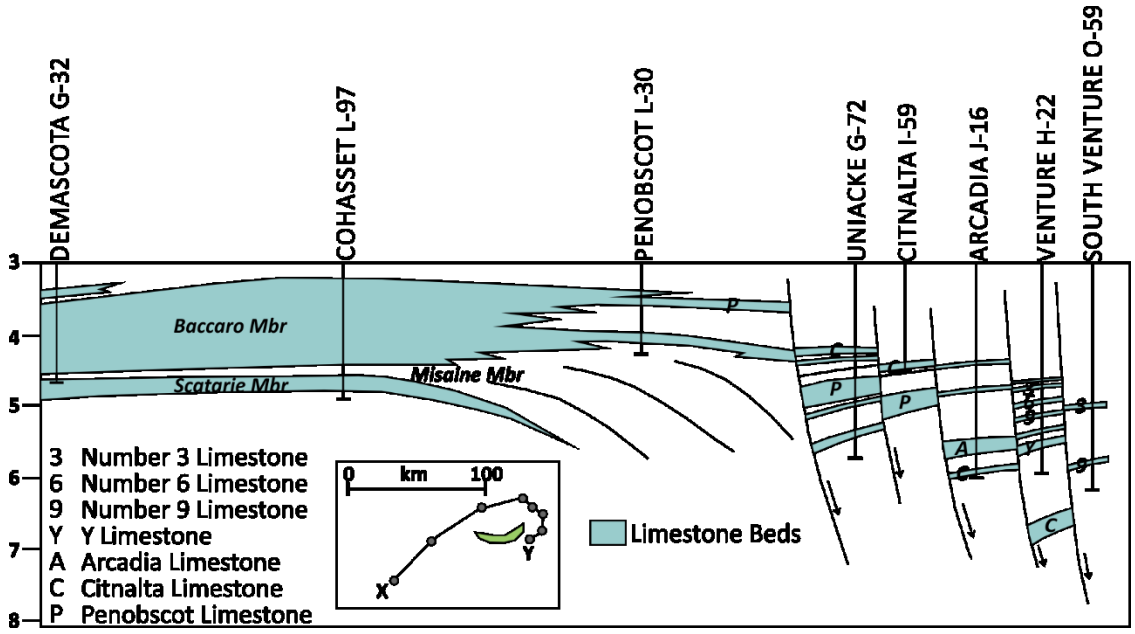

Figure 5.4: Diagram illustrating the stratigraphic discontinuity of the Abenaki Formation due to listric faulting near Sable Island (Wade and MacLean 1990).

The autotracking process required activating the desired seismic horizon in the input window and choosing the 2D autotracking mode in the seismic interpretation process tool. In the seismic interpretation window, a seed point was generated by clicking on the given seismic reflection where the horizon was interpreted. The software traced the horizon for as far as possible within that seismic interpretation window. Seed confidence was controlled by the interpreter, and is independent for each horizon; for this study confidence was kept between 0.6 – 0.8 (60 – 80 %). Autotracked horizons were used to generate horizon interpretation grids (every tenth inline and crossline), and were extensively reviewed, compared, and corrected to ensure accuracy.

Autopicking was used to fill in the autotracked interpretation grid, which served as the seed points for the autotracking. The autotracking process involves activating the

desired seismic horizon in the input window and choosing the 3D autotracking mode in the seismic interpretation process tool. Seed confidence is controlled by the interpreter, and is independent for each horizon; for this study confidence was kept between 0.6 – 0.8 (60 – 80 %). Autotracked horizons were used to generate horizon surfaces, and were extensively reviewed, compared, and corrected to ensure accuracy.

5.2.4: Fault Interpretation

The faults were interpreted on the seismic data by identification of vertical offset sub-horizontal seismic reflections in inline and crossline sections (Figure 5.5).

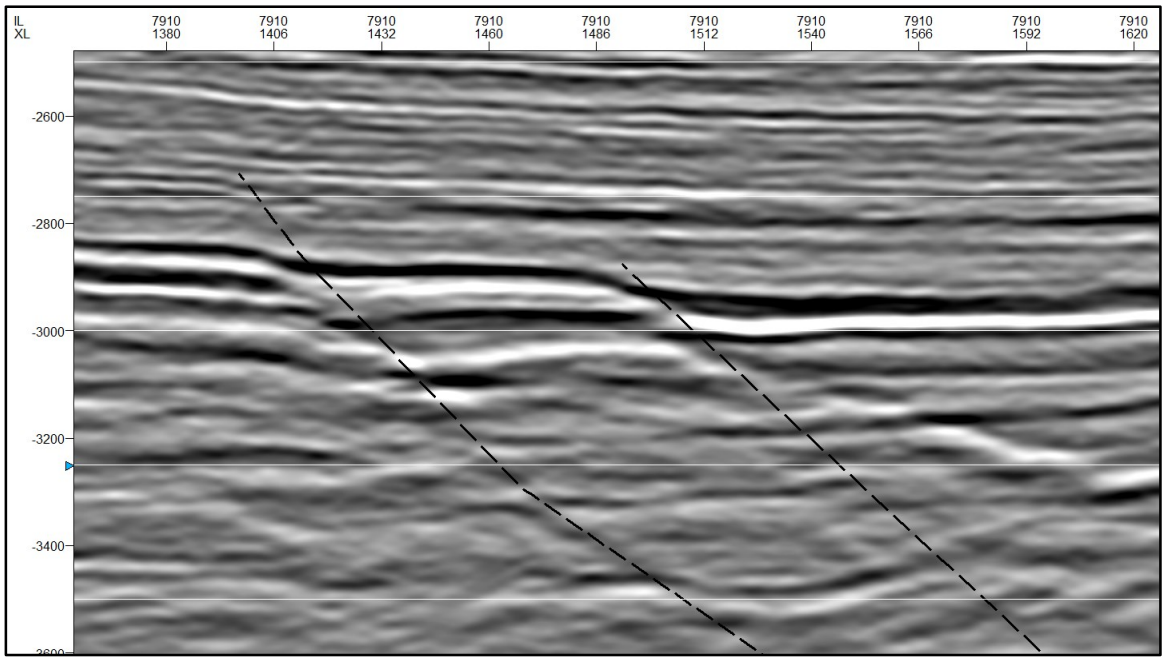

Figure 5.5: Seismic section demonstrating the vertical offset of sub-horizontal seismic reflections that were used to identify and map faults within the study area Vertical scale in ms TWT, with 5X vertical exaggeration.

Within the study area, 83 faults were interpreted, of which 72 were within the model boundary polygon and were used to generate the fault model. Of the 11 faults eliminated from the model, 9 were outside the boundary and 2 were within but were antithetic faults (see next section for further explanation).

5.2.5: Fault Model

The fault model boundary was defined to include the Uniacke, Citnalta, Arcadia, Venture, and South Venture fields (Figure 5.6). The fault model and pillar grid tools were

used to convert the fault interpretations into the pillars that define the 3D IJK grid the model is based on. An IJK 3D grid was generated (as opposed to a XYZ, which is based on the Cartesian system) and then the fault interpretations were converted into the grid using the fault model tool. Once the fault model was created, the faults were extended to a top limit defined by the O Marker horizon and bottom limit of -4500 ms by cutting or extending the pillars. After this, the faults were individually reviewed in a 3D window to make corrections where:

(a) faults crossed - will cause problems with later gridding processes
(b) faults were distorted - pillars have been deformed during transformation into the fault model
(c) antithetic faults - because of software limitations, will cause problems with the later gridding process.

Faults in (a) and (b) above had the pillar structures corrected, reviewed in a 2D interpretation window to ensure a good fit to the seismic data, and re-input into the fault model (Figure 5.7); faults in category (c) were removed. Trends were added to the end of selected faults within the fault model to isolate segments (different fields). These segments allow for the creation of Fault Plane Profiles (FPPs) to compare fault juxtaposed permeable units.

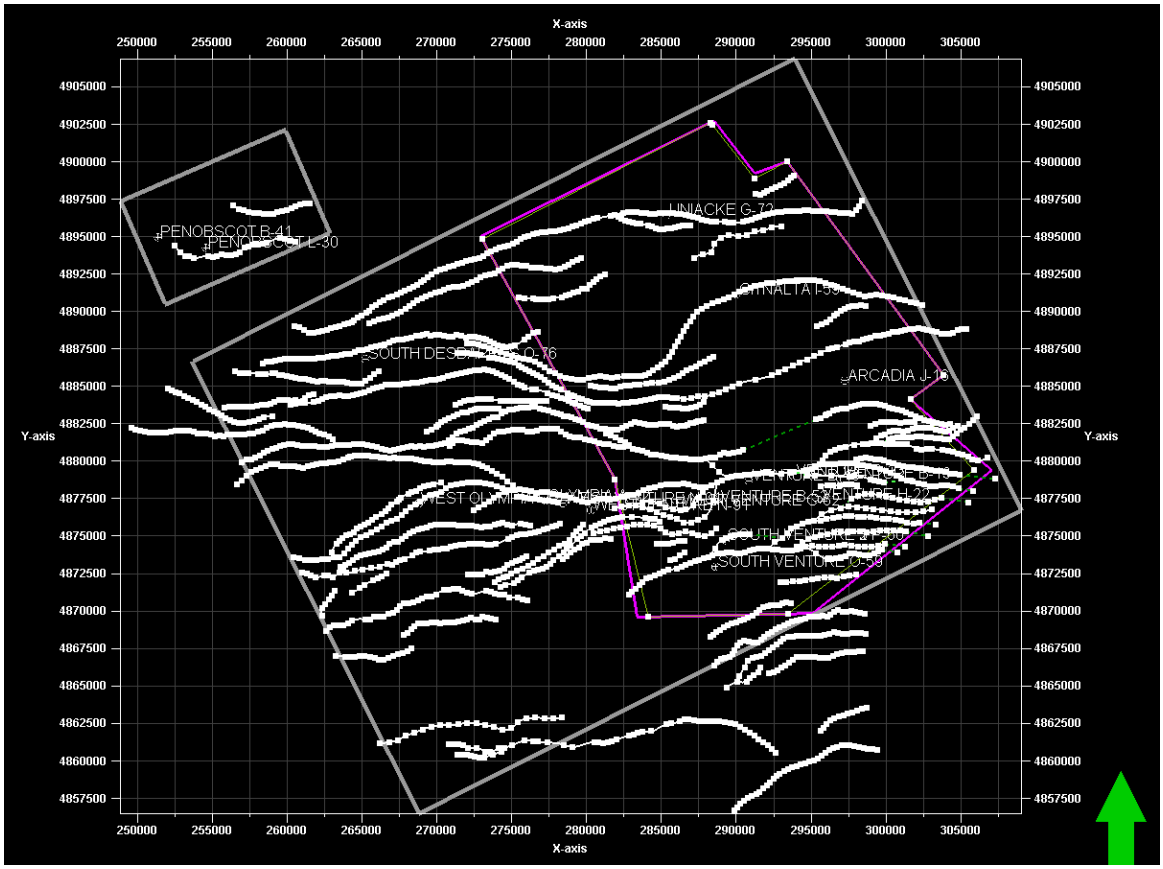

Figure 5.6: Faults (white) modelled within the study area (grey outline) and model area (purple outline). Also shown are trend lines (green dashed lines) used to isolate segments for later fault plane profiling.

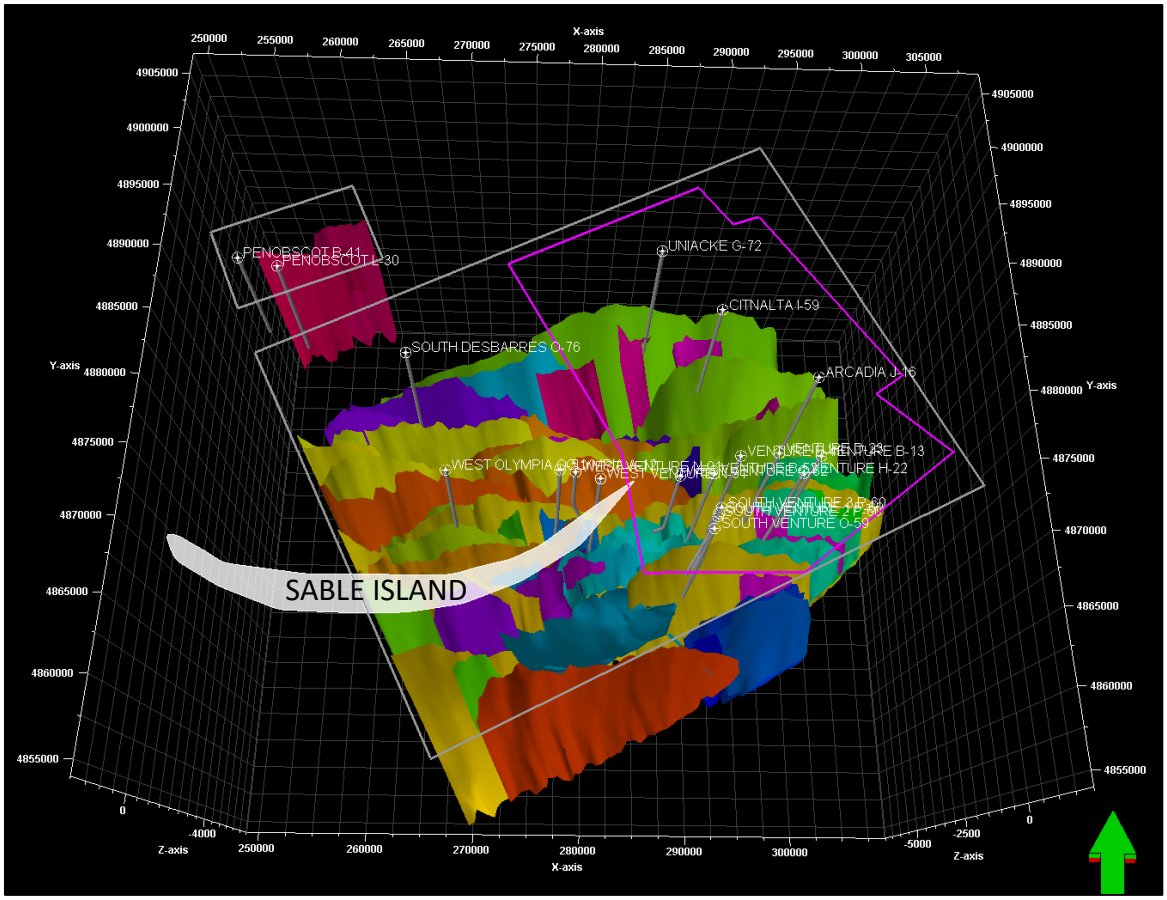

Figure 5.7: 3D fault interpretation model within the study area (grey outline) and model area (purple outline) with labelled wells and corresponding well trajectories. Faults generally trend southwest-northeast to west-east. XY grid for scale is based on UTM zone 21 and is in meters. Z axis is time-based and units are ms TWT. 5X vertical exaggeration has been applied. View is from south to north.

5.2.6: Pillar Gridding

Once the fault model was constructed and reviewed, pillar gridding was completed. Pillar gridding is the process of using the faults in the fault model as the basis for generating the 3D grid for the remaining modelling. The gridding process first created a 2D skeleton grid (no z-values) between the mid-points of key pillars; the top and bottom grids were then generated from the top and bottom points of the key pillars. The geocellular grid is further distorted from a Cartesian grid when horizons and zones are put in. This creates cells whose grid boundaries are defined by faults and horizons so that fluid flow calculations are accurate and efficient - with a Cartesian system, the cells would have been prohibitively small and computationally intensive.

Problems in the fault model that were not visible at the fault model stage were identified and corrected, then the pillar gridding was repeated; this process was completed iteratively until a pillar grid of good quality and high cell orthogonality was generated.

5.2.7: Horizons Modelling

The "make horizons" process was completed following pillar gridding by inputting the seismic interpretations for each horizon. Each horizon type (conformable, erosional, or base) was assigned before the horizons were created (Table 5.2). The horizons were modelled across all the segments.

Table 5.2: Input summary for horizon modelling

Horizon Code	Horizon	Horizon Type
OMK	O Marker	Conformable
SV0	South Venture 0 Sand	Conformable
SV6	South Venture 6 Sand	Conformable
SST2 Canyon Top	Sandstone 2 Canyon Top	Erosional
SST2 Canyon Base	Sandstone 2 Canyon Base	Erosional
3 LST	3 Limestone	Conformable
6 LST	6 Limestone	Conformable
9 LST	9 Limestone	Conformable
9LSTb	9 Limestone Base	Erosional
Y LST	Y Limestone	Conformable
Y LST Base	Y Limestone Base	Erosional
Z LST	Z Limestone	Conformable
Z LST Base	Z Limestone Base	Erosional
CIT TCE	Citnalta Top Carbonate Envelope	Conformable
CIT BCE	Citnalta Bottom Carbonate Envelope	Erosional
PEN TCE	Penobscot Top Carbonate Envelope	Conformable
PEN BCE	Penobscot Bottom Carbonate Envelope	Erosional
-4250	Surface at -4250 ms	Base

The distance to fault was set to 250 m, which determines the distance that the horizon interpretations are ignored and the horizon is extrapolated to the fault plane - this provides for a cleaner model nearer the faults.

5.2.8: Zone Modelling

Zones were inherently generated between the horizons input in the "make horizons" process; these initial zones are known as stratigraphical intervals. Further zonal subdivision - sub-zones - at the flow unit level were achieved using the "make zones" process with the well tops as input and several choices of algorithm as to how the wells tops are extrapolated between the stratigraphic intervals. The zones were built from the base horizon with proportionally equal volume corrections and the thickness calculation set to True Vertical Thickness (TVT). Table 5.3 below summarizes the stratigraphic intervals and corresponding zones modelled.

Table 5.3: Zone Index for each stratigraphic interval, including average lithology (based on CanStrat data, and depositional environment and seismic interpretation).

Stratigraphic Interval	Zones	General Lithology
O Marker - South Venture Sand 0 "OMK - SV0"	OMK	Limestone
	UNI 1 SST	Sandstone
	UNI 1 SH	Shale
	UNI 2 SST	Sandstone
	UNI 2 SH	Shale
	UNI 3 SST	Sandstone
	UNI 3 SH	Shale
South Venture Sand 0 - South Venture Sand 6 "SV0 - SV6"	SV0	Sandstone
	SH SV0	Shale
	SH 2 SV0	Shale
	SV1	Sandstone
	SH SV1	Shale
	SV2	Sandstone
	SH SV2	Shale
	SH SV2 Hot	Shale
	SV3	Sandstone
	SH SV3	Shale
	SV4A	Sandstone
	SH SV4A	Shale
	SV4B	Sandstone
	SH SV4B	Shale
	SV4C	Sandstone
	SH SV4C	Shale
	SH 2 SV4C	Shale
	SV4D	Sandstone

Stratigraphic Interval	Zones	General Lithology
South Venture Sand 0 - South Venture Sand 6 "SV0 - SV6" (continued)	SH SV4D	Shale
	SV4E	Sandstone
	SH SV4E	Shale
	SV5	Sandstone
	SH SV5	Shale
South Venture Sand 6 - Sand 2 Canyon Top "SV6 - SST2 Canyon Top"	SV6	Sandstone
	SH SV6	Shale
	SST 1	Sandstone
	CIT ZONE 1	Sandstone
	SH SST 1	Shale
	B43 ST SST	Sandstone
	SH B43 ST SST	Shale
	ST SST 2	Sandstone
	SH ST SST 2	Shale
	B13 ST SST	Sandstone
	SH B13 ST SST	Shale
Sand 2 Canyon Top - Sand 2 Canyon Base "SST2 Canyon Top - SST2 Canyon Base"		Shale
Sand 2 Canyon Base - 3 Limestone "SST2 Canyon Base - 3 LST"	SST2	Sandstone
	CIT ZONE 2	Sandstone
	SH SST2	Shale
	SST A	Sandstone
	SH SST A	Shale
	SST B	Sandstone
	SH SST B	Shale
	SST C	Sandstone
	SH SST C	Shale
	SV7	Sandstone
	SH SV7	Shale
3 Limestone - 6 Limestone "3 LST - 6 LST"	3 LST	Limestone
	SST 3	Sandstone
	SH SST 3	Shale
	SST 4A	Sandstone
	SST 4B	Sandstone
	SH SST 4B	Shale
	SST 4C	Sandstone
	SH SST 4C	Shale
	SST 4D	Sandstone
	SH SST 4D	Shale
	SST 5	Sandstone
	SH SST5	Shale

Stratigraphic Interval	Zones	General Lithology
6 Limestone - 9 Limestone “6 LST - 9 LST”	6 LST	Limestone
	SST 6	Sandstone
	SH SST 6	Shale
	SST 7	Sandstone
	SH SST 7	Shale
	SST 8	Sandstone
	SH SST 8	Shale
9 Limestone - 9 Limestone Base “9 LST - 9 LST Base”		Limestone
9 Limestone - Y Limestone “9 LST Base - Y LST”	SST 9	Sandstone
	SH SST 9	Shale
	SST 10	Sandstone
	SH SST 10	Shale
	SST 11	Sandstone
	SH SST 11	Shale
	SST 12	Sandstone
	SH SST 12	Shale
	SST 13	Sandstone
	SH SST 13	Shale
Y Limestone - Y Limestone Base “Y LST - Y LST Base”		Limestone
Y Limestone Base - Z Limestone “Y LST Base - Z LST”	CIT ZONE 3	Sandstone
	CIT ZONE 3 SH	Shale
	CIT ZONE 4	Sandstone
	CIT ZONE 4 SH	Shale
Z Limestone - Z Limestone Base “Z LST - ZLST Base”		Limestone
Z Limestone Base - Citnalta Top Carbonate Envelope “Z LST Base - CIT TCE”	CIT ZONE 5	Sandstone
	ARC ZONE 1	Sandstone
	ARC ZONE 2	Sandstone
	ARC ZONE 3	Sandstone
	ARC ZONE 4	Sandstone
	CIT ZONE 5 SH	Shale
	ARC ZONE 5	Sandstone
	ARC ZONE 6	Sandstone
	CIT ZONE 6	Sandstone
	CIT ZONE 6 SH	Shale
	CIT ZONE 7	Sandstone
	CIT ZONE 7 SH	Shale

Stratigraphic Interval	Zones	General Lithology
Citnalta Top Carbonate Envelope - Citnalta Base Carbonate Envelope "CIT TCE - CIT BCE"	CIT LST TCE	Limestone
	CIT LST SH	Shale
	CIT LST 2	Limestone
	CIT LST 2 SH	Shale
Citnalta Base Carbonate Envelope - Penobscot Top Carbonate Envelope "CIT BCE - PEN TCE"	CIT Zone 8	Sandstone & Shale
	CIT Zone 8 SH	Shale
	CIT Zone 9	Sandstone
	CIT Zone 9 SH	Shale
	CIT Zone 10	Sandstone
Citnalta Base Carbonate Envelope - Penobscot Top Carbonate Envelope "CIT BCE - PEN TCE" (continued)	CIT Zone 10 SLT	Siltstone
	CIT Zone 11	Sandstone
Penobscot Top Carbonate Envelope - Penobscot Base Carbonate Envelope "PEN TCE - PEN BCE"		Limestone
Penobscot Base Carbonate Envelope - Surface at -4250 ms "PEN BCE - -4250 Base"		Shale

5.3: Geometrical (Properties)

Geometrical modelling was used to generate properties (fault, zones, and pressure indices) using predefined system variables.

5.3.1: Zones Index

A zone index was generated using the geometrical modelling tool, which allowed for the creation of a discrete property were the cells were assigned to a value according to their zone. This allowed the model to be displayed or filtered based on the zone(s) of interest.

5.3.2: Pressure Index

A pressure index was generated using the geometrical modelling tool, which allowed for the formation of a discrete property where the cells were assigned a pressure value (the average pressure for the flow unit in that zone) according to the zone and segment (Appendix C). This allowed the model to be displayed or filtered based on the zone(s) and segment(s) of interest, which was especially important in creating the FPPs.

5.4: Facies Model

Facies modelling to assess variations in permeability across the model requires upscaling of the lithology log. First, the petrofacies log was calculated within the software, and is based on the CanStrat lithology log, the density log, and the Vsh log. A nested "If" statement (Equation 5.1) was used to determine the petrofacies based on these logs:

LITH = If (Lithology_CS = 27, 7, If (Lithology_CS = 26, 9, If (V_{sh} <0.55 And DEN >2.55, 5, If (V_{sh} <0.5 And DEN > 2.5, 4, If (V_{sh} <0.6 And DEN >1, 3, If (V_{sh} >0.5, 2, If (V_{sh} > 0.65, 1, 0)))))))

Equation 5.1: Petrofacies log (LITH) calculation, where Lithology_CS is the CanStrat lithology log; V_{sh} is the shale volume log; and DEN is the density log. See Table 5.4 for correlation between equation, CanStrat lithology code, and facies calculated.

Table 5.4: Correlation between Equation 5.1, CanStrat code and lithology, and calculated petrofacies.

Equation Term (Equation 5.1)	CanStrat Lithology Code	CanStrat Interpreted Lithology	Equation Calculated Petrofacies
Lithology_CS = 27, 7	27	Limestone	Limestone (use CanStrat, do not calculate)
Lithology_CS = 26, 9	26	Marlstone	Marlstone (use CanStrat, do not calculate)
V_{sh} <0.55 And DEN >2.55, 5	n/a	n/a	Tight Sand & Silt (ϕ <4 %)
V_{sh} <0.5 And DEN > 2.5, 4	n/a	n/a	Sand & Silt (ϕ 4-9 %)
V_{sh} <0.6 And DEN >1, 3	n/a	n/a	Sand (ϕ >9 %)
V_{sh} >0.5, 2	n/a	n/a	Shale
V_{sh} > 0.65, 1, 0	n/a	n/a	Shale

This equation allowed for six petrofacies to be assigned: (1) limestones, (2) marlstones, (3) tight sand and silt (ϕ <4 %), (4) sand and silt (ϕ 4-9 %), (5) sand (ϕ >9 %), and (6) shale. These lithologies approximate different permeability regimes because there is (in a general sense) a direct relationship between increasing porosity and permeability.

Although a more accurate determination of permeability is possible (through various methods), it was beyond the scope of this project to do so.

Layers were then added in each stratigraphic interval of the model, creating enough layers so that each would be approximately 2 ms thick. The calculated lithology log was then upscaled in each interval based on the number of layers using the "most of" method, where the program will select the value that is most represented in the log for a particular cell (in terms of MD length) and assign it to the cell.

Finally, the facies modelling tool was used to integrate the upscaled lithology logs (discrete data) into the geocellular model using a stochastic method called "sequential indicator simulation". For each stratigraphic interval, the facies to be included in the zone were selected and the sequential indicator simulation method was selected. This method created a stochastic distribution of the petrofacies property using the pre-defined histogram, while honouring directional settings and extensional trends. The tool also runs a parallel deterministic algorithm that populates the model through indicator kriging, where values are optimally interpolated based on regression against observed values of surrounding data points and weighted according to spatial covariance.

5.5: Data Organization and Presentation for Interpretation

5.5.1: Databases and Spreadsheets

The data analyzed and generated during this thesis were organized and displayed to facilitate their interpretation. Data organization includes the creation of several databases that captured original data from the sources, and results as they were generated from the various analysis steps discussed above. Maintaining databases for the analysis results was especially important as it allowed for comparisons between earlier and later iterations, enabling the effect of qualitative choices to be evaluated. Databases (and associated spreadsheets) created include:

- Well Database:
    - .LAS files
    - Core logging program
    - Bit size and casing program

    - Checkshot surveys
    - Deviation surveys
    - Lithology logs
- Well Tops Database
    - BASIN database formation well tops (based on multiple interpreters)
    - BASIN database production well tops (based on multiple operators)
    - Formation well tops (adjusted/corrected for this study)
    - Flow unit well tops (a result of this thesis)
    - Petromod™ well tops (a result of this thesis used as an input for Wong et al. 2016)
    - Excess pressure well tops (data sourced from pressure analysis Excel spreadsheet)
- Pressure Database:
    - Individual pressure data for each well (as downloaded from the BASIN online database)
    - All Excel spreadsheets generated during pressure data analysis
- Seismic Horizon Database:
    - Interpretation faults
    - Interpretation of carbonates
    - Interpretation of Venture Field
    - Interpretation of model area
    - Interpretation of entire study area
- Geocellular Model Database:
    - 3D grid model (with zones, flow units, and pressure data) – Versions 1 to 5
    - 3D grid (with zones, flow units, and pressure data) – Final (Version 6)
    - Fault Model (with faults, trends, boundary) – Final (Version 5)
    - 3D grid (with zones and facies data) – Versions 1 to 3
    - 3D grid (with zones and facies data) – Final (Version 4)

5.5.2: Excess Pressure-Depth Plots

Pressure-depth plots are a powerful and effective method for visualizing a range of pressure data for interpretation of fractures pressures and gradient(s), fluid type(s), fluid pressures, hydrocarbon-water contacts, and reservoir connectivity. For this thesis, excess pressure-depth plots were generated to enable comparison of the excess pressure to depth for observable correlations and trends, with the data classified by flow unit. It was important to identify the data points based on flow unit to assess reservoir connectivity, as location of changes in pressure gradients and magnitude of excess pressure relate to changes in rock properties (primarily permeability), which are linked to stratigraphy and lithology. These plots were produced after the pressure data had undergone extensive review and were created for each field individually and all the fields combined. Overlapping pressures from two or more wells, or pressure plotting on a common fluid gradient can be indicators of reservoir connectivity.

5.5.3: Fault Plane Profiles

Fault plane profiles (FPPs) are cross sections of a fault plane that show both the hanging wall and footwall cutoffs (Allan 1989). FPPs are an important tool for prospect assessment and for understanding seal behavior in fields. A FPP shows what is juxtaposed across the fault, demonstrating areas of sand-sand and sand-shale juxtaposition and defining potential fault-dependent leak points. Juxtaposed lithology leak points (JLLPs) identify where hydrocarbons may cross leak from the footwall into the hanging wall. The leak is assumed to occur along the entire length of the sand-sand juxtaposition. There were two types of FPPs generated, the first were based on flow units to highlight permeable units, and the second were filtered on only flow units with recorded pressure data.

The excess pressure data was populated into the reservoirs of the appropriate segments of the model to generate a 3D visualization of the reservoir pressure and fluid systems across the area. The FPPs were regenerated for both faults based on the excess pressure data to provide insight on the effectiveness of the juxtaposition connections from a pressure perspective. The lack of data in many reservoirs (no data, poor quality

data, or not collected within a particular block) is an acknowledged, unresolvable limitation of the analysis. It is reasonable to assume that excess pressure and fluids are migrating through these units based on juxtaposition connections in other faults or top seal transmissibility.

5.5.4: Seismic Cross Sections

Composite (not inline or crossline) seismic cross sections were generated through the model area, across the expansion trend, to assess the reservoir connectivity and identify potential pressure migration pathways. The cross sections were generated with three different properties: (1) flow units, (2) excess pressure results, and (3) facies results. These cross sections were then examined for lateral and vertical reservoir fluid and pressure migration opportunities that could rationalize the current excess pressure distribution in the Sable Subbasin model area.

Chapter 6: Results and Discussion

At depth, hydrocarbon reservoirs and associated aquifers of the Sable Subbasin are observed to be at extremely high excess pressures, interpreted here as a combined result of ongoing hydrocarbon generation (Wong et al. 2016) and isolation of reservoir compartments (observed in the sub-regional geocellular model presented here). One means of pressure generation is via the reservoir fluid volume increase associated with conversion of kerogen to hydrocarbons (Barker 1990; Tissot et al. 1987). Ongoing hydrocarbon generation occurs in the mature to overmature shales that enclose pressure compartments at depth within each fault block / expansion trend. Other mechanisms for pressure generation are described (Forbes et al. 1992; Jansa and Urrea 1990; Mudford and Best 1989; Mudford et al. 1991; Wielens 2003; Williamson 1995; Williamson and Smyth 1992; Yassir and Bell 1994), but none are suggested to occur recently in the Scotian Basin and so are inconsistent with the limited capacity of thin topseals in the Sable Subbasin to retain pressure over more than tens of thousands of years (according to seal leak rates from Deming (1994) and permeabilities from Mudford and Best (1989) and Mudford et al. (1991)). Pressure release through seals (whether by mechanical leak, Darcy-type flow of water, or flow of gas once capillary entry pressure of seals is exceeded) is interpreted based on the Deming (1994) paper to be geologically rapid requiring a recent source of pressure to maintain the pressures observed here.

Migration out of the deepest, highest pressure compartments at leak off pressures occurs via mechanical leak through seals (based on observed LOP data in excess pressure-depth plots) or by slow Darcy-type flow of water through seals. Pressure compartments at depth are also isolated in each fault block / expansion trend by a combination of faulting, deposition in a distal setting, and diagenesis. Referring to the seismic transect (Figure 6.1) from the geocellular model and well data; in each fault block / expansion trend, net-to-gross ratios increase upwards, reflecting progradation of the shelf, and the offset of each major listric fault (that separate expansion trends / major fault blocks) and internal blocks (within fault blocks) diminishes. Based on the model and subsequent fault plane profiles,

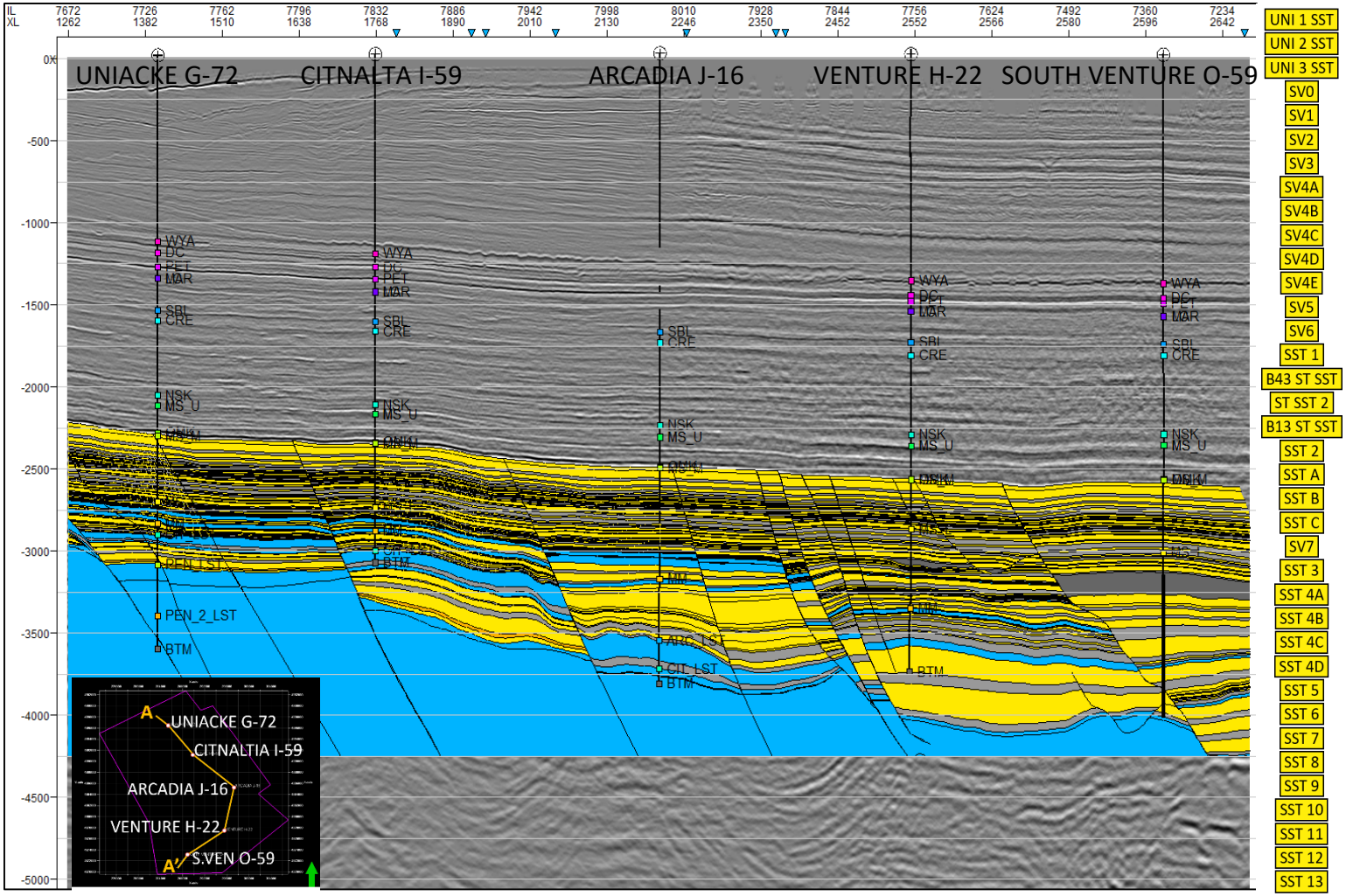

Figure 6.1: Seismic transect from A to A' with 5 wells included (5X vertical exaggeration). The cross section shows the flow units across the expansion trend. The increasing space is due to movement along the listric growth faults that can be easily observed.

cross fault juxtaposition of permeable pressure cells becomes increasingly common upward until the unfaulted high net-to-gross sands of the Missisauga interval where full connectivity between sands is interpreted to occur by occasional cross fault juxtapositions and erosional incision of sands into each other. This pattern of connectivity pathways observed in each fault block / expansion trend allows for the dispersal of excess pressure within the modeled area and this forms a template for how pressure dissipation may occur throughout the basin.

In the deep reservoir compartments, especially those located distally within each expansion trend, excess pressure is retained until it exceeds the (mechanical) seal capacity of the enclosing shales. Assuming pressure influx exceeds pressure outflux via Darcy-type flow, once the pressure has reached mechanical seal capacity, either new fractures are generated or existing fractures may be opened (or a combination of both) within the top seals or locally for very limited distances at faults. As the fluids escape, fluids migrate out and pressure is released until the fractures close; if pressure generation is ongoing, this process may repeat. This interpretation is supported by observations in the excess pressure-depth plots from the study area, where pressures in the deeper reservoir compartments plot near to leak-off pressures.

Excess pressure is released from the deepest reservoirs following mechanical seal failure as either water or gas escape. Alternatively, pressure can be released when water escapes via Darcy-type flow below leak off pressures, and pressure can also be released when gas accumulates to the point where buoyancy exceeds the capillary entry pressure and gas can flow through the topseal by multiphase Darcy-type flow. Fluids, predominantly water and gas, migrate upwards through fault juxtaposition connections of permeable strata with gas subsequently filling structural highs within each pressure cell. Eventually, gas and displaced water reach the shallower, hydrostatically pressured reservoirs where they cannot increase reservoir fluid pressure because of being an unlimited volume system (reservoir units subcrop to seafloor approximately 75 km to northeast).

A key observation in the wells and propagated through the model is that large pressure differences are observed across the juxtaposition connections between pressure cells (in the interval between the “leak off” and “hydrostatic” systems). These “stepped decreases” in excess pressure upwards are observed in each fault block / expansion trend. This threefold segregation of pressure distribution (and mechanisms) is seen in each fault block and partially reflects Downey’s (1990) observations regarding the behavior of faults in fluid and pressure connectivity. The impedance of fluid movement and pressure release at intermediate depths in the Sable Subbasin requires ongoing pressure influx (from either deeper strata or shales enclosing the sands) and some inhibition that is interpreted to be either the result of low transmissibility fault juxtapositions windows between permeable pressure cells or reduction of permeability distally within each expansion trend (rapid distal degradation is observed in each fault block via well control and/or seismic amplitudes) – or both. Development of fault material such as gouge, cemented sands, or fine-grained material as a result of cataclasis may impede Darcy-type flow to water across juxtaposition windows or may form a capillary seal to hydrocarbons. The result may be slow ongoing leak of water or episodic or ongoing leak of hydrocarbons across capillary seals.

The excess pressure-depth plot from the Venture field (this also has the most pressure data points of the fields included in this study) best exemplifies the excess pressure systems of the Sable Subbasin, where large pressure steps can be observed between the major reservoirs (Figure 6.2). Individual reservoirs having distinct pressure characteristics are plotted in clearly separate groupings while multiple reservoirs having similar reservoir pressure values plot along common excess pressure/depth trends, inferring connectivity. Major reservoirs include (from deep/highest excess pressure to shallow/hydrostatic pressure): Sand 13 – Sand 10, Sand 8 – Sand 6, Sand 5 – Sand 4, Sand 3, Sand C, Sand B, Sand A, and Sand 2.

The South Venture excess pressure-depth plot also shows large pressure steps between the major reservoirs, however there are significantly fewer data points collected in the deeper excess pressured system than in the Venture Field (Figure 6.3). The

hydropressured system (-3750 to -4250 m TVDSS) has multiple data points plotting along a common gradient, inferring connectivity is present. This may infer a shared water leg, but the gas legs off of this may not be in communication with each other. Within the deeper excess pressured system, there are only six data points, however, four of the six plot along a common pressure/depth trend, again inferring connectivity. This could imply a more worthwhile exploration target due to implied larger reservoir size.

The remaining fields (south to north), Arcadia, Citnalta, and Uniacke, do not have as many data points as the Venture and South Venture fields, therefore their individual excess pressure-depth plots were less informative about their individual (fault block / expansion trend) pressure systems (Appendix D). Data from the all five fields were plotted as a single excess pressure-depth plot (Figure 6.4), which enabled reasonable extrapolation of trends between the five fields. The data from the Arcadia, Citnalta, and Uniacke fields plots well within the data from the Venture and South Venture fields, with a few anomalies (from the Uniacke field) plotting beyond the fracture gradient in the deep "leak off" pressure system. There are 3 possible reasons for this: (1) there is a problem with the data or the tests used to gather the measurements (2) they are perfectly valid and correct measurements that are possible due to uniquely strong seal lithologies able to retain significantly higher pressures than would be normally expected at that depth; (3) perhaps the fracture gradient is not a hard linear relationship, rather it is more of a diffuse zone that is more influenced by geology than previously considered.

Three pressure systems are observed in the excess pressure-depth plot for all the fields: (1) shallower hydrostatic pressured, (2) stepped excess pressured, and (3) "leak off" pressured. Multiple data points sourced from different fields plot along common excess pressure-depth trends, inferring that there is not only connectivity within individual fault blocks but between the fault blocks of the expansion trend. Consequently, it is reasonable that observations and interpretations regarding fluid and pressure migration through cross fault juxtaposition windows in the data-rich Venture and South Venture blocks (11 and 4 wells respectively) can be applied to the data-poor Arcadia, Citnalta, and Uniacke blocks (1 well in each).

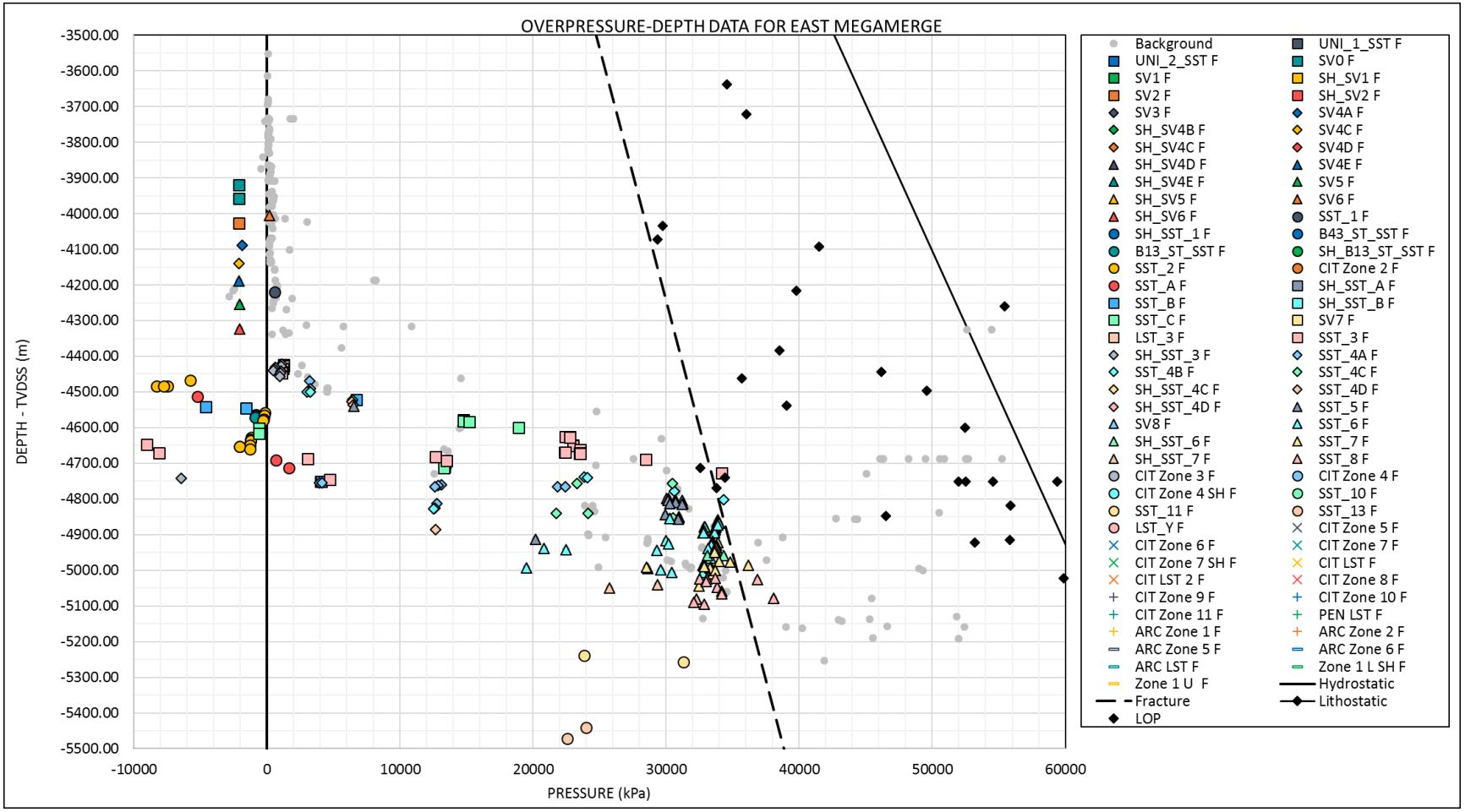

Figure 6.2: Excess pressure-depth plot for the Venture Gas Field, including exploration and productions wells. Full table of data plotted available in Appendix B. Larger versions of this figure and plots for individual fields available in Appendix D.

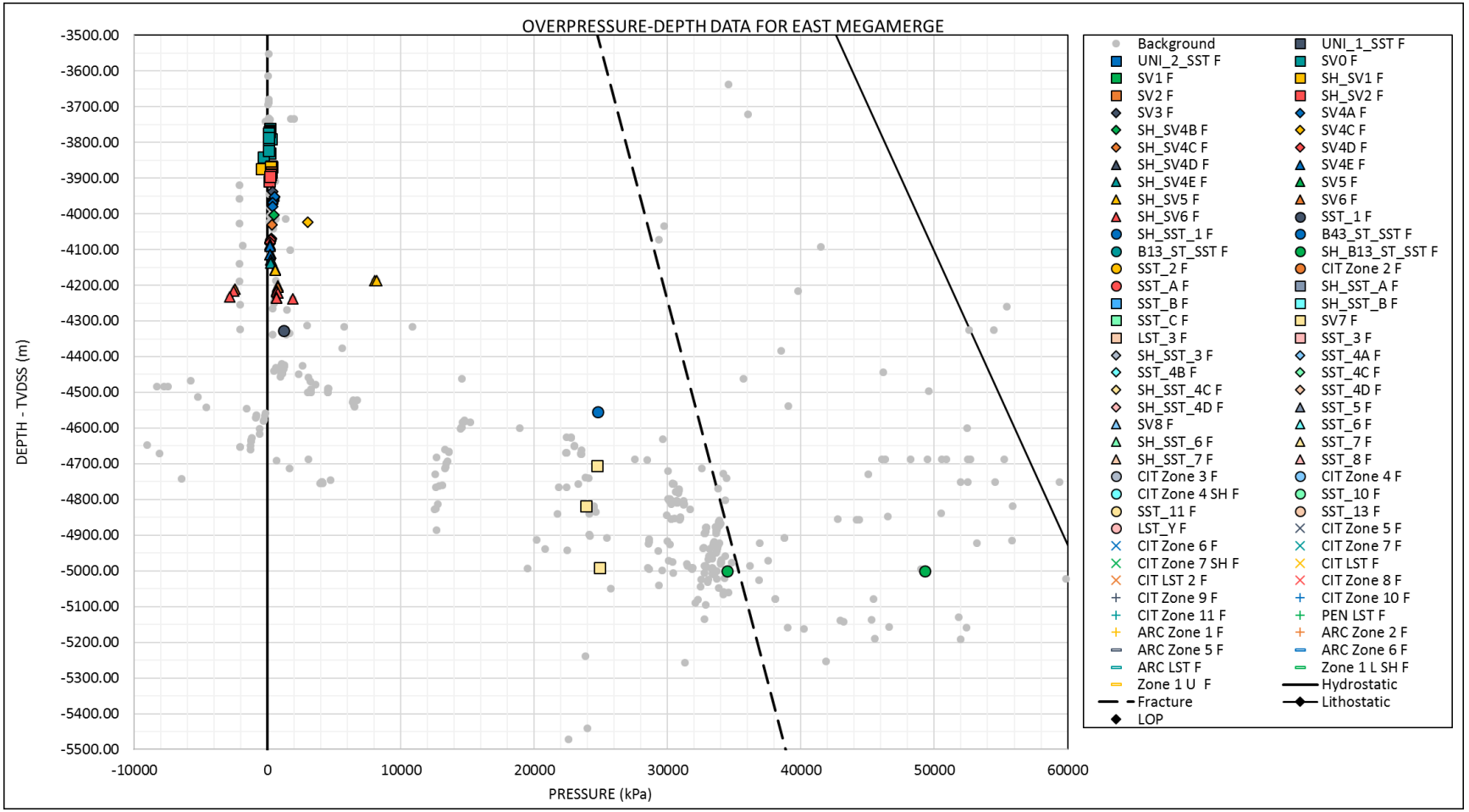

Figure 6.3: Excess pressure-depth plot for the South Venture Gas Field, including exploration and production wells. Full table of data plotted available in Appendix B. Larger versions of this figure and plots for individual fields available in Appendix D.

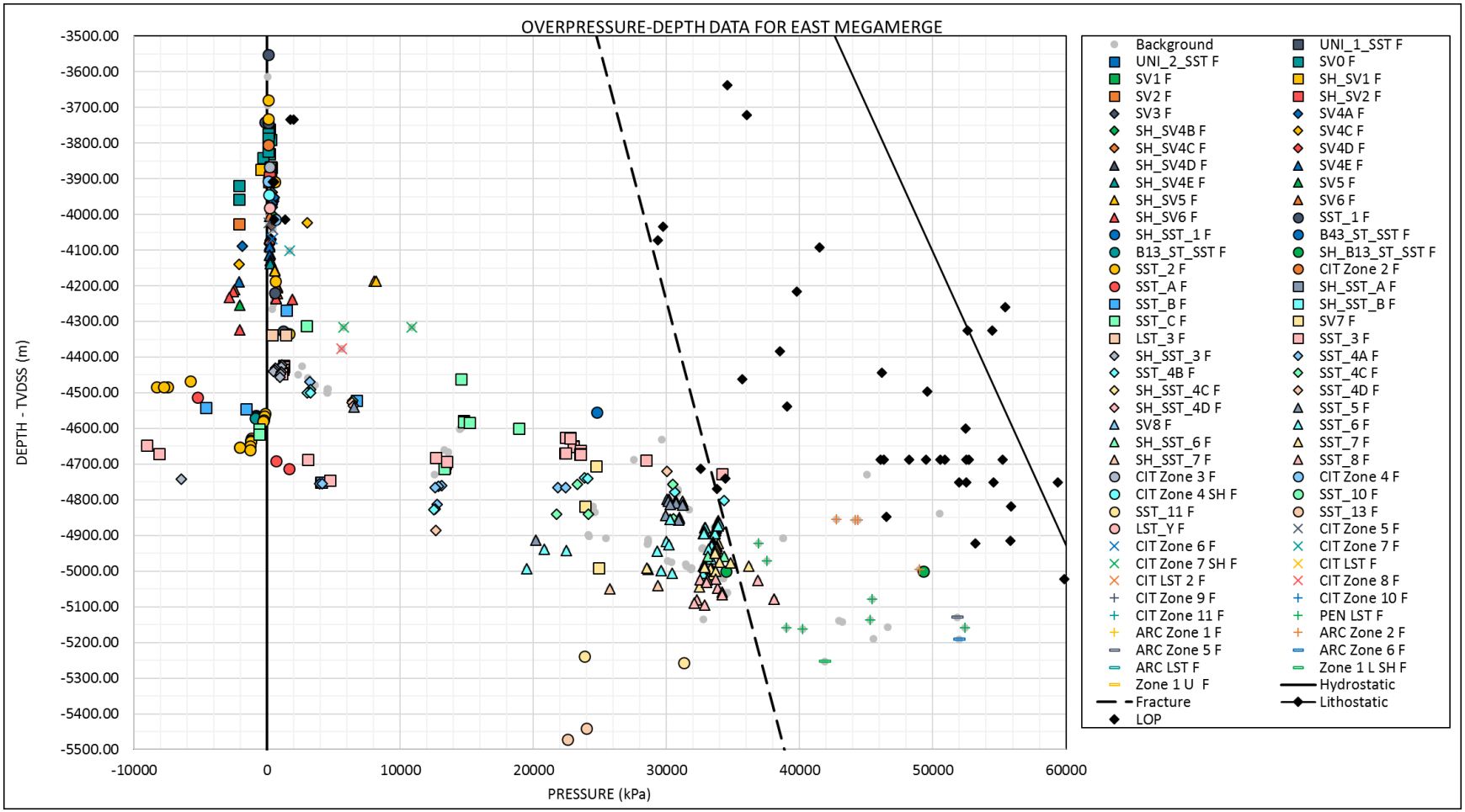

Figure 6.4: Excess pressure-depth plot for all gas fields in study area, including exploration and production wells. Full table of data plotted available in Appendix B. Larger versions of this figure and plots for individual fields available in Appendix D.

In order to investigate the juxtapositional relationships between pressure cells, fault plane profiles were analyzed to examine connectivity between permeable strata. Fault plane profiles (FPPs) for two faults have been selected for inclusion in this thesis (although could be generated for any fault within the model area): Venture B-13 crestal fault, and Venture H-22 splay fault. The Venture B-13 fault occurs within the Venture field, where the fault provides opportunities for fluids and associated pressure to migrate vertically from deeper to shallower pressure systems while staying within the field. The Venture H-22 splay fault also occurs within the Venture field; however, this fault is one of a series that link pressure cells / flow units of the Venture field expansion trend.

The FPP for the Venture B-13 crestal fault reservoirs (flow units) demonstrates the juxtaposition of the permeable units within the field. The fault does not have a large delta throw at the top, but the throw does increase with depth with greater throw observed by the juxtaposition of the deeper units (Figure 6.5). The FPP for the Venture H-22 splay fault reservoirs demonstrates similar juxtaposition of the permeable units as seen in the Venture B-13, however the overall throw of the fault is larger than the Venture B-13 crestal fault with more juxtaposition connections between different units across the fault (Figure 6.6). The Venture H-22 fault is a splay off the larger South Venture bounding fault that separates the South Venture field from the Venture field, therefore it is reasonable that the fault has a higher delta throw. The juxtaposition connections for both faults are simplified and compared in Figure 6.7.

The FPPs for both the Venture B-13 crestal fault and Venture H-22 splay fault demonstrate numerous juxtaposition connections between (stratigraphically) deeper and shallower reservoirs. When the same FPPs are instead viewed with the pressure data (associated with the reservoirs), it is immediately apparent that there are juxtaposition connections between excess pressured reservoirs and hydrostatic pressured reservoirs (Figure 6.8 and Figure 6.9 respectively). This again supports the conclusion that these juxtaposition windows provide opportunities for the deeper excess pressured systems to equilibrate laterally and vertically by “stair stepping” up the permeable units along the fault(s).

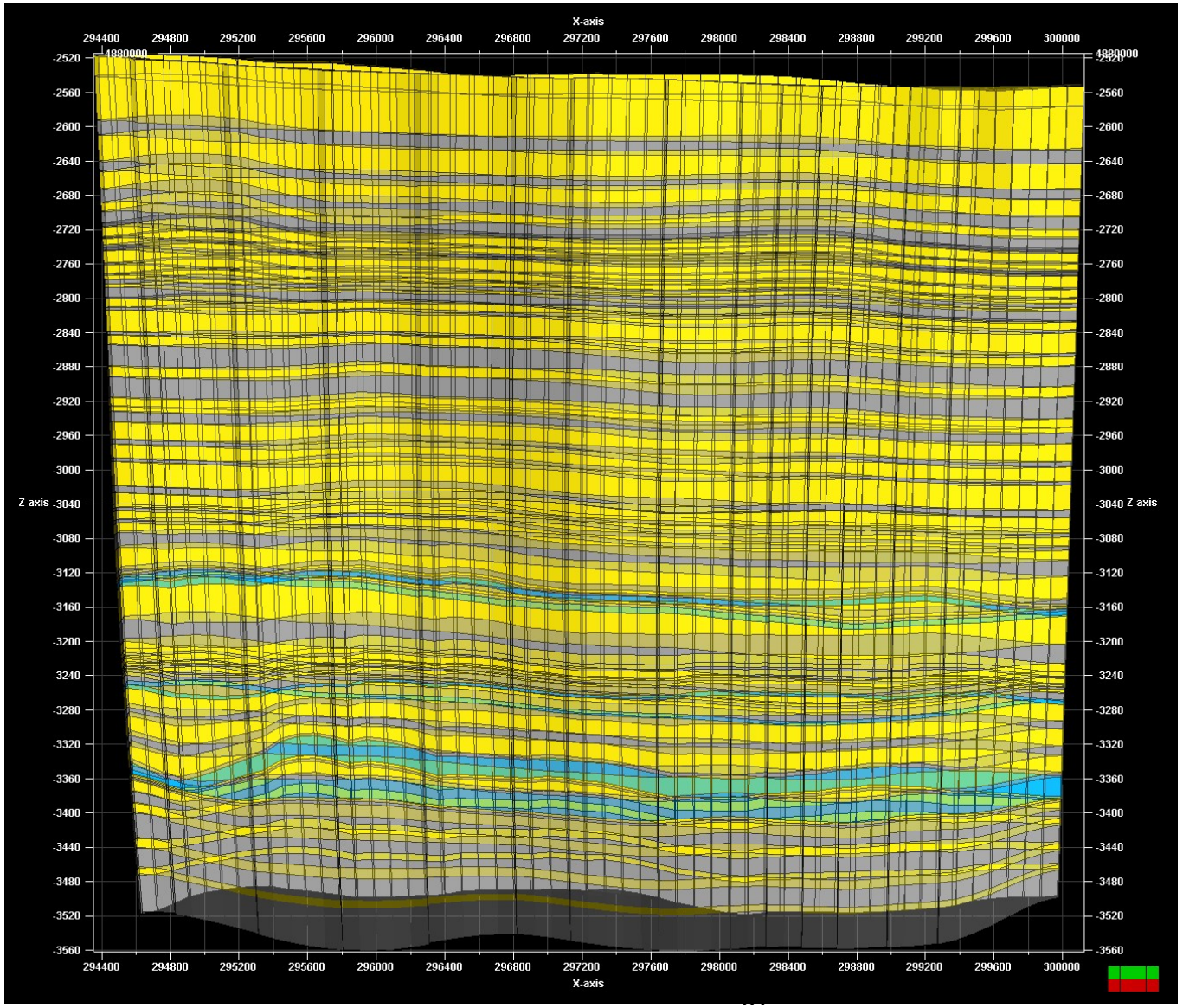

Figure 6.5: Fault plane profile for Venture B-13 crestal fault flow units (5X vertical exaggeration; orthogonal view; north projected into page). Units on the north side of the fault are solid-filled; units on the south side are gridded. The north side of the fault is formed by the Venture Splay 1 segment (west) and the south side of the fault is the Venture segment. Shales (grey) and limestones (blue) are not interpreted as flow units. Larger version available in Appendix H.

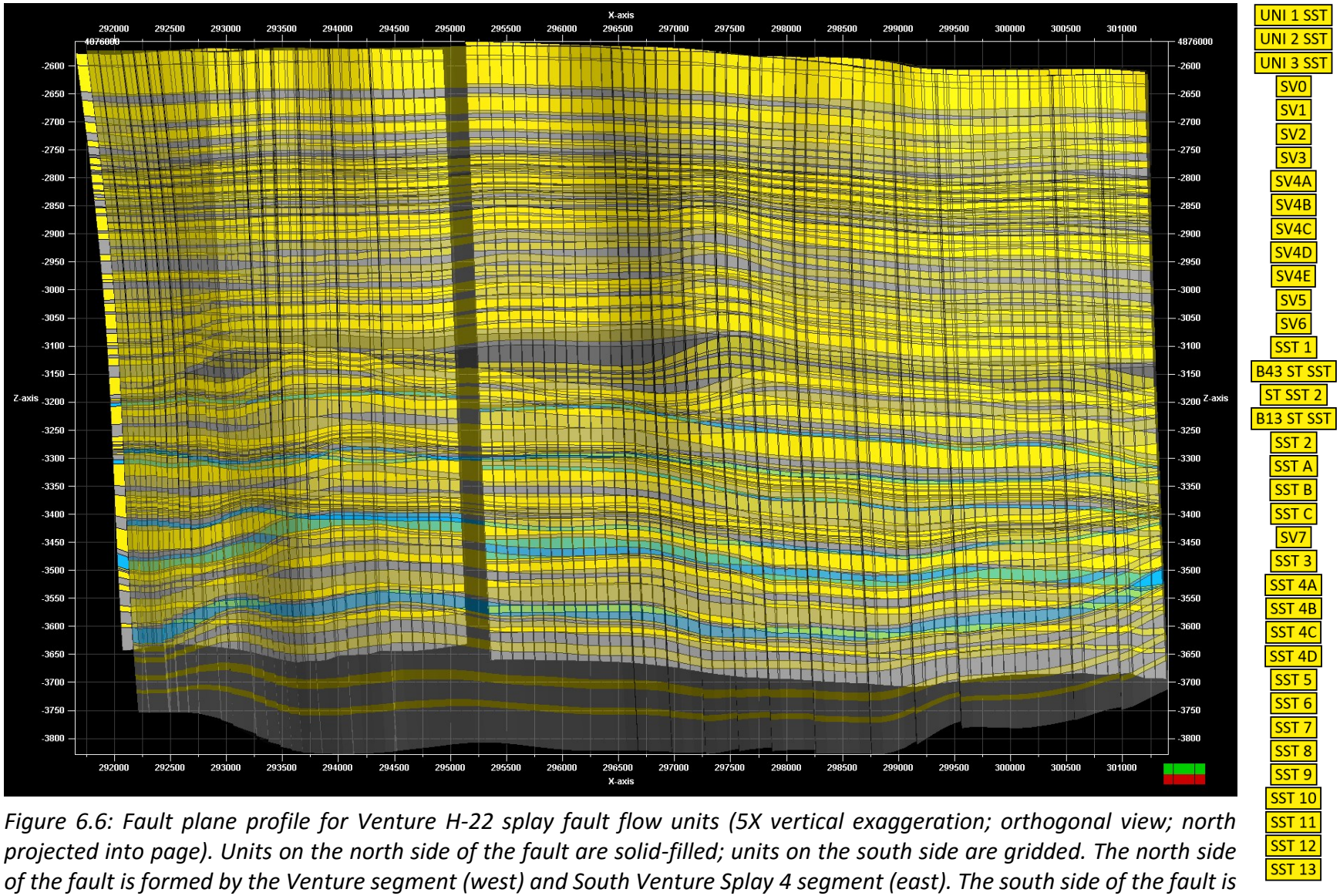

Figure 6.6: Fault plane profile for Venture H-22 splay fault flow units (5X vertical exaggeration; orthogonal view; north projected into page). Units on the north side of the fault are solid-filled; units on the south side are gridded. The north side of the fault is formed by the Venture segment (west) and South Venture Splay 4 segment (east). The south side of the fault is the South Venture Splay 3 segment. Shales (grey) and limestones (blue) are not interpreted as flow units. Larger version available in Appendix H.

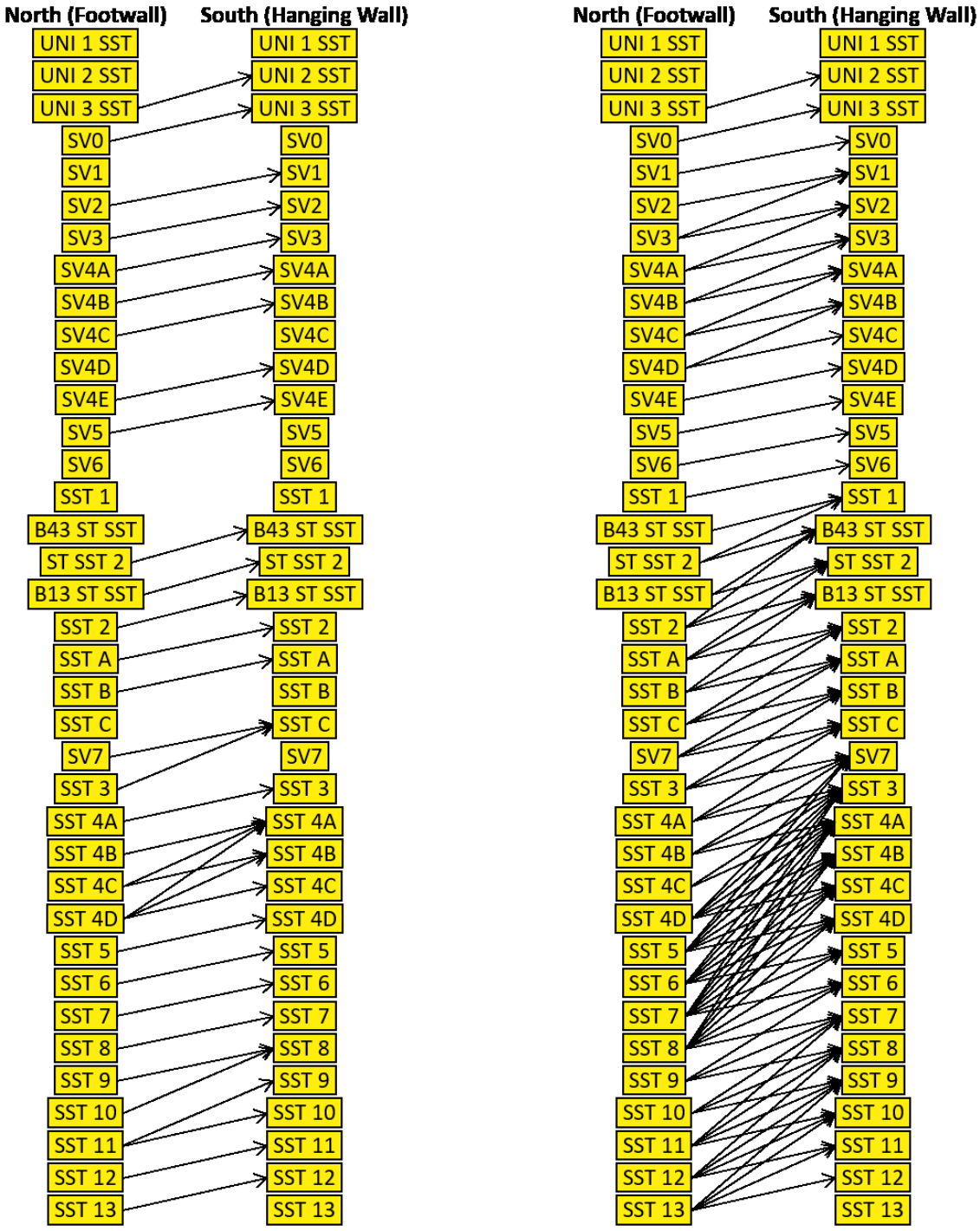

Figure 6.7: (Left) Simplified connectivity diagram across the Venture B-13 crestal fault with arrows indicating potential flow directions between flow units based on fault juxtaposition. (Right) Simplified connectivity diagram across the Venture H-22 splay fault with arrows indicating potential flow directions between flow units based on fault juxtaposition. Note that the Venture H-22 fault has more juxtaposition connections than the Venture B-13 fault, likely due to the greater throw along the fault.

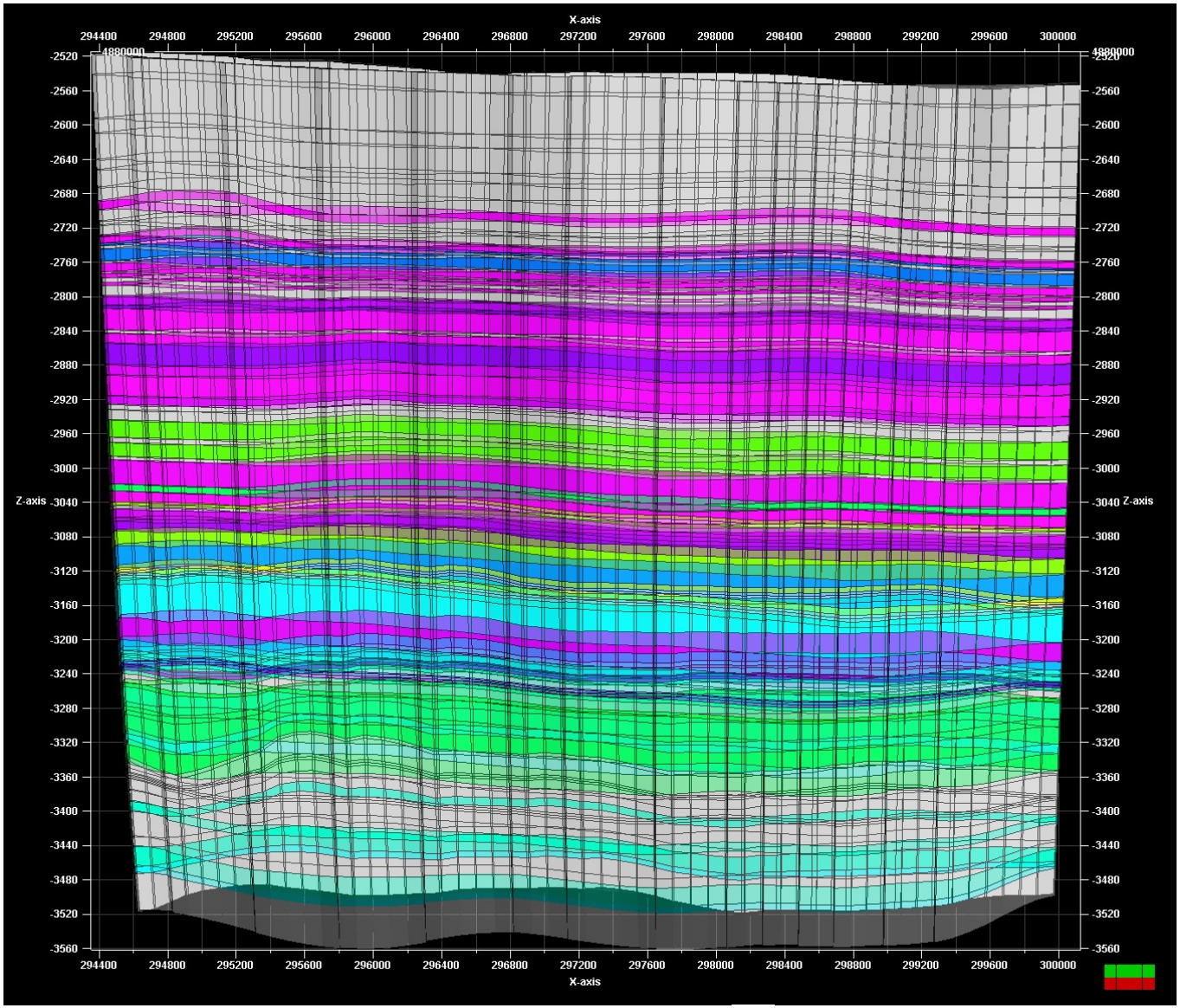

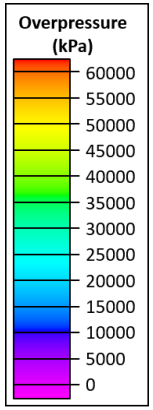

Figure 6.8: FPP for Venture B-13 crestal fault flow units with associated pressure data (5X vertical exaggeration; orthogonal view; north projected into page). Units on the north side of the fault are solid-filled; units on the south side are gridded. The north side of the fault is formed by the Venture Splay 1 segment (west) and the south side of the fault is the Venture segment. Units that are grey do not have a pressure measurement within the segment. Pressure data are available in Appendix B.

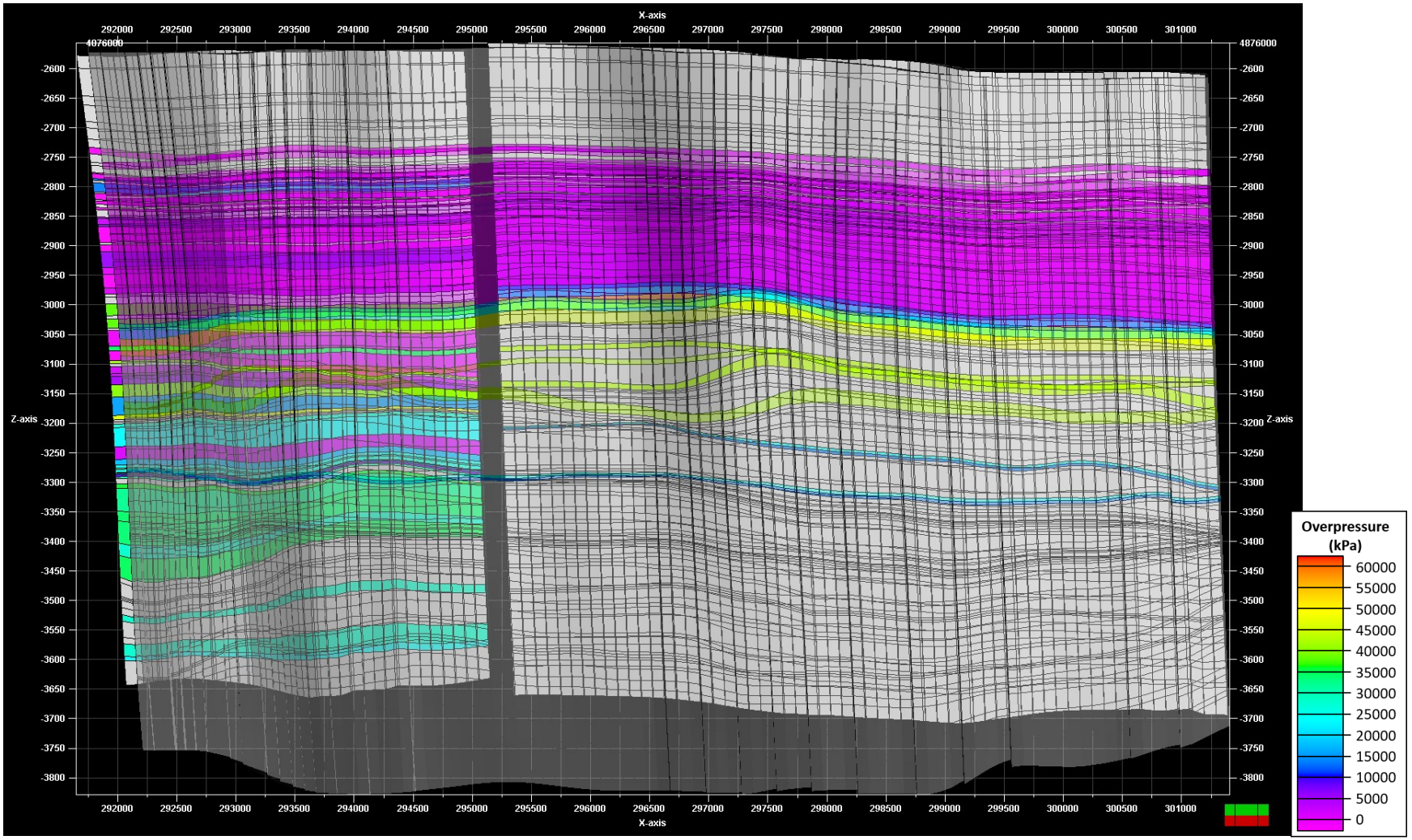

Figure 6.9: FPP for Venture B-13 crestal fault flow units with associated pressure data (5X vertical exaggeration; orthogonal view; north projected into page). Pressure data are available in Appendix B. Units on the north side of the fault are solid-filled; units on the south side are gridded. The north side of the fault is formed by the Venture segment (west) and South Venture Splay 4 segment (east). The south side of the fault is the South Venture Splay 3 segment. The pressure data is similar but not the same for the Venture and South Venture segments, therefore the difference with respect to the segments is displayed on the north side of the fault.

Table 6.1: Flow units with average excess pressure values for Venture B-13 Crestal Fault.

Flow Unit	Pressure (kPa)
SV0	2186
SV2	-2084
SV3	12555
SV4A	-1858
SV4B	-2099
SV4D	2214
SV4E	1298
SV5	5853
SH_SV5	5455
SH_SV6	-2040
SST_1	8817
B43_ST_SST	37143
B13_ST_SST	-849
SH_B13_ST_SST	34126
SST 2	40799
SST_A	1166
SST_B	37815
SH_SST_B	39226
SST_C	44925
SST_3	26962
SH_SST_3	893
SST_4A	12986
SST_4B	29614
SST_4C	26866
SST_4D	6371
SH_SST_4D	6499
SST_5	30531
SST_6	35477
SH_SST_6	33706
SST_7	33103
SH_SST_7	27541
SST_8	35682
SST_11	27555
SST_13	23263

Table 6.2: Flow units with average excess pressure values for FPP Venture H-22 Splay Fault.

Flow Unit	North Segments		South Segment
	Venture	South Venture Splay 4	South Venture Splay 3
SV0	2186	101	101
SV1		302	302
SH_SV1		263	263
SV2	-2084	243	243
SH_SV2		186	186
SV3	12555	400	400
SV4A	-1858	430	430
SV4B	-2099		
SH_SV4B		470	470
SV4C		3009	3009
SH_SV4C		339	339
SV4D	2214	222	222
SH_SV4D		176	176
SV4E	1298	215	215
SH_SV4E		282	282
SV5	5853	579	579
SH_SV5	5455	683	683
SV6		751	751
SH_SV6	-2040	888	888
SST_1	8817	1205	1205
SH_SST_1		24749	24749
B43_ST_SST	37143		
B13_ST_SST	-849		
SH_B13_ST_SST	34126	41881	41881
SST 2	40799		
SST_A	1166		
SST_B	37815		
SH_SST_B	39226		
SST_C	44925		
SV7		24517	24517
SH_SV7		12566	12566
SST_3	26962		
SH_SST_3	893		
SST_4A	12986		
SST_4B	29614		
SST_4C	26866		
SST_4D	6371		

Flow Unit	North Segments		South Segment
	Venture	South Venture Splay 4	South Venture Splay 3
SST_5	30531		
SST_6	35477		
SH_SST_6	33706		
SST_7	33103		
SH_SST_7	27541		
SST_8	35682		
SST_11	27555		
SST_13	23263		

The juxtaposition connections observed in the two faults presented here are observed in numerous locations within the study area, suggesting that these connections are not unique to the Venture field or between the South Venture and Venture fields. In fact, based on these observations, it is reasonable to extrapolate the interpretation across the other fault blocks / expansion trends in the study area. The fault juxtaposition connections between the permeable strata between the fields provides the opportunity for fluids and associated pressures to migrate from one fault block into the next, and so forth. It also allows the fluids and associated pressures to migrate laterally from deeper excess pressured systems to shallower hydropressured systems as it “steps” up via the fault juxtapositions of different stratigraphic flow units.

The repeated observance of permeable unit cross fault juxtapositions suggests that following permeability, connectivity is a primary control on the migration and dissipation of pressure in the Sable Subbasin. The faulting throughout the Subbasin has resulted in extensive cross-fault connectivity, which in turn has caused the hydrocarbons of the basin to become trapped in many smaller traps and fields comprised of stacked reservoirs. The complexity associated with developing the smaller traps is increased by the different pressure systems associated with the stacked reservoirs since a basic concept of reservoir management in producing gas fields is to minimize the downhole cross-flow between hydrocarbon-bearing reservoirs having significantly different pressures.

As previously discussed, permeability is the primary control factor on reservoir connectivity. Facies models were generated along the same FPPs that were used to compare flow unit and pressure system juxtaposition, to compare facies across the faults (Figure 6.9 and 6.10). This was important because facies have a strong correlation to permeability; certain facies are typically associated with higher permeabilities and vice versa. Six facies were calculated across the model based on Vsh, density, and CanStrat lithology logs:

(1) limestone

(2) marlstone

(3) tight sand and silt (ϕ <4 %)

(4) sand and silt (ϕ 4-9 %)

(5) sand (ϕ >9 %)

(6) shale

When the facies FPPs are compared to the flow unit FPPs (Figure 6.4 and 6.5) and pressure FPPs (Figures 6.7 and 6.8), there is an obvious correlation between the more permeable facies and the flow units where pressure data was successfully obtained. It is also interesting to note that there are more permeable facies in the upper section, which is hydropressured, and fewer (more isolated) permeable facies modelled in the deeper, excess pressured systems. Normal compaction with depth would also contribute to this observed trend.

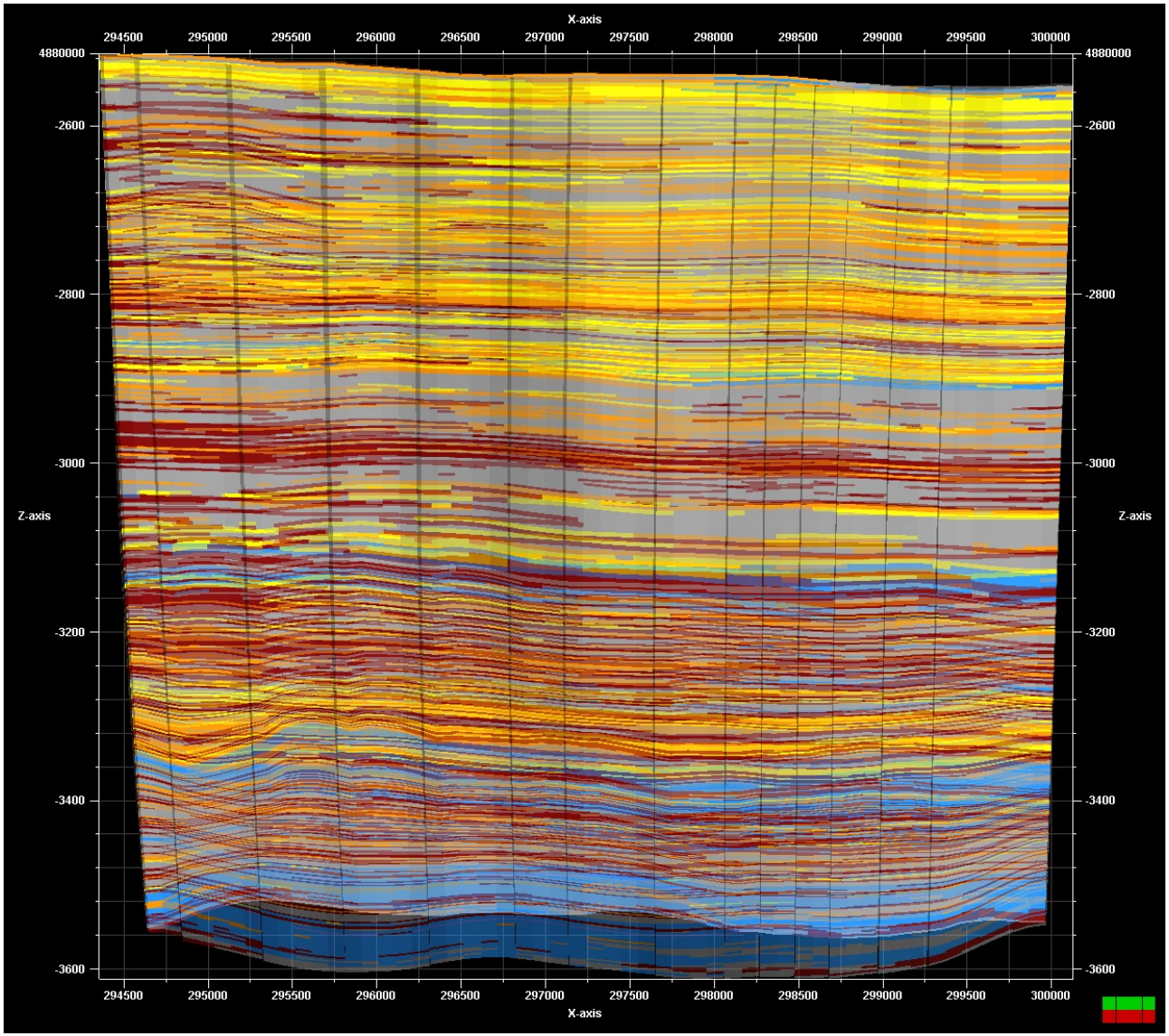

Figure 6.10: FPP for Venture B-13 crestal fault facies (5X vertical exaggeration; orthogonal view; north projected into page). Units on the north side of the fault are solid-filled; units on the south side are gridded.

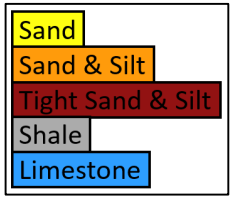

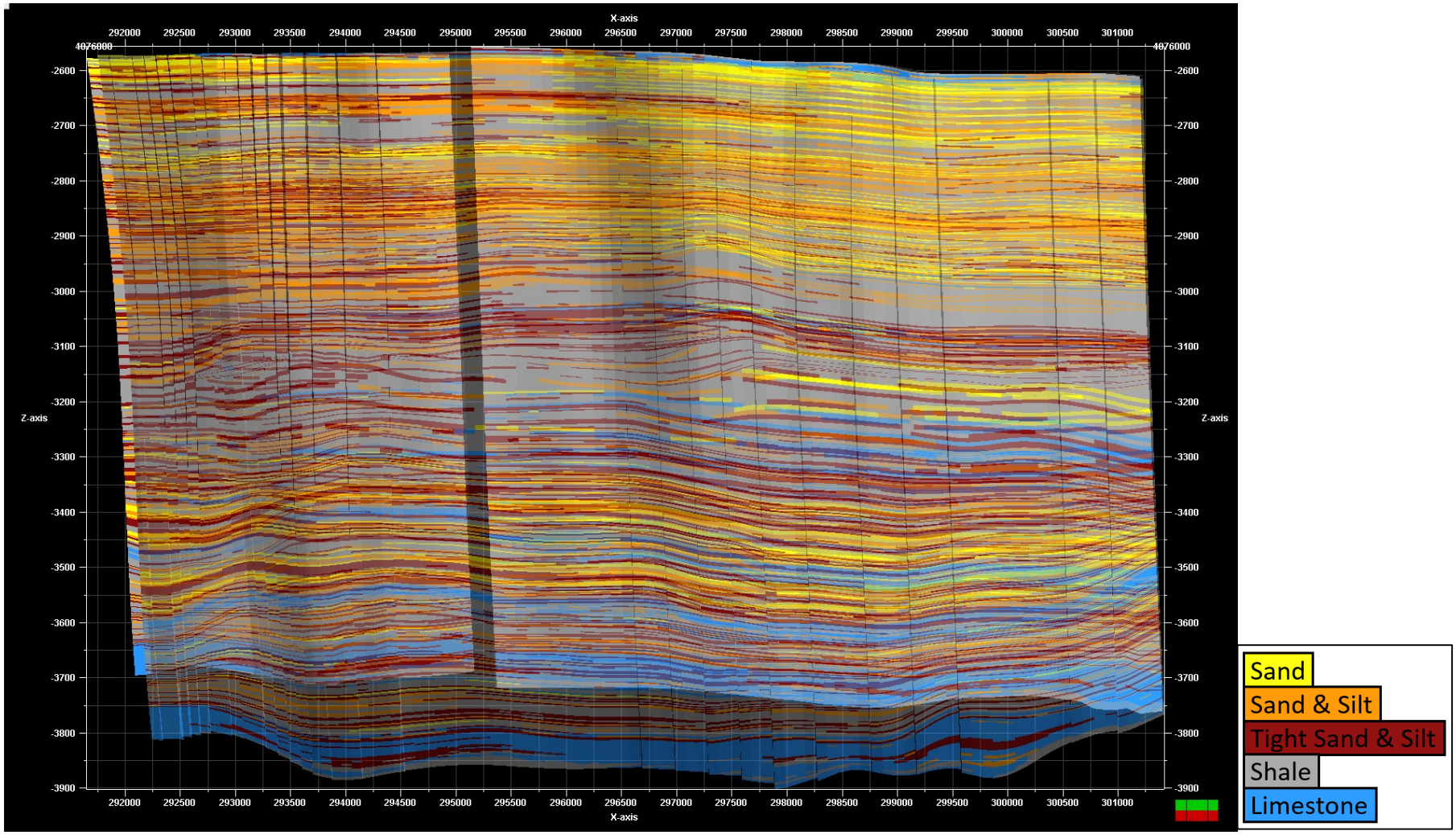

Figure 6.11: FPP for Venture H-22 splay fault facies (5X vertical exaggeration; orthogonal view; north projected into page). Units on the north side of the fault are solid-filled; units on the south side are gridded.

The above interpretations have been integrated in a seismic transect through the entire modelled expansion trend to demonstrate how interpretations from the Venture and South Venture fields can be applied to the remaining fault blocks in the expansion trend (Figure 6.12). Several studies have suggested late hydrocarbon generation as a mechanism for excess pressure, therefore potential entry points into the pressure systems of the Sable Subbasin have been annotated into Figure 6.12. Possible entry points include the enclosing shales of the pressure cells, and source rocks of the South Venture Field. Deeply buried mature to overmature shales that enclose the pressure cells provide a pressure and fluid phase input (hydrocarbon generation) to the limited-volume reservoir systems of multiple fault blocks within the expansion trend. 1D thermal modelling of the South Venture O-59 well (Wong et al. 2016) supports late to ongoing hydrocarbon generation of source rocks (Tithonian-age) within this fault block. Fault juxtaposition windows between the South Venture fault block and the adjacent Venture fault block allow fluids and associated pressure to migrate laterally and vertically via “stair stepping” up the permeable strata.

Mechanical failure (green arrows) is likely in several reservoirs based on excess pressure-depth plots and geocellular modelling of pressure. In Figure 6.12, the plotted excess pressures are greater than 25,000 kPa in several deep aquifers, putting the sands and seals at or very near to fracture pressure. These are likely experiencing mechanical failure, allowing the excess pressure to migrate vertically into shallower units.

Finally, fault juxtaposition opportunities (blue arrows) occur in numerous locations, which is emphasized by the common trends observed in the seismic cross section:

(1) deeper excess pressured system inferred to be in a mechanical failure pressure regime in multiple segments

(2) intermediate excess pressured system not at mechanical failure but sufficiently pressured to lead to reservoir fluids and associated pressuring crossing faults at juxtaposition windows of permeable units

(3) shallower hydrostatic pressure system that has minimal juxtaposition across faults, but allows excess pressure and fluids to disseminate through larger unconfined compartments extending across multiple segments (less isolation than (1) and (2)).

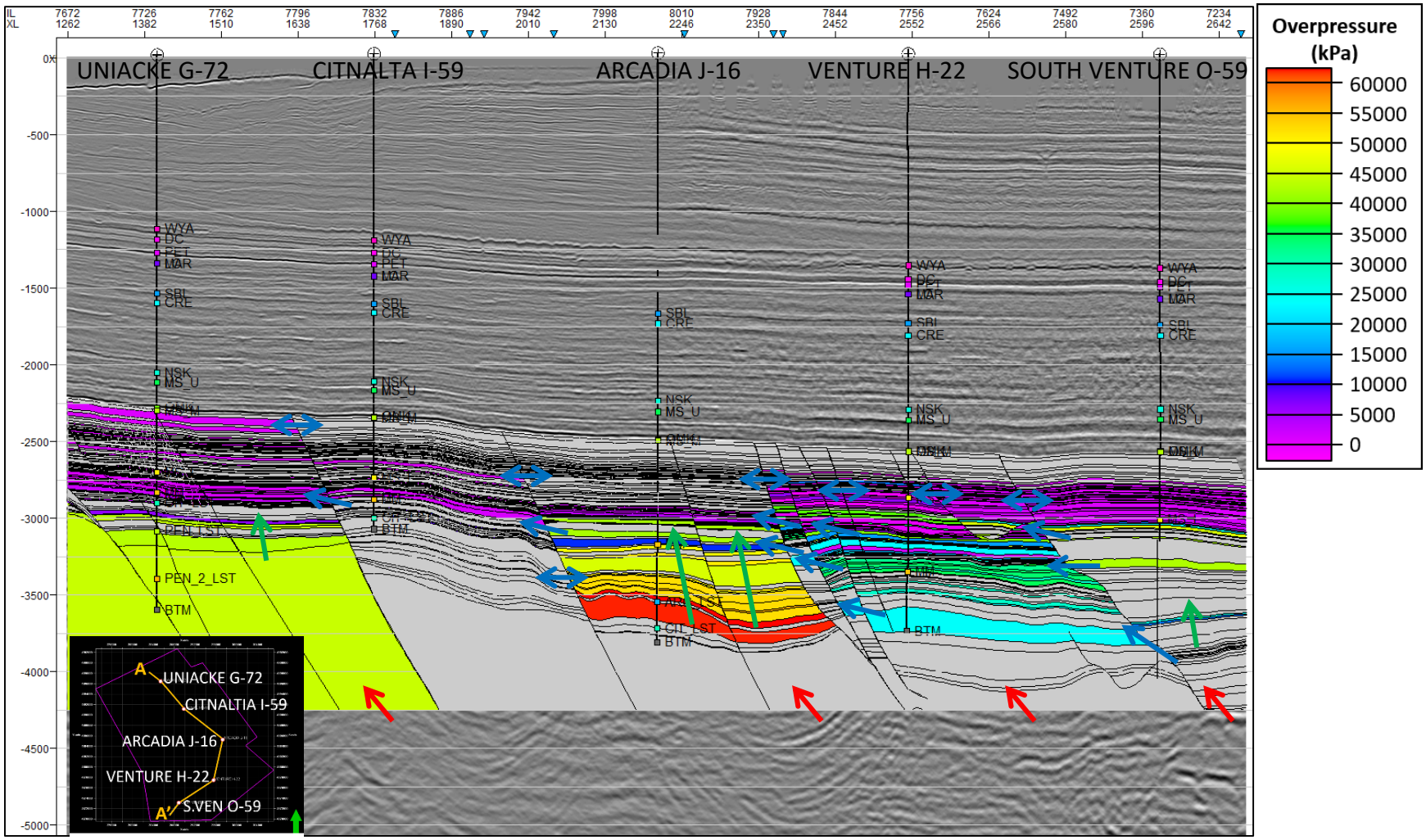

Figure 6.12: Seismic transect (5X vertical exaggeration) from A to A'. This section shows the pressures across the expansion trend (associated with the formation of the subbasin) with predominantly hydrostatic pressure systems at the top and excess pressured systems in the deeper flow units. Although there are flow units that do not have pressure data, it is reasonable to assume they will be similar to the adjacent segments. Arrows indicate potential entry points (red), mechanical failure points (green) and cross fault juxtaposition points (blue). Larger version available in Appendix I.

Chapter 7: Conclusions & Final Recommendations

7.1: Conclusions

The initial objectives for this thesis were to identify potential pressure sources within the Sable Subbasin, determine how pressure could migrate and dissipate, and clarify the role of faults and fault juxtaposition of permeable units.

Understanding reservoir connectivity is critical to the successful and safe commercial hydrocarbon development and production from the Sable Subbasin in the Scotian Basin, and any basin globally. Fluid communication through cross-fault juxtaposition connectivity is a principle control on pressure migration and distribution, and is a function of permeability. The producing commercial reservoirs of the Sable Subbasin have well established high net-to-gross ratios (deeper reservoirs less so), with the thin encasing shales serving as seals and potentially as a source for ongoing or late hydrocarbon generation. The shales of the Subbasin within this study area are tens of meters thick and have permeabilities of 10^{-20} m^2 to 10^{-22} m^2 (Mudford and Best 1989; Mudford et al. 1991) which at face value would be insufficient to confine excess pressures for longer than tens of thousands of years (Figure 7.1) (Deming 1994). However gas generation within shales (capillary seals to water (Williamson and Smyth 1992)) or underestimates of permeabilities may extend the effectiveness of shale pressure seals into the millions of years range.

Whatever the absolute timing of movement through shales, migration of water and hydrocarbons from one pressure cell to another also occurs (and probably much faster) if fault juxtapositions windows between (sufficiently) permeable units are present. However, if the reservoir quality is poor or the juxtaposition connections are choked, Darcy-type flow of water (irrespective of capillary leak) will likely be impeded.

Considering hydrocarbons, if the threshold capillary entry pressure is reached, capillary leak of hydrocarbons through a water-wet seal occurs (when hydrocarbons reach sufficient buoyancy to displace water in fine capillaries). Hydrocarbons have limited miscibility with formation water due to interfacial tension (water molecules have

asymmetric charge with positive at the hydrogen ends and negatives at the oxygen end). If the threshold capillary pressure is reached but pressure is not dissipating as fast as it is being generated (influx > outflux), then mechanical failure of the rocks will occur. If there are no hydrocarbons present, capillary leak is irrelevant, mechanical leak will happen if Darcy-type flow of water between shales is slow and pressure builds up to fracture pressure.

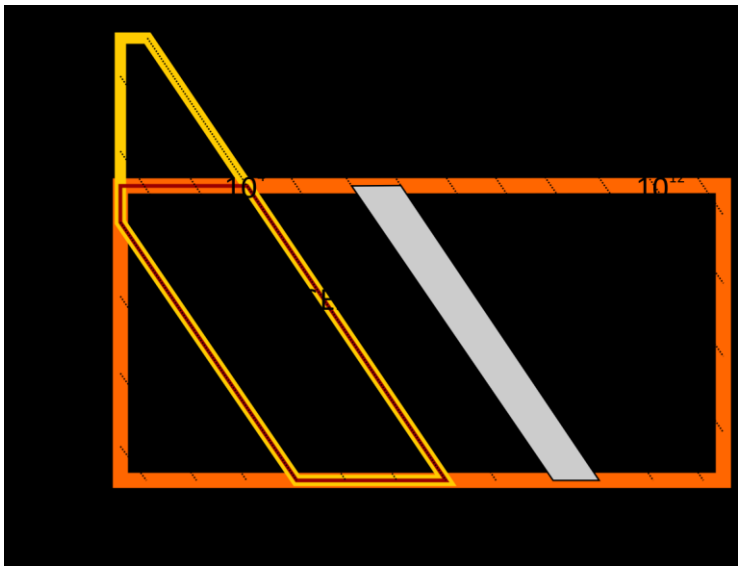

Figure 7.1: Maximum times over which a shale of a given thickness (y axis) and permeability (x axis) can confine excess pressures (Deming 1994). Grey shaded area indicates approximate minimum permeability required to sustain a 100-1000 m thick seal over 1 my. Yellow outline indicates average Sable Subbasin shale permeability of 10^{-20} to 10^{-22} m^2, while orange outline indicates shale thickness from 10 to 1000 m. Red outline indicates overlap of thickness and permeability, suggesting the maximum time shales of these conditions could impede flow is 10^4 years.

Substantial research has been done on the role of faults in compartmentalization, where faults "must have sealed" or "must have leaked". However, the behavior of a fault is not homogeneous along its' surface, with significant variability due to shale gauge, cataclasis, and mineralization; these are occasional, very local phenomena. Simply, "stair stepping" occurs where permeable units are juxtaposed; each permeable unit is filled before migration continues up to the next.

Based on work by Neele et al (2012), four potential connections are possible along faults (Figure 7.2):

(1) Partial self juxtaposition;

(2) Full self juxtaposition;

(3) Non-juxtaposition (juxtaposition seal);

(4) Cross reservoirs juxtaposition.

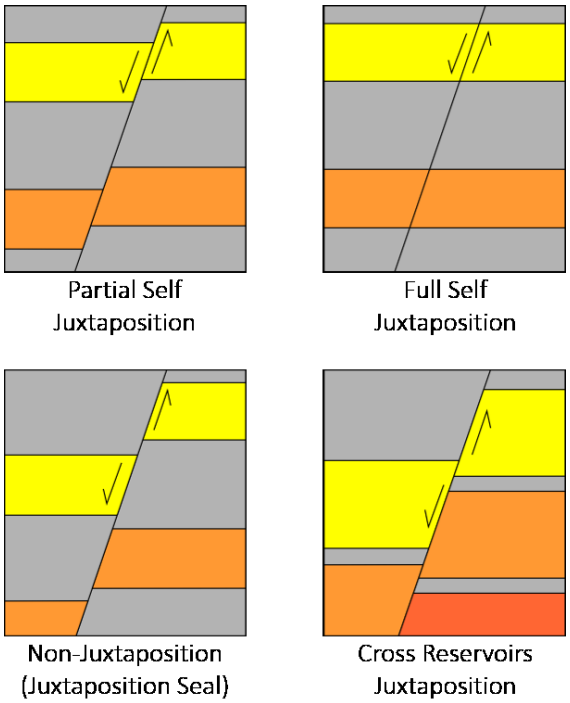

Figure 7.2: Juxtaposition relationships proposed by Neele et al (2012).

The different juxtaposition relationships observed within the geocellular model of the Sable Subbasin, and provide different opportunities for fluids and associated pressures to migrate and dissipate

The location of the faults in each expansion trend can also make a significant difference in the ability of pressure and associated reservoir fluids to “stair step” through juxtaposed permeable units. Faults more distally located tend to encounter lower permeability lithologies, which in turn have lower Darcy flow. The cross sectional area remains the same, however the permeability is reduced so the effective or available area for migration is also reduced and the system will be slower to equilibrate.

Previous work has considered disequilbrium compaction (due to rapid sedimentation) and hydrocarbon generation as two of the main potential mechanisms for pressure generation. Shales above the excess pressured reservoirs do not show any of the

postulated indicators of disequilibrium compaction; indicators are reversals of the acoustic, resistivity, and density measurements. Recent 1D thermal modelling work on the South Venture O-59 well suggests that there is late (to ongoing) generation of gas in the deep source rocks (Wong et al. 2016). This generation is supplying fluids and associated pressure to the petroleum systems of the Subbasin. When combined with the general basis of Darcy's Law and the regional geology (particularly the seals), ongoing hydrocarbon generation is the reason there is still excess pressure present in the basin and why it has not yet dissipated.

Ongoing hydrocarbon generation (supported by South Venture O-59 1D modelling) is causing a more rapid influx of hydrocarbons than are being dissipated through fault juxtapositions or contiguous reservoirs within the region. This has led to the inferred mechanical failure of the deeper reservoirs by building up pressure above fracture pressure (i.e. Venture Field - Sandstone 13), and significant excess pressuring of the middle reservoirs (i.e. Venture Field - Sandstone 8), where pressures appear to be releasing slowly at local choked juxtaposition connections. The offset between the hanging wall and footwall is not as large in shallower reservoirs compared to the deeper ones, and the net-to-gross ratio increases upwards with progradation of the shelf. This means there are more permeable units juxtaposed over larger surface areas allowing for increased connectivity, therefore considerably larger compartments as confirmed by seismic profiles. The hydrostatically pressured systems at the top of the region eventually subcrop to surface in the northeast of the Subbasin (beyond the model boundary), providing a final outlet for pressure and fluid dissipation.

The conclusion from this research is that fault juxtaposition relationships (combined with seal leakage, seal failure and erosional contacts) control the connectivity between permeable units (potential reservoirs) in the region. The permeability of the units at the fault juxtapositions is primarily dependent on the position in the expansion trend, with more distal locations demonstrating decreased permeability and correspondingly decreased connectivity. The combination of available reservoir volumes, area-dependent fault transmissibility, and ongoing hydrocarbon generation have led to

the present distribution of excess pressured systems and fluids at depth. Deeper sands release fluids and pressure through top seal leakage, mechanical failure and/or by exceeding the fracture closure pressure, eventually allowing the fluids and associated pressures to migrate vertically and laterally to the shallower hydropressured sands by choked cross fault leak of distal (within expansion trend) reservoirs or “fault rocks”. This arrangement is repeated within each fault block of the expansion trend and between the expansion trends within the modelled area. Faults in this part of the Sable Subbasin demonstrate two of three migration pathways suggested by Downey (1994): (1) at depth, hydrocarbons with (sufficient) excess pressures are able to migrate along the fault plane (or through mechanical failure of seals), and (2) at intermediate depths, hydrocarbons migrate by “stair stepping” up permeable units that are juxtaposed across the fault (Figure 7.3).

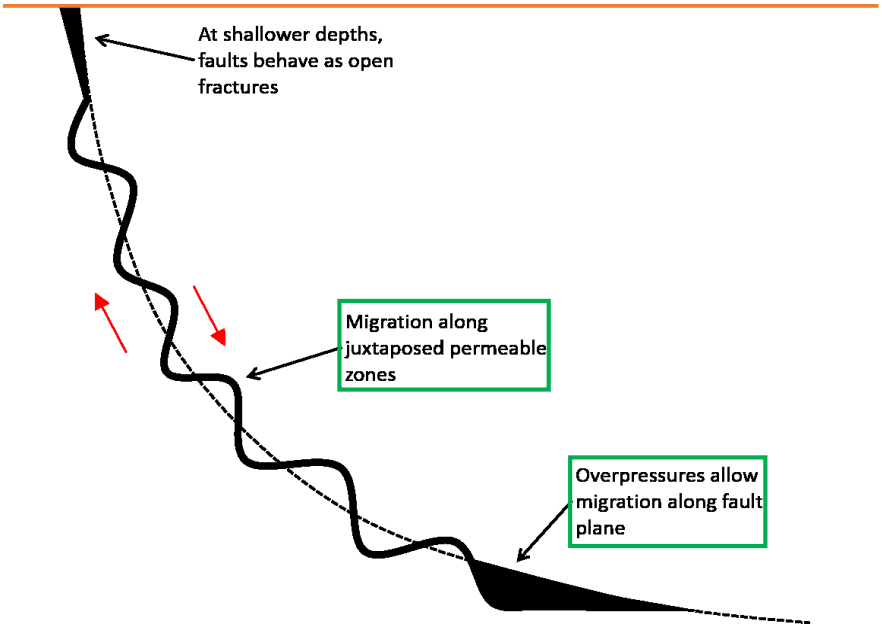

Figure 7.3: Hydrocarbons can migrate along the fault plane at shallow depth where they behave as open fractures, or juxtaposed permeable zones, or due to excess pressure at depth (Downey 1994). The green boxes define the behaviours suggested by Downey (1994) that are supported by observations and interpretations of fault juxtapositions the Sable Subbasin expansion trends included in this study.

7.2: Final Recommendations

Further work is required to refine the model. Accessing the original operator digital data on pressure buildups for each pressure point would allow for extrapolation to reservoir pressure when build up was still occurring, and would potentially improve screen for valid versus invalid data. Undertaking a complete petrophysical analysis for each well to provide detailed lithology, porosity, and permeability values at each wellbore and horizon that can then be populated through the contained reservoir volume using Petrel™. This would enable analysis of the calculated pore space and the permeability product in the reservoir overlap area along fault planes, and investigation into possible links with rates of fluid and reservoir pressure migration. Examining shale mineralogical compositions and thicknesses to determine whether there is a relationship between the preferred failure mechanism leading to fluid and pressure transfer between reservoirs - along fault planes, across fault planes at reservoir-reservoir juxtapositions, or via breaching of top seals.

Finally, the model created for this thesis is a static model; a dynamic model would better serve to recreate and better predict excess pressure in undrilled sections of the region. To create a dynamic model, a 'layer-cake' velocity model would be required first. Thermal modelling of more wells would provided further insight on the thermal and maturation history of the region, which in turn could increase knowledge surrounding excess pressure mechanisms in the Sable Subbasin. Modelling can be completed using Eclipse Reservoir Simulation over long time spans, or PetroMod Thermal Modelling.

Bibliography

Allan, U.S. 1989. Model for hydrocarbon migration and entrapment within faulted structures. AAPG Bulletin **72**(7): 803-811.

Asquith, G., and Krygowski, D. 2004. Basic Well Log Analysis. 244.

Atwater, G.I., Miller, E.E., and Wiggins, G.B. 1986. Effect of decreased porosity with depth on oil and gas reserves in south Louisiana sandstone reservoirs. AAPG Bulletin **49**: 334.

Barker, C. 1990. Calculated volume and pressure changes during the thermal cracking of oil to gas in reservoirs. AAPG Bulletin **74**: 1254-1261.

Berg, R.R. 1975. Capillary pressures in stratigraphic traps. AAPG Bulletin **59**(6): 939-956.

Bjorkum, P.A. 1996. How important is pressure in causing dissolution of quartz in sandstones? Journal of Sedimentary Research **66**: 147-154.

Bruce, C.H. 1984. Smectite dehydration - its relation to structural development and hydrocarbon accumulation in northern Gulf of Mexico basin. AAPG Bulletin **68**: 673-683.

Burger, H., Sheehan, A., and Jones, C. 2006. Introduction to Applied Geophysics. 624.

Catuneanu, O., Abreu, V., Bhattacharya, J.P., Blum, M.D., and Dalrymple, R.W. 2009. Towards the Standardization of Sequence Stratigraphy. Earth-Science Reviews **92**: 238-271. doi: 10.1016/j.earscirev.2008.12.003.

Cayley, G.T. 1987. Hydrocarbon migration in the Central North Sea. *In* Petroleum Geology of Northwest Europe: Proceedings of the 4th Conference on Petroleum Geology of NW. Europe. pp. 549-555.

Christians, A. 2015. Late Cretaceous to Cenozoic Reactivation of Central Scotian Slope Salt Bodies and the Impact on Slope Depositional Systems. p. 247.

CNSOPB, C.-N.S.O.P.B. 2016. Depth to pre-Mesozoic and pre-Carboniferous basements (including Petroleum Rights). . Geological Survey of Canada.

Deming, D. 1994. Factors necessary to define a pressure seal. AAPG Bulletin Bulletin **78**: 1005-1009. doi: 10.1306/A25FE40F-171B-11D7-8645000102C1865D.

Downey, M.W. 1990. Faulting and hydrocarbon entrapment. Leading Edge: 20-22.

Downey, M.W. 1994. Hydrocarbon Seal Rocks. *In* The Petroleum System - from Source to Trap. *Edited by* W.G. Dow and L.B. Magoon. AAPG, Tulsa. pp. 159-164.

Forbes, P.L., Ungerer, P., and Mudford, B.S. 1992. A two dimensional model of overpressure development and gas accumulation in venture field. AAPG Bulletin **76**: 318-338.

Goulty, N.R. 1998. Relationships between porosity and effective stress in shales. First Break **16**: 413-419.

Gussow, W.C. 1954. Differential entrapment of oil and gas: a fundamental principle. AAPG Bulletin **38**(5): 816-853.

Hansen, D., Shimeld, J., Williamson, M.A., and Lykke-Andersen, H. 2004. Development of a major polygonal fault system in Upper Cretaceous chalk and Cenozoic mudrocks of the Sable Subbasin, Canadian Atlantic margin. Marine and Petroleum Geology **21**: 1205-1219.

Harris, J.P., and Fowler, R.M. 1987. Enhanced prospectivity of the Mid-Late Jurassic sediments of the South Viking Graben, northern North Sea. *In* Proceedings of the 3rd Conference of Petroleum Geology of North West Europe. *Edited by* J. Brooks and K. Glennie. Graham & Trotman. pp. 879-898.

Hunt, J.M. 1990. Generation and migration of petroleum from abnormally pressured fluid compartments. AAPG Bulletin **74**: 1-12.

Hunt, J.M., Whelan, J.K., Eglinton, L.B., and Cathles, L.M. 1994. Gas generation - a major cause of deep Gulf Coast overpressure. Oil and Gas Journal **92**: 59-63.

Jansa, L.F., and Urrea, V.H.N. 1990. Geology and diagenetic history of overpressured sandstone reservoirs, Venture gas field, offshore Nova Scotia, Canada. *In* American Association of Petroleum Geologists Bulletin. pp. 1640-1658.

Jowett, E.C., Cathles, L.M., and Davis, B.W. 1993. Predicting depths of gypsum dehydration in evaporitic sedimentary basins. AAPG Bulletin **77**: 402-413.

Katsube, T.J., and Williamson, M.A. 1994. Effects of diagenesis on shale nano-pore structure and implications for sealing capacity. Clay Minerals **29**: 451-461.

Kidston, A.G., Brown, D.E., Smith, B.M., and Altheim, B. 2005. The upper Jurassic Abenaki formation offshore Nova Scotia: a seismic and geologic perspective.

Luo, M., Baker, M., and Lemone, D. 1994. Distribution and generation of the overpressure system, eastern Delaware basin, western Texas and southern New Mexico. AAPG Bulletin **78**: 1386-1405.

Mackenzie, A.S., and Quigley, T.M. 1988. Principles of geochemical prospect appraisal. AAPG Bulletin **72**: 399-415.

McCarthy, K., Rojas, K., Niemann, M., Palmowski, D., Peters, K., and Stankiewicz, A. 2011. Basic petroleum geochemistry for source rock evaluation. Oilfield Review **23**: 32-82.

Mitchum, R., Vail, P., and Sangree, J. 1977. Seismic stratigraphy and global changes of sea level, part 6: stratigraphic interpretation of seismic reflection patterns in depositional sequences. *In* Memoir 26: Seismic stratigraphy - applications to hydrocarbon exploration. *Edited by* C. Peyton. AAPG, Tulsa. pp. 117-133.

Mondol, N. 2010. Seismic Exploration. *In* Petroleum Geoscience. Springer Science, New York. pp. 375-402.

Mudford, B.S., and Best, M.E. 1989. Venture Gas Field , Offshore Nova Scotia : Case Study of Overpressuring in Region of Low Sedimentation Rate. AAPG Bulletin **73**: 1383-1396.

Mudford, B.S., Gradstein, F.M., Katsube, T.J., and Best, M.E. 1991. Modelling 1D compaction-driven flow in sedimentary basins: a comparison of the Scotian Shelf,

North Sea and Gulf Coast. Geological Society, London, Special Publications **59**: 65-85. doi: 10.1144/GSL.SP.1991.059.01.05.

Mukhopadhyay, P.K. 1993. Analyses and Interpretation of Geochemical and Source Rock Data from Scotian Shelf Wells. *In*, Halifax. p. 234.

Neele, F., ten Veen, J., Wilschut, F., and Hofstee, C. 2012. Independent assessment of high-capacity offshore CO2 storage options. Energy/Geological Survey of the Netherlands. The Netherlands.

NRCan. 2016. BASIN Database. Natural Resources Canada.

Osborne, M.J., and Swarbrick, R.E. 1997. Mechanisms for generating overpressure in sedimentary basins: a reevaluation. AAPG Bulletin **81**: 1023-1041.

Richards, B., Fairchild, L.H., Vrolijk, P.J., and Hippler, S.J. 2008. Reservoir Connectivity Analysis, Hydrocarbon Distribution, Resource Potential and production Performance in the Clastic Plays of the Sable Subbasin, Scotian Shelf. Central Atlantic Conjugate Margins Conference, Halifax 2008: Extended Abstracts: 165-185.

Sales, J.K. 1997. Seal strength vs trap closure - a fundamental control on the distribution of oil and gas. *In* AAPG Memoir 67: Seals, traps, and the petroleum system. *Edited by* R.C. Surdam. AAPG, Tulsa. pp. 57-83.

Shanmugan, G., Bloch, R.B., Mitchell, S.M., Beamish, G.W.J., Hodgkinson, R.J., Damuth, J.E., Staume, T., Syvertsen, S.E., and Shields, K.E. 1995. Basin-floor fans in the North Sea: sequence stratigraphic models versus sedimentary facies. AAPG Bulletin **30**(4): 477-511.

Sheriff, R.E. 1992. Vertical and Lateral Seismic Resolution and Attenuation: Part 7: Geophysical Methods. *In* ME 10: Development Geology and Reference Manual. American Association of Petroleum Geologists, Tulsa. pp. 388-389.

Silva, R.L., Wong, J.C., and Wach, G. 2015. Source rocks and petroleum systems of the Scotian Basin. CSEG Recorder **40**(8): 22-27.

Smith, B.M., Makrides, C., Altheim, B., and Kendell, K. 2014. Resource Assessment of Undeveloped Significant Discoveries on the Scotian Shelf. Canada-Nova Scotia Offshore Petroleum Board.

SOEP. 1997. Development Plan Application - Volume 2: Sable Offshore Energy Project. p. 245.

Tissot, B.P., Pelet, R., and Ungerer, P. 1987. Thermal history of sedimentary basins, maturation indices, and kinetics of oil and gas generation. AAPG Bulletin **71**: 1445-1466.

Vrolijk, P., James, B., Myers, R., Maynard, J., Sumpter, L., and Sweet, M. 2005. Reservoir connectivity analysis - defining reservoir connections and plumbing. *In* 14th SPE Middle East Oil & Gas Show and Conference. pp. 1-23.

Wach, G., Pimentel, N., and Pena dos Reis, R. 2014. Petroleum systems of the central Atlantic margins, from outcrop and subsurface data. *In* 33rd Annual GCSSEPM

Foundation Bob F. Perkins Research Conference. *Edited by* J. Pindell and B. Horn and N. Rosen and P. Weimer and M. Dinkleman and A. Lowrie and R. Fillon and J. Granath and L. Kennan. GCSSEPM, Houston, Texas. p. 68.

Wade, J.A., and MacLean, B.C. 1990. Geology of the Continental Margin of Eastern Canada. *Edited by* P.J. Griffin and J.O. Wheeler. Geological Survey of Canada, Ottawa. pp. 190-235.

Watts, N.L. 1987. Theoretical aspects of cap-rock and fault seals for single- and twophase hydrocarbons columns. Marine and Petroleum Geology **4**: 274-307.

Weston, J.F., MacRae, R.A., Ascoli, P., Cooper, M.K.E., Fensome, R.A., Shaw, D., and Williams, G.L. 2012. A revised biostratigraphic and well-log sequence-stratigraphic framework for the Scotian Margin, offshore eastern Canada. Canadian Journal of Earth Sciences 49: 1478-1503. doi: 10.1139/e2012-064.

Wielens, J.B.W. 2003. Overpressures on the Scotian Shelf. Geological Survey of Canada, Open File 1557: 142p.

Williamson, M.A. 1995. Overpressures and hydrocarbon generation in the Sable sub-basin, offshore Nova Scotia. Basin Research 7: 21-34. doi: 10.1111/j.1365-2117.1995.tb00092.x.

Williamson, M.A., and Smyth, C. 1992. Timing of gas and overpressure generation in the Sable Basin offshore Nova Scotia: implications for gas migration dynamics. Bulletin of Canadian Petroleum Geology 40: 151-169.

Wong, J.C., Skinner, C.H., Richards, F.W., Silva, R.L., Morrison, N., and Wach, G. 2016. 1D thermal model of South Venture O-59, Sable Subbasin (Scotian Basin, Nova Scotia). In The Atlantic Geoscience Society 42nd Colloquium and Annual Meeting. Edited by T. Fedak and B. Grantham and R. Raeside and C. White. Atlantic Geoscience Society, Truro NS. p. 68.

Yassir, N.A., and Bell, J.S. 1994. Relationships between pore pressure, stresses, and present-day geodynamics in the Scotian Shelf, offshore eastern Canada. AAPG Bulletin 78: 1863-1880.

Yilmaz, O. 2008. 3D Seismic Exploration. In Seismic Data Analysis: Processing, Inversion, and Interpretation of Seismic Data. Edited by S. Doherty. SEG, Tulsa. pp. 1001-1194.